Innovative laminate structures for tubular elements

Postma, Tiemen

Award date:
2012

Awarding institution:
University of Bath

Innovative laminate structures for tubular elements

Tiemen Rudolf Postma

A thesis submitted for the degree of Doctor of Philosophy

University of Bath

Department of Mechanical Engineering

April 2012

Abstract

The performance of peristaltic pumps is mainly governed by their tubing or hose materials. Research and development in this area is therefore very important for peristaltic pump manufacturers to keep in front of the competition and to open up new applications to enable further market penetration. Another aspect of this is of course price; performance and cost have to be in balance.

As an approach to fabricate a new tube material, the field of negative Poisson's ratio (or: auxetic) materials is explored. The combined deformations of tensile, compression and shear in a peristaltic pump tube may well benefit from the specific characteristics of auxetic materials. Materials can be designed to keep their dimensions constant in directions perpendicular to an applied load. This is referred to as “auxetic balancing”. Finite element modelling shows that lowering the Poisson's ratio will rapidly decrease the maximum stresses in the cross-section of an occluded tube. Optimum values for the Poisson's ratio are found to be between −0.1 and +0.1, preferentially being 0.

The re-entrant honeycomb structure is selected for initial trials, but manufacturing of this structure at the desired dimension proved to be too difficult at this time. Instead, electrospun nanofibre membranes are selected as the reinforcement structure. A liquid silicone elastomer is used as the matrix material. Key characteristics for the new material are derived from baseline test results on existing tubing.

Laminates are manufactured from electrospun nylon6 nanofibre membranes coated with a liquid silicone rubber. Compression moulding is used to cure the nylon6-silicone rubber laminate, to give two effects: it ensures impregnation of the membrane and the compression deforms the nanofibre structure in such a way that it will become auxetic through-the-thickness. Flat sheet laminates of 2 mm thickness are manufactured with 14 layers of reinforcement. A reinforcing effect and substantial lowering of the through-the-thickness Poisson's ratio is observed for the laminates at low strains. At higher strains (>50%) the effect of the reinforcement diminishes and the Poisson's ratio of the laminate and pure silicone rubber equalises. Finally, tubular laminates are manufactured and the resulting tubes are tested in a peristaltic pump with some promising results (>1 million occlusions before failure). Tube performance is not yet at the required level, but with further optimisation of the laminating process, mould design and (post-)curing large steps forward can be made.

Table of contents

Table of figures

Glossary

Cusp

The cusp is the area at the inside of the tube where the tube folds during occlusion (see picture). Sometimes the cusp is also referred to as "*cheek*", but then it includes the whole area up to the outside of the tube.

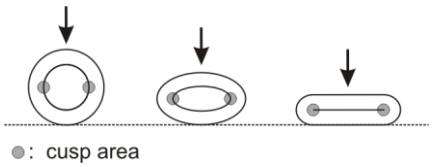

Dimensions

The dimensions of peristaltic pump tubing are normally given as:

[inner diameter (or bore)] x [wall thickness] x [length]

The length may be omitted to denote the cross-sectional tube size alone.

Heavy duty

This generally refers to the higher demanding industrial application area of peristaltic pumps requiring large flows and/or high pressures (up to 16 bar). In these applications mostly hose pumps are used (see *Hose* below).

Hose

Refers to a pump element in a peristaltic pump reinforced with cord layers. The peristaltic pumps that use these hoses are also called "*hose pumps*".

Life (or: hose/tube life)

Life means generally time it takes to the fatal hose/tube burst. At that time there is a direct connection through the wall between the inside and outside surface of the tube or hose. The product that is being pumped will end up partly in the pump housing and the hose has failed. Besides this there can also be other performance indicators to consider the hose as failed, e.g. unable to deliver the desired flow due to insufficient hose/tube recovery or backflow. Delamination can cause the first, abrasion of the inner surface the second.

Low duty

This generally refers to the lower demanding dosing and metering application area of peristaltic pumps requiring low flows and/or low pressures (up to 4 bar). In these applications mostly tube pumps are used (see *Tube* below).

Medium duty

Refers to the application area in between low and heavy duty and involves not too demanding applications between 4 and 8 bar of discharge pressure.

Overcompression (or: overocclusion)

Occluding a tube or hose between two surfaces requires a distance between them of twice the wall thickness (thinning of the wall caused by the Poisson's ratio is not taken into account). More occlusion than this double wall thickness is referred to as overcompression and is for instance necessary to pump against back pressure.

Spallation

This is material from the inner surface of the tube that is rubbed loose by abrasion due to the peristaltic action of the pump. It mainly occurs in the cusp at the discharge side, but can also take place elsewhere in the tube. This material will come into the product stream and should therefore be prevented as much as possible.

Tube

Tube refers to a pump element in a peristaltic pump without cord layer reinforcement. The peristaltic pumps that use these tubes are also called "*tube pumps*".

1 Introduction

This research is about tubing for a peristaltic pump. The tube is often considered as the heart of such a pump. Therefore the tube is a vital part of the pump and an important subject of research and development.
In the next sections the principle of peristaltic pumping will be explained followed by a historical overview on peristaltic pump and tube development. Then the current art in pump tubing will be presented and finally the objectives for this research are given.

1.1 Peristaltic principle

Peristaltic pumps are positive displacement pumps and use the movement of peristalsis to transport fluids. Peristalsis is known from nature and can be found in animal and human bodies in for instance their digestive tract [1]. After swallowing food it is transported down the oesophagus by a wavelike radial contraction of muscles lying around it along its length. This makes the ball of food go forward towards the stomach and prevents it from going back to the mouth. Something similar happens in the small intestine after the food has passed through the stomach.

In peristaltic pumps the tract is replaced by a pump element (an elastomeric tube or hose) and the muscles by a pressing element (rollers or shoes) mounted on a rotor. A schematic view of the working principle of the peristaltic pump is shown in Figure 1.1. The pictures show a peristaltic pump, in this case with a hose and pressing shoes, at several stages of the first pumping cycle when starting the pump. At the suction side a pressing shoe runs into the hose and will then fully occlude it. Further rotation of the rotor pushes the pressing shoe further through the hose. Behind this pressing shoe the hose will recover from flat to its original cross-sectional shape. This recovery creates a vacuum by which new medium is sucked into the pump hose. In front of the pressing shoe the medium is pushed forward in the hose releasing it into the discharge line. As soon as the pressing shoes runs out from the hose at the discharge side, the pressing shoe at the opposite side of the rotor runs into the hose at the suction side. This way always one pressing shoe will fully occlude the hose, separating the suction from the discharge and preventing backflow.

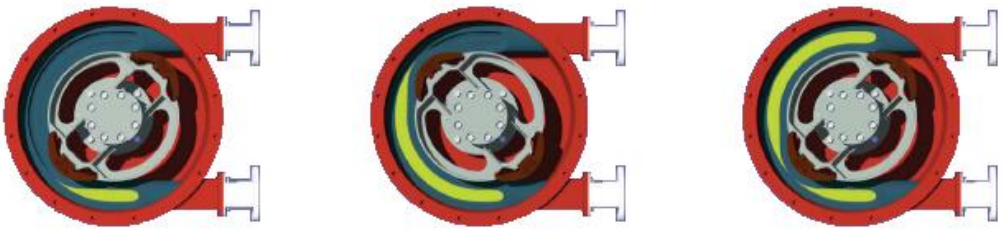

Figure 1.1: Schematic view of the peristaltic pump principle [© Watson-Marlow Bredel].

The peristaltic pumps have several features that make them very useful in certain applications. First of all, the medium being pumped is contained inside the tube or hose and does not come into contact with (moving) metal parts of the pump. Therefore corrosive and abrasive products are no problem for the peristaltic pump. Another important feature involves high-viscosity and high-density products. The vacuum created by the tube or hose recovery can be up to around 95% and with this the pump has very good suction capabilities. The final main feature of the peristaltic pump is its gentle pumping action which will transport the medium virtually as a plug flow. Delicate and shear sensitive products are therefore also very suitable for the peristaltic pump with a minimal chance of damaging these products.

1.2 Historical background of peristaltic pumps

First mentions of peristaltic pumps date from the late 19th century. A patent was granted to Eugene E. Allen in 1881 on an “instrument for the transfusion of blood” [2]. The idea was to use an elastic tube to contain the blood for transfusion in surgery. An external mechanism could then transport the blood through the tube by means of a peristaltic movement. This would reduce the introduction of air or coagulated blood into the bloodstream, the cause from which many patients died in those days.

Whether or not Allen’s design worked well is not clear. But in the decades thereafter it was tried to improve the peristaltic pump. Many more patents were granted on various new ideas on applications and improved pump design. Where many applications still involved medical ones [3,4], some came up with new usages such as a vacuum pump [5] or a gas meter [6].
Improvement in pump design often addressed the weakest point of the peristaltic pump, the tube. Because of the occlusion of the tube, in these early pumps inside wear was a big problem especially in the cusp (the location where the tube wall folds). Also axial stretching of the tube during the pumping action reduced tube life

and therefore limited the usefulness of the pump. It was still early days in rubber technology (Goodyear invented sulphur curing of rubber only in 1839), so solutions to improve life of the tube were mainly sought in mechanical aspects of the tube and the pump. Axial stretching of the tube was countered by either changing the number or size of the rollers or the track length of occlusion. To reduce wear inside the tube to a minimum attempts were made for instance to built-in compression regulation to prevent the tube from being occluded more than necessary. Another approach often used was to change the cross-sectional shape of the tube from annular to a free shape to accommodate occlusion and this way attempt to obtain a longer tube life. Some examples of these shapes are shown in Figure 1.2, with some also including fixtures to keep the tube from moving sideways. Other innovations comprised of vacuum assisted tube recovery to limit flow drop over life to a minimum.
This way many variations of the peristaltic pump came into existence by the end of the 19th century, having rotors with 1 to 4 horizontally or vertically placed rollers and a tube occlusion track varying between 90° and 360° [7-13].

Figure 1.2: Examples of alternative cross-sectional shapes of peristaltic tubes adopted from late 19th century patents.

Into the next century innovation continued on peristaltic pumps in attempts to make the pump cheaper, easier to construct and more durable. This resulted in many more variations of peristaltic pumps being developed to increase pump and tube life. This manifested itself in for instance pumps with up to 8 rollers placed on the rotor, eccentric rotors, and leather or thin steel bands around the rollers of the rotor [14-27]. Also a linear type was developed [28]. On the tube side more cross-sectional shapes were devised and (partial) reinforcement was introduced [21,28]. This reinforcement was either used to increase hoop strength for better pressure resistance, or to strengthen the tube wall where it contacts the roller. Other improvements in pressure resistance were obtained by enclosing the tube with the pump casing as much as possible [19]. At the same time the manual crank to operate the pump was slowly replaced by (electric) motors with reduction gears.

This also opened up the opportunity to place the pump in devices for medical applications like blood transfusions [26].

After World War II more possibilities became available for tube materials. In the decades before this war a number of synthetic rubbers like polyisoprene (IR), polybutadiene (BR), chloroprene (CR) and styrene butadiene rubber (SBR) were already invented. During this war natural rubber became scarce because most of the producing countries were under Japanese control. The demand for rubber to use in military vehicles (e.g. tires) in the U.S. and Germany was of course very high so the production capacity of synthetic rubber took off quickly. The discovery of silicone rubber in 1943 and its later found medical benefit of no blood clotting made this new found material useful as a tube for the peristaltic pump. Heart-lung machines were first used in 1951, which operates using the roller or peristaltic pump invented by Dr. Michael E. DeBakey [29,30]. This renewed medical application is interesting, especially when keeping in mind the pump's original application of blood transfusion. Besides tires, the military vehicles in World War II also required a large number of hoses. This demand led to improved and cheaper production techniques for rubber hoses by using extrusion instead of moulding and new ways to apply fabric reinforcements. Peristaltic pumps however kept mainly using tubes in their designs for a long time, so cord or other fabric reinforcement was hardly found in them. This could be due to the compression forces involved in occluding the tube and the remaining focus on the lower flow rates. This lower flow rates only need relative small tubes and it is difficult to get fabric reinforcement into a thin tube wall. Also the cost aspect must have played an important role in the limited use of fabric reinforced tubing, i.e. hoses.

Despite all the attempted innovations to make the peristaltic pump successful, nearly a century later the technique was still in its infancy. In a 1957 German patent [31] a typical tube life of only 10 hours is mentioned. This may be acceptable for transfusion or dispensing purposes (where the tube will be disposed after use), but for any form of industrial use this life time is much too short. In the years after some progress was made to improve the peristaltic pump, but it took until the first half of the 1980s for the real breakthrough. This was achieved by the company *Watson-Marlow*, founded in 1956, which were at that time commercially producing peristaltic pumps mainly for medical applications. First step in the breakthrough was a new pump head with a rotor design that was able to accommodate variable tube sizes, different materials and hardness' [32]. The second step was the discovery to use a thermoplastic elastomer tube material (Marprene®) and its market launch in 1984.

This material exhibits very good fatigue properties and tube life could be extended to more than 1,000 hours. These kinds of lifetimes are useful for industrial applications and because of this success Watson-Marlow became world leader in peristaltic pumps.

Meanwhile, in 1971 the foundations were set in The Netherlands for a new line of peristaltic pumps for heavy duty applications. The company *Bredel* were designing machines to spray concrete mixtures (mortar) at construction sites. Spraying the mortar required a pump, but at that time this was a problem because no available pump was really able to handle this very abrasive product. Trying to solve this problem and looking at the properties of the mortar, a pump operating with the peristaltic principle would be very suitable for this. The flow range and pressure capabilities of existing peristaltic pumps were however far too low. Therefore the peristaltic pump and hose were scaled up and redesigned to a larger size and strength to meet the demands for mortar pumping. This was so successful that Bredel in 1973 decided to focus its activities on the production and development of this new peristaltic pump. In the following years more and more applications for this pump were found and more sizes and hose materials became available. Ever since the start Bredel is world market leader in these heavy duty industrial hose pumps.
In 1996 Watson-Marlow took over Bredel and the newly formed company Watson-Marlow Bredel is now able to serve the whole spectrum of (rotary) peristaltic pumps. Currently Watson-Marlow Bredel is world leader with around 50% market share for the whole range of peristaltic pumps.

1.3 Current art

Heavy duty industrial peristaltic pumps use rubber hoses reinforced with 2 to 6 cord layers depending on the size. During hose manufacturing these cord layers are applied by a spiral winding technique winding the cords themselves or by winding calendared plies. Like in all pressure hoses the winding angle is around the equilibrium angle of approximately ±54° with respect to the length axis to limit the length and diameter change of the hose [33]. It was however quickly found that stretching of the hose by the rollers during pumping needed to be countered. This was first done by adding axial reinforcement (steel wiring) to the 54° carcass [34]. A problem with this added axial reinforcement was an increased bending stiffness of the hose. To avoid this as well as other construction issues, it was found that by changing the angles of the cord layers to ±63° the hose remains at the same

position in the pump. Lengthening of the hose by internal pressure is now compensated by the extra length needed from stretching. This hose construction was patented in 1976 [35] and became the most important pillar of Bredel's success as this patent kept competitors from using the same idea.

The Bredel 4-ply hoses changed a little afterwards. It appeared that this larger angle in the outer two plies only was sufficient to keep the hose in place. The inner two plies could now be chosen at smaller angles in such a way that the angle of the 4 plies together averages to equilibrium angle of 54°. The advantage of this two-angle construction is mainly better occlusion behaviour as is schematically shown in Figure 1.3. This is better because over-compression of the side parts can be less and possible solids in the product being pumped are not pushed into the cusp. Also hose recovery after occlusion is improved. Later developments and improvements in materials and production techniques reduced this advantage somewhat, but Bredel's hoses are still superior in high demanding applications.

Nowadays, development focuses mainly on gentler hose occlusion and hose material improvement. Also alternative materials like thermoplastic elastomers are investigated and been applied [36,37].

Figure 1.3: Schematic view of the occlusion behaviour for (a) "two-angle" Bredel hose where the hose closes from the cusp to the middle and (b) "one-angle" hose where the hose closes from the middle to the cusps. The picture shown in (b) is also valid for tubes without reinforcing cord layers.

In the smaller low duty peristaltic pumps the current top art in tubing is produced by W.L. Gore & Associates and it is sold under the trade names STA-PURE™ and CHEM-SURE™. The tube material here is a membrane of expanded PTFE (ePTFE) impregnated with a liquid elastomer, silicone in the case of STA-PURE™ and perfluoro polyether in the case of CHEM-SURE™. This impregnated membrane is then rolled up around a mandrel like a Swiss roll up to the required wall thickness and curing of the final tube is done by compression moulding [38,39]. The finished product is then basically a tube constructed of a "PTFE reinforced elastomer laminate".

From now onwards the focus will be specifically on STA-PURE™. This tube has a number of advantages over other peristaltic tubing as is shown in Table 1.1. Of course there are also a number of drawbacks and they are also mentioned here.

STA-PURE™ tubing	
Advantages	**Disadvantages**
Long life	Risk of delamination
Good hoop strength (→ good pressure resistance)	Limited suction capabilities
Flow consistency over life	“Sweating” through the tube wall
Virtually no spallation	Very expensive
Has all approvals for use in pharmaceutical, medical and food applications (e.g. USP Class VI)	

Table 1.1: Advantages and disadvantages of STA-PURE™ compared to other peristaltic tubing.

Especially the last disadvantage of the high cost is a large one and it inhibits the growth to full potential for a tube of this performance. This brings us to the objectives of this research, which involves finding an alternative to STA-PURE™, but at a lower cost.

1.4 Objectives

The current STA-PURE™ tubing works well but is too expensive to extend Watson-Marlow’s market penetration in areas where they cannot compete right now with other pump types. To increase accessibility into these areas, peristaltic tubing should become available with at least similar performance capabilities as STA-PURE™, but at a much lower price.

Even though it goes a bit too far to achieve this within this research, as a basic product specification this would ultimately mean:

- In the mid range 500/600 series of the Watson-Marlow pumps, the price of a single tube (element) should be in the order of £5 − £10.
- Performance wise, tube life should be aimed at 6 months although 1 year would be ideal. At a reference duty point of 100 rpm this would mean well over 50 million occlusions (with a two-roller rotor) that the tube has to endure during 6 months of continuous pump duty.
- During its life, the tube has to be able to withstand average discharge pressures of:

    * 5 bar for large tubes (bore > 12 mm)
    * 7 bar for middle size tubes (6.4 mm ≤ bore ≤ 12 mm)
    * 10 bar for small tubes (bore < 5 mm)
- Tube life needs to be consistent.
- Most popular tube sizes are those with bores between 6.4 and 12.7 mm and wall thicknesses of 2.4 to 4.8 mm. It would be beneficial for new tubes to have the same dimensions as current tubing, so it can fit directly into existing pumps.

In order to achieve such an alternative, novel tubing material or material combination has to be developed. For intellectual property reasons the use of PTFE must be avoided. The objective is to find a concept for such a tubing material in terms of properties and behaviour. Also manufacturing routes have to be investigated on how to make this material and how to produce tubing from this material. Finally some prototype testing in a pump should be done to demonstrate potential and feasibility of the material design in the actual application of peristaltic tube elements.

In the next chapters of this thesis all these topics are addressed. In chapter 2 a key material property is identified for peristaltic tube performance and a literature review is made on this property. In the following chapter the methods and approaches are described on how this property can be introduced into a tubing material. Several material designs and manufacturing routes are discussed in here as well. Using existing peristaltic tubing materials, a baseline for several (mechanical) properties of peristaltic tubing is established in chapter 4 in order to know what their typical range or value should be. Chapter 5 shows the effect of the earlier identified key material property on the occurring stresses and strains inside a peristaltic tube by means of finite element modelling. The final two chapters describe the manufacturing, characterisation and testing of the selected laminate material that could be used for peristaltic pump tubing. In chapter 6 only as flat sheet laminates to accommodate standard material tests, but in chapter 7 also as tubular laminates. These tubular laminates acted as first prototypes and have been put to test in a peristaltic pump.

2 Literature review

This literature review will focus on the field of auxetic materials. When in service, the tube will undergo tensile and compression forces simultaneously. This causes internal stresses in the material as a consequence of its positive Poisson's ratio. This is especially the case in the cusp of the tube. Local compression causes material to bulge out of the tube's inner surface when the tube is occluded, as is schematically shown in Figure 2.1. In the pump with full (over)occlusion on the tube this causes wear and tube material is abraded from the cusp. This is the mechanism for spallation (the formation of debris) and the markings of this process can eventually be seen inside the tube as "tram rails" along its occluded length. Here is why auxetic materials become interesting to use in the peristaltic tubing application. Incorporation of auxetic materials, which have a negative Poisson's ratio, can balance or even inverse this effect by tuning the tube's overall Poisson's ratio. This should result in better occlusion behaviour as the cusp area will then be relieved from the excessive compression loads. It is likely this affects peristaltic tube performance positively and is the key to meet the desired objectives.

The review first gives some basic theory on elastic properties. Secondly auxetic behaviour will be explained, followed by a description of a number of material variations that can exhibit auxetic behaviour like foams, polymers, composites and microstructures. Finally some concluding remarks are given on the findings from this review.

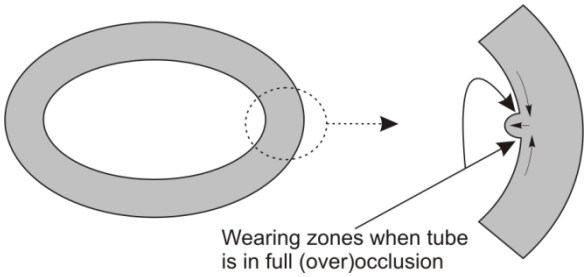

Figure 2.1: Schematic representation of bulging material from the tube wall when occluded.

2.1 Elastic properties

Deformation involves a stress and a strain in a material. For instance, stretching a material will result in an elongation in that direction. The theory of elasticity is developed to describe this material behaviour. From an engineering point of view three properties are often used to characterise the elastic behaviour of a material. These properties are the Young's modulus (E), the shear modulus (G), and the bulk

modulus (K). In addition to these three moduli also a fourth parameter, the Poisson's ratio (ν), is often used.

The Young's modulus is linked to the material's linear (elastic) response to strain and it is the measure of stiffness. The Young's modulus (E) is defined as the ratio between stress (σ) and strain (ε):

$$E = \frac{\sigma}{\varepsilon} \tag{2.1}$$

For most materials linear response occurs only at small deformations, so this relation is limited to small strains (< 0.2%).

The shear modulus (G) is a measure of how easy the material will deform under shear stress. This is also called the modulus of rigidity and is defined as the ratio between shear stress (σ_{xy}) and shear strain (ε_{xy}):

$$G = \frac{\sigma_{xy}}{\varepsilon_{xy}} \tag{2.2}$$

The bulk modulus (K) is the volumetric response of the material to uniform pressure (p). It is a measure of incompressibility and is defined as:

$$K = -V\left(\frac{\partial p}{\partial V}\right) \tag{2.3}$$

Stretching a material in one direction will cause a response in the transverse direction. The Poisson's ratio describes this response and it is defined as:

$$\nu_{xy} = -\frac{\varepsilon_y}{\varepsilon_x} \tag{2.4}$$

This is when deformed (either tensile or compression) in the x-direction.

For homogeneous isotropic materials these properties can be described by the following equations [40]:

$$G = \frac{E}{2(1+\nu)} \tag{2.5}$$

$$K = \frac{E}{3(1-2\nu)} \tag{2.6}$$

$$E = \frac{9KG}{(3K+G)} \tag{2.7}$$

$$\nu = \frac{1}{2}\left(\frac{3K-2G}{3K+G}\right) \tag{2.8}$$

The equations show that these properties are interdependent and only two of them need to be known to calculate the other two. Providing positive moduli, two extreme situations for the Poisson's ratio can be considered using equation (2.8). A material that is easy to shear (compliant) but also incompressible (G << K) will have a Poisson's ratio approaching +½. On the other hand, when G >> K (so easy to compress but difficult to shear) the Poisson's ratio becomes negative, approaching –1. The consequences of ν being between –1 and +½ on a material and the way it is perceived will be outlined in the next section.

2.2 Auxetic behaviour

In everyday life certain phenomena are experienced as normal, like an object that will fall to the floor under the influence of gravity. It can even be that something is considered normal while it is actually an exception to normal behaviour, like ice floating on water. For almost all substances the solid state has a higher density than the liquid state and will sink to the bottom. Nevertheless, we all take ice skating for granted.

In the scope of this section another phenomenon is seen as normal: a positive value of the Poisson's ratio. Our intuition tells us when stretching a material, it is supposed to elongate in the direction of stretching, but contract in the transverse direction. And similarly, under compression the material will become shorter in the direction of compression, but will expand (or "bulge") in the transverse direction.
In the 19th century [41] Poisson himself and others found the, as it was then called "stretch-squeeze ratio", to be ¼ for isotropic materials based on the elastic uni-constant hypothesis. In this time the general thought was for a material to be isotropic and homogeneous, the stretch-squeeze ratio is fixed. Small deviations in the value were then supposed to be caused by anisotropy. Wertheim however found in his experiments on metals this value to be near ⅓ [41]. He however did not rule

out the possibility of other values, as around 1860 many other values for the stretch-squeeze ratio were reported, like 0.294 for tempered steel and 0.387 for brass. They were still pretty near the aforementioned values of ¼ and ⅓, but some elastic materials investigated, like cork, jelly and india-rubber, were found to have very deviating values. Results like these of course led to a lot of discussions in the scientific world of the second half of the 19th century. The author of [41] derived (in article 169d) the stress-squeeze ratio to be between 0 and ½ for isotropic materials. He also makes a remark about the possibility of *negative* dilatation in anisotropic materials like certain types of wood. From experiments on pyrite crystals done by W. Voigt, a *negative* Poisson's ratio was observed and had a calculated value of nearly –⅐ [42].

Today we know the Poisson's ratio can (in the isotropic case) theoretically be anywhere in the range of $-1 \leq \nu \leq +\frac{1}{2}$ as can be shown from equation (2.8). This means the Poisson's ratio does not necessarily need to have a positive value. Even though it is known for well over a century now that negative Poisson's ratio materials could exist, this phenomenon still feels counter-intuitive and was for a long time regarded as some kind of anomaly in nature.

Material	**Poisson's ratio** [51]	**Material**	**Poisson's ratio**
Aluminium	0.334	Polymers [52]:	
Brass	0.340	Polyethylene (PE)	0.4 – 0.42
Bronze	0.14	Polypropylene (PP)	0.4 – 0.45
Cast iron, gray	0.211	Polycarbonate (PC)	0.39 – 0.44
Copper	0.340	Polyamide (Nylon®)	0.38 – 0.42
Lead	0.431	PTFE (Teflon®)	0.44 – 0.47
Magnesium	0.350	PMMA (acrylate)	0.4 – 0.43
Molybdenum	0.307	Polyvinylchloride (PVC)	0.37 – 0.43
Steel, cast	0.265		
high carbon	0.295	Natural rubber	0.4997 [53]
stainless (18-8)	0.305		
Titanium (99% Ti)	0.24	Concrete [54]	0.17
Zinc	0.331	Cork [43]	0.064 – 0.097
		Glass [55]	0.19 – 0.26

Table 2.1: Poisson's ratios of various materials.

Looking at Table 2.1 it is clear that intuition will tell you a positive Poisson's ratio is normal. Most every day materials have a positive Poisson's ratio around 0.25 to 0.33, so it is not a surprise that the scientists from the 19th century thought it to be a constant. An interesting behaviour can be seen in cork. This material has a Poisson's ratio close to 0 [43] what means there is almost no dimensional change in

cork transverse to the loading direction in tension as well as in compression. This property is thankfully used in wine bottle stoppers where a pressure increase inside the bottle would jam a larger (positive) Poisson's ratio stopper in the bottle's neck.

In 1987 Roderic Lakes presented a material with a negative Poisson's ratio [44] by converting a positive Poisson's ratio open-cell polyester foam into a negative one. This was basically the first description of a purposely produced and investigated isotropic material of this kind. Negative Poisson's ratios are mentioned in the literature before e.g. [45-47] but are not discussed. From this time onward more and more attention was focussed on negative Poisson's ratio materials. In order to overcome the long describing phrase "negative Poisson's ratio materials" this new class of materials is referred to as anti-rubber [48], dilatational [49] and auxetic materials. The latter one is derived from the Greek word "auxetos" ($\alpha\upsilon\xi\varepsilon\tau\sigma\sigma$), which means "that may be increased" referring to the increasing width and volume when the material is stretched [50]. The term "auxetic materials" is now generally adopted as the name for the negative Poisson's ratio class of materials.

Visualising auxetic behaviour can be done the easiest by deforming a 2-dimensional honeycomb structure. Figure 2.2 shows a hexagonal and a re-entrant structure and the effect of vertical stretching on horizontal deformation. The hexagonal structure exhibits a positive and the re-entrant structure a negative Poisson's ratio.

Auxetic materials have some interesting and useful properties in general, but also compared to their positive Poisson's ratio counterparts. Two of them were already suggested by Lakes in his 1987 Science paper [44]. To bend a conventional, positive Poisson's ratio in two opposing directions a saddle shape will form (anticlastic curvature). On the other hand, an auxetic material can accommodate the double bent dome-shape form (synclastic curvature). Evans proved in 1991 this is indeed the case when he found synclastic curvature upon bending sandwich panels with an auxetic foam core [56]. The second feature of auxetic materials suggested by Lakes is the higher indentation resistance or hardness. He experimentally verified this in 1993 [57]. Basically, all material properties with the term $(1+\nu)$ in the denominator should improve for auxetic materials. Keeping this in mind and going back to the equations in section 2.1, another example of increasing property can be seen in equation (2.5): the shear modulus G. It is indeed demonstrated by Choi and Lakes that the shear modulus increases for polymeric foams [58]. Also toughness should increase. Especially the fracture toughness should improve compared with

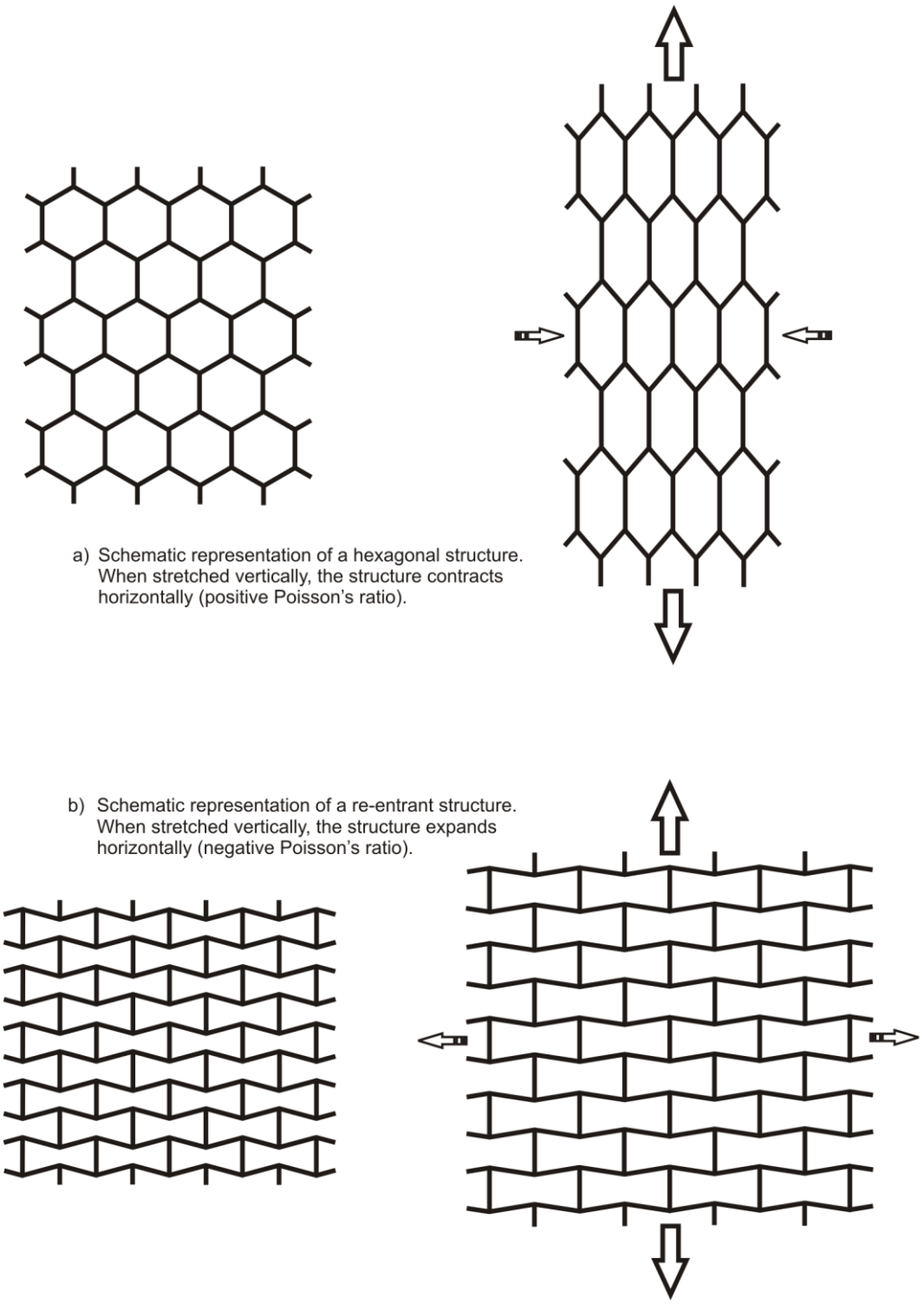

Figure 2.2: Hexagonal and re-entrant honeycomb structures showing the effect of positive (a) and negative (b) Poisson's ratio upon tensile deformation.

conventional materials provided that the Poisson's ratio is sufficiently negative, because the critical stress for unstable crack growth of an isotropic elastic material is proportional to the Poisson's ratio by $[1/(1-\nu^2)]^{1/2}$ [59]. This increase in (fracture) toughness is indeed observed for conventional and re-entrant open cell copper foams [59,60], for polymeric foams [58] as well as in carbon fibre / epoxy laminates [61].

Since 1987 more and more natural materials are recognised to exhibit auxetic behaviour and also earlier findings could be explained. For elements it was found that 69% of the cubic metals show a negative Poisson's ratio when deformed in the [110]-direction [62]. The minerals α-cristobalite (a crystalline form of SiO_2) and natrolite (a zeolite) were also found to behave auxetically due to the deformations in their crystal structure [63,64]. Also in biological materials auxetic behaviour is observed. Cat skin [65], cow teat skin [66], cancellous bone [67] and crystalline cellulose from Norway spruce [68] all show negative Poisson's ratios when deformed because of their microstructures. How a material's microstructure can cause auxetic behaviour will become clear from the following sections.

2.3 Foams

As already mentioned above, the first deliberately made isotropic material with a negative Poisson's ratio was a foam. For such a foam, Roderic Lakes envisioned cubic unit cells with all the faces bent inwards [44]. This re-entrant cell configuration will give for pulling at any two opposite sites an expansion in the other two directions as well. And on the other hand, pushing at any two opposite sites will cause the whole cell to contract. To make the auxetic foams Lakes devised a way to transform conventional open-cell polyester foams with various cell sizes. An oversized piece of the foam is triaxially compressed in a mould with typical volumetric compression ratios between 1.4 and 4. This triaxial compression causes the cell ribs to buckle. This configuration is then fixed by heating the mould with the compressed foam slightly above the softening temperature and subsequently cool it to room temperature. Of these foams the Poisson's ratios were found to be negative up to values as low as –0.7. Lakes also made metal foams auxetic by triaxial compression at room temperature causing plastic deformation of the cell ribs. The auxetic foams were found to be more resilient in all three orthogonal directions than conventional foams.

Later, Friis et al. describe the fabrication of other foamed materials made auxetic based on the triaxial compression technique and compared them against the original ones [69]. The materials involved a thermoplastic polyester urethane foam, a thermosetting RTV silicone foam and a metallic copper foam. Here is also found that the re-entrant auxetic foams are more resilient than the conventional foams. The Young's moduli of the re-entrant foams are lower than for the conventional foams [69,70].

In the following decade or so, a lot of effort was put by various researchers into downsizing auxetic structures (like the re-entrant structure in Figure 2.2) to a molecular level, mainly with modelling or other computational techniques [50,71-75]. Because the theory of elasticity contains no length scale, the elastic behaviour is size independent and consequently not limited to normal foam cell sizes. Auxetic behaviour could therefore also be found in microstructures with scale sizes < 1 μm [44]. The main advantage to be gained by designing and synthesising these molecular auxetics is an increase in stiffness [50]. To simulate the re-entrant structure, Evans et al. suggest a structure of benzene rings connected with acetylene chains and calls it (n,m)-flexyne for the hexagonal structure and (n,m)-reflexyne for the re-entrant structure with n and m the number of acetylene links in the diagonal and vertical branches from the benzene ring respectively (see Figure 2.3) [50]. This will create a two-dimensional structure with auxetic behaviour and anisotropy can be introduced by changing values of n and m. Although there has been success in synthesising building blocks for this type of structures [76] and despite advances in the field of macrocyclic chemistry, it seems to have lost the attention for developing auxetic materials.

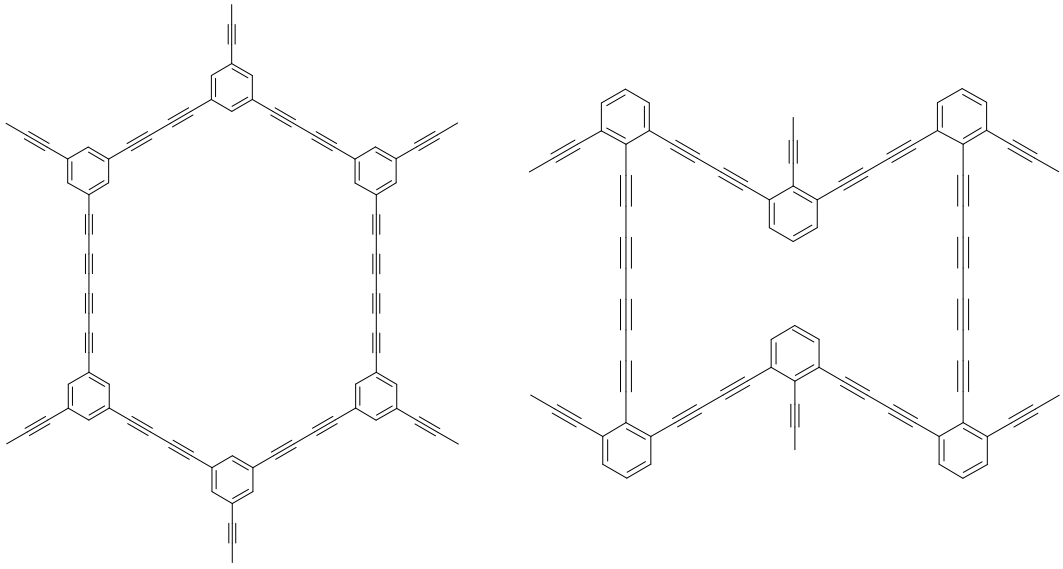

Figure 2.3: The structures of (n,m)-flexyne (left) and (n,m)-reflexyne (right), here with n=2 and m=4.

Other molecular designs predicted to have a negative Poisson's ratio are based on three-dimensional inorganic self-assembling structures e.g. through hydrogen bonding or coordination to metals [73], spiral or helix structures of polydiacetylene [72,75] and certain phases of carbon nitride [77].

Meanwhile research was also focussed back to the cellular foams. Up to 1997 the fabrication of the auxetic foams was somewhat arbitrary. Chan and Evans therefore studied the processing parameters of the triaxial compression technique on different foams [78]. These parameters are the heating temperature, heating time and the volumetric compression ratio and guidelines are presented to keep a better control of the process:

- The heating temperature should be 5-20 °C below the softening temperature of the foam to prevent collapse of the cells, but still a maximum of stress relaxation in cell structure.
- The heating time should be until the centre of the foam has reached the desired heating temperature.
- The volumetric compression ratio has an upper limit at the foam's densification point, when opposite cell ribs will touch each other. The lower limit is governed by the point where cell ribs start to buckle. Any volumetric compression ratio between these limits will vary the amount of re-entrancy and hence the degree of auxeticity.

In a next step Chan and Evans further developed the process to be able to make larger foam blocks auxetic [78]. When the foam block is too large, the creasing effect will come into play when trying to compress it too much. The foam will locally collapse. To overcome this effect, a multistage triaxial compression technique is introduced, gradually decreasing the size of the foam. For each stage the heating time is needed to be determined again because of change in the foam's density.

Various polyethylene foams are tried to be converted into auxetic ones by Brandel and Lakes [79]. Large cell (1-2 mm) foams could easily be made auxetic using the triaxial compression technique. Attempts of doing the same for microcellular (0.1 mm) polyethylene foams proved to be more difficult. The microstructure seems to densify and hardly any change in cell shape occurred, causing only a minimal auxetic effect in only a few samples. A reason for this was found in DSC and extraction tests which indicated that the microstructured polyethylene was crosslinked to a certain extent, what prevented the cell ribs to buckle inwards during the transformation process.

In order to better understand the influence of the cell geometry on deformation behaviour of the foams, polyether and polyester urethanes with various pore densities were studied [80]. These foams are made auxetic by the triaxial compression technique. Besides only just comparing these conventional foams against their auxetic counterparts, in all foams the cell ribs were chemically thinned

by a NaOH solution decreasing the foam's stiffness. Results from tensile and compression tests show that rib flexure and hinging dominates compression and tension for auxetic foams and also under compression for conventional foams. However for conventional foams under tension also rib stretching is observed, especially for the thinner ribs.

Further studies on these foams gave full sets of elastic properties, i.e. measured in all three orthogonal directions [69,81]. General conclusion is a strong dependence of the tensile and compressive properties on the amount of strain as this changes the shape of the foam cells. Poisson's ratios in the auxetic foams are not linear dependent on strain in one direction. At higher tensile and compression strains some of the cell ribs are at the end of their "free movement" and the ribs need to stretch in order to accommodate further deformation [70]. Depending on the cell geometry, the Poisson's ratio can even change sign at sufficient large deformation [82]. In addition also the shear deformation is studied by measuring the static and dynamic shear modulus and the loss tangent δ. The shear moduli as well as the loss tangent are found to be higher for the auxetic foams than for the conventional ones. Because the shape of the loss tangent curves is identical for the conventional and the auxetic foams, the higher value is solely a consequence of the auxetic structure and not caused by a chemical or molecular change [81].

Similar results were found later by Scarpa et al. [83] when investigating grey open cell polyurethane foam. Even though only low absolute values for the Poisson's ratio were obtained (–0.02 to –0.04) for the auxetic foam, auxetic behaviour was well noticeable. Besides determining the Young's modulus and the loss tangent for the conventional and the auxetic foam, the measurements were extended with acoustic impedance and absorption behaviour. Especially sound absorption at low frequencies is much better for the auxetic form of the polyurethane foam. This was later generalised for auxetic foams and quantified by Chekkal et al. to be for frequencies up to 1,500 Hz [84].

Recently, a novel manufacturing technique, derived from a "half mould" process, has been described by Bianchi et al. to produce auxetic foams with an arbitrary shape and in bulk quantities [85]. In this technique a flat pad of polyurethane foam was placed against a curved mould. This was vacuum bagged and a technical vacuum was applied inside the bag. This caused the bag material to push the foam along mould following its shape. Similar heating and cooling steps as described earlier caused the foam to collapse and stay permanently deformed. The behaviour of the foam was auxetic and the properties were distributed homogeneously

throughout the foam. Since the heating is done in an autoclave, the size and shape of the foam is basically only limited by the available facilities.

Applications for auxetic foams will be in the field that specifically exploits the features of auxeticity and distinguishes it from conventional foams. One important feature is the compression load characteristics of the auxetic foams, static as well as dynamic as a result of densification of the foam structure.
Improved indentation resistance combined with the general feature of synclastic curvature would make auxetic foams ideal for mattresses or other cushion material. In more extreme high strain rate large displacement (crushing) tests, auxetic foams clearly show a time-load history but this is not found for conventional foams [83]. A property like this, combined with a higher loss tangent would make the auxetic foam ideal for structural integrity elements under dynamic loading. An interesting analysis is made by Lim on a functionally graded beam [86]. In this analysis Poisson-curving is studied by a (gradual) change in Poisson's ratio from positive to negative in the thickness direction of the beam. Such a graded structure can be attained when varying the density of the re-entrant ribs from low to high across the material. This introduced anisotropy leads to significant beam thickening or thinning when bent. Having the negative Poisson's ratio at the inner curve of the beam a strong axial stiffening effect occurs.
Sound insulation is another area of applications for the auxetic foams. This is useful for instance in the automotive industry to dampen noise in the passenger section of the car. The light weight of foam is then also an advantage.

2.4 Microporous polymers

The auxetic foams described in the previous section exhibit Poisson's ratios to lowest values of around –0.7 to –0.8. Lower values are inhibited by the material's cellular structure. Also the auxetic foams are often more or less isotropic when the applied triaxial compression to fabricate them is uniform and this limits the theoretical lower limit to –1. In order to achieve lower values of the Poisson's ratio anisotropy must be present in the material. Derived from classical elasticity theory it can be shown that for an orthotropic material the Poisson's ratios in the three planes can theoretically have any real value, providing that at least one of them is negative [87]:

$$\left| \nu_{xy} \right| \leq \left(E_x / E_y \right)^{1/2} \qquad (2.9)$$

where ν_{xy} is the Poisson's ratio as defined in (2.4) and E_x and E_y are the Young's moduli in the x- and y-direction respectively.
One known highly anisotropic material is expanded polytetrafluoroethylene (PTFE). Investigating this expanded PTFE more closely in relation to the Poisson's ratios it can exhibit, was the beginning of a new class of auxetic materials: microporous polymers. The research done on these microporous polymers is outlined in the following sections, describing the microstructure and modelling, fabrication methods, auxetic polymer fibres and films. Finally, the specific for auxetic materials interesting properties indentation resistance and ultrasonic absorption are illustrated.

2.4.1 Basic microstructure and modelling

As already mentioned, a highly anisotropic material is expanded PTFE and it can exhibit large negative Poisson's ratios. The auxetic behaviour has its origin in the microstructure of the polymer material. Expanded PTFE shows a highly porous fibrillar network with nodes at the junctions. The amount of anisotropy is governed by the way the PTFE is expanded, the drawing conditions. These drawing conditions can be partly uniaxial, partly biaxial and complete biaxial. Highest anisotropy is expected in partial uniaxial expanded PTFE. Caddock and Evans did an extensive study on this material in 1989, looking at the microstructure under deformation and the mechanical properties with respect to the Poisson's ratio [88]. Poisson's ratio values as low as –12 were found when stretched in the drawing direction. Believed is that two mechanisms play a role in tensile deformation explaining the negative Poisson's ratio. First the fibrils are stretched and the nodes are pushed aside. Secondly, when more and more of the fibrils get fully stretched the nodes start to rotate, causing an extra lateral expansion. A schematic representation of this mechanism is shown in Figure 2.4. Further stretching gives plastic deformation what will break up the nodes and hence the microstructure. This behaviour is a good example of the theoretical model for tensile network microstructure allowing rotation of nodes on a micro-level [87]. It is indeed confirmed that these theoretical predictions from the model and experimental data correlated well for the expanded PTFE [89].

The model for the node-fibril structure used in [87] and [89] was extended by Alderson and Evans by deriving expressions for the Young's modulus and Poisson's ratios for various node and fibril configurations [90]. Since the Young's modulus represents the linear elastic behaviour at small deformations only, this model focuses on the deformation step from 1 to 2 as shown in Figure 2.4. The movement

of the fibrils with respect to the nodes is divided in three separate mechanisms, similar as above described for cellular foam structures: hinging, flexure and stretching. Comparison of model results with experimental data gives a reasonable understanding about what is happening when stretching a node-fibril structure. In fact, using this extended model also leaves out the necessity for rotation of the nodes to achieve the description of the Poisson's ratio versus strain. Although showing useful trends, there are some deviations between model and practice. This is mainly because the calculations use fibril hinging followed by stretching, while in real life these effects will occur simultaneously. The calculations on flexural movement of the fibrils gave similar results as the ones for hinging. Even though flexure of fibrils will occur, the flexure mechanism can be omitted from the model as it cannot be distinguished from the hinging mechanism.

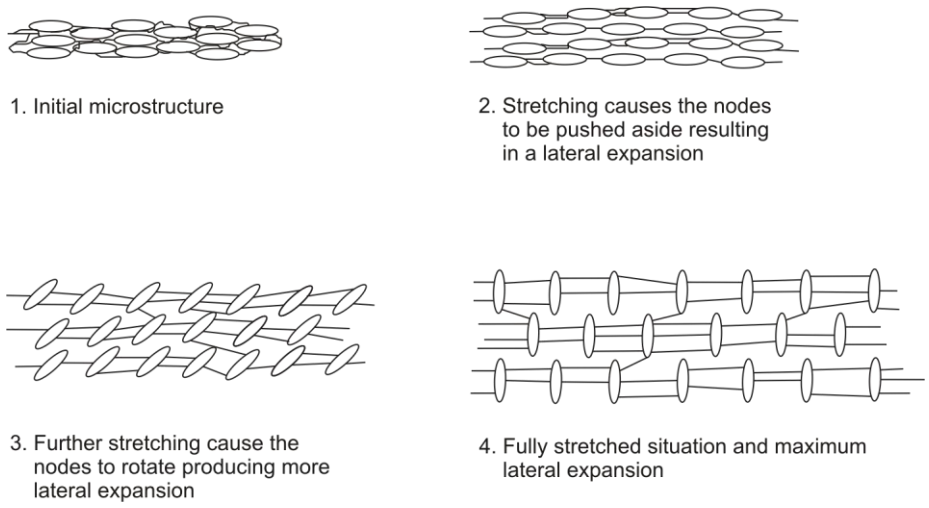

Figure 2.4: Schematic representation of the deformation mechanism of the expanded PTFE microstructure when subjected to tensile loading (after [88]).

The part of the model to visualise the tensile deformation by hinging alone is shown in Figure 2.5 and the auxetic behaviour can easily be visualised when this structure is stretched horizontally. The rectangles with aspect ratio a:b are representing the nodes in the microstructure. They are connected with lines of length l representing the fibrils on their corner points. The angle α will change with the amount of tensile deformation, starting with 90° in the non-deformed state and decreases to 0° in the fully stretched state. With further deformation the stretching mechanism comes into play and the fibrils will elongate first elastically and then plastically. The Poisson's ratio will therefore be strain dependent.

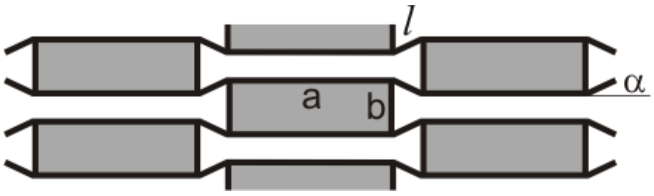

Figure 2.5: The node-fibril model with the parameters describing the microstructure of auxetic polymers [89,90].

An important conclusion of the study by Caddock and Evans [88,89] is that the microstructure makes the material auxetic, and it is not an intrinsic property of PTFE. This conclusion opened the search for other polymer materials that could also exhibit this node-fibril microstructure.

2.4.2 Fabrication methods and its effects on the microstructure

All fabrication methods for the auxetic microporous polymers use finely divided powder as a start. Based on several techniques from ceramic and metal powder processing, this powder is shaped into an auxetic product. In the following subsections these methods are described, as well as their influences on the microstructure and the reasons behind changing fabrication methods.

2.4.2.1 Three-stage method: compaction, sintering and extrusion

The first material found after expanded PTFE was ultra high molecular weight polyethylene (UHMWPE) [91]. The basic fabrication route for this auxetic polyethylene was devised and consists of three stages. The first stage is “compaction” of fine UHMWPE powder in order to make it sufficiently dense. Compaction involves the destruction of the original bulk powder arrangements and can go as far as elastic or even plastic deforming of neighbouring particles to increase contact area. The powder is compacted to 0.04 GPa at an elevated temperature of 110 °C for 20 minutes. The second stage involves “sintering” of the polyethylene particles at a temperature just below the melting point, in this case 160 °C. The third and final stage is “ram extrusion” of the UHMWPE by pushing it through a die in the form of a cylindrical rod. The extrudate expands radially when it leaves the die what was thought to be the fibril creating step in the process to produce the auxetic polyethylene [91,92]. Negative Poisson’s ratios of –1.24 in the radial direction were obtained at low applied strains. At higher strains the Poisson’s ratio increased to 0.00, possibly due to plastic deformation.

Improving this fabrication method to be able to produce larger sizes of auxetic polyethylene, a detailed investigation is published in 1995 through a trilogy of articles, each describing the different stages in this process: compaction [93],

sintering [94] and extrusion [95]. The effects of all variables in every production step are studied and the optimum processing conditions could be determined. All three stages are important to eventually produce the auxetic polyethylene. Pressure and temperature are key parameters in the compaction stage in order to get the required contact area between the particles. This is the foundation step for an end product with good structural integrity. In the sintering stage the temperature is the most important factor, because only surface melting of the particle should occur. The die geometry in the extrusion stage is critical in order to form the auxetic product with a high structural integrity.

In 1996 the next polymer that can exhibit auxetic behaviour is found. Polypropylene (PP) was made auxetic by using the compaction, sintering and extrusion method [96]. PP powder can be obtained in many particle sizes and shapes. From this study on the powder morphology however it is found to be crucial that the particles are large enough (~300 μm) and have a sufficiently rough surface (depth variation of at least 1 μm). Otherwise no auxetic PP is obtained because the nodes will be too small for fibrillation and insufficient contact area between the particles can be created during the compaction stage. The obtained Poisson's ratios are relatively small, with the lowest value –0.22 at 1.6% strain, much smaller than the values found for PTFE and UHMWPE. However, model calculations as used in [90] indicate larger negative values for ν should be possible in PP. This requires the nodes in the microstructure to be more circular, instead of the elliptical nodes (approximately a 4:1 aspect ratio) obtained with the PP in this study.

The microporous auxetic polymers PTFE, UHMWPE and PP show a nonlinear strain dependent behaviour of the Poisson's ratio. To what extent the model from Figure 2.5 is able to describe this is verified in a study from 1997 where theoretical and experimental results of Poisson's ratio versus strain are compared for three different forms of auxetic UHMWPE [97]. These three forms of auxetic polyethylene are fabricated using the three-stage compaction-sintering-extrusion method using three different barrel and extrusion die geometries. Using Scanning Electron Microscopy (SEM) the geometrical parameters (a, b, l, α) were determined to make the model calculations. Obviously the parameters are not a fixed value but are within a certain range. Experimental values for ν versus strain were obtained through compression measurements and fitted reasonable well within the theoretical predictions using the geometrical parameter ranges determined through SEM.

2.4.2.2 Two-stage method: sintering and extrusion

Research continued on the node-fibril microstructures of the various auxetic polymers [98]. In the meantime (1996-1998) also polyamide (nylon) was fabricated with the node-fibril microstructure. In order to study the fibrils, it was necessary to fabricate a highly fibrillar structure. UHMWPE and nylon were used as the polymers. The increased fibrillar structure (in all directions) is produced using the sintering and extrusion stages on the polymer powder only. The compaction stage is omitted because this stage mainly gives the polymer its structural integrity [93] and without compaction it also better simulates the structure in tension. It will result in an extrudate with a poor structural integrity, but none is really required here. Examining the microstructures using SEM, a clearer understanding is obtained on fibril deformation under tension. Firstly, from previous research in [88] and [90], it is believed that in the node-fibril microstructures the nodes consist of amorphous material, while the fibrils are crystalline. Secondly, at the location where fibril and node are connected, a transition zone of amorphous and crystalline material is believed to exist. Based on this, a mechanism is proposed for fibril deformation. At the end of the hinging deformation step, stretching also begins. Stretching makes the fibril longer and thinner, but at the same time material is drawn from the amorphous-crystalline transition zone on the outside of the node. Through an ordering effect induced by the applied stress this adds the material to the fibril until the transition zone is depleted. Further stretching will elastically elongate the fibril, followed by plastic deformation. The plastic deformation can be seen by a necking effect of the fibril. Even further stretching will eventually cause the fibril to break. All these deformation stages are present in the material indicating a high level of inhomogeneities. This is the case for all the studied polymers regardless of the way they are produced [98].

Continued research was conducted on the high fibrillar UHMWPE fabricated through the two-stage process of sintering and extrusion only, involving the determination of its auxeticity and mechanical properties [99,100]. UHMWPE produced via the three-stage process, so including compaction, is too tough to make samples for examining the axial direction properties of the extrudate. With the two-stage process the material has a much higher porosity, so is less dense and less tough. As mentioned before [98], the structural integrity of the produced UHMWPE was poor using sintering and extrusion only. However, from [95] it was known that the die geometry used for the extrusion stage also influences the structural integrity. First objective of this research [99] was then to find the die geometry best suitable for the two-stage process in order to make high fibrillar auxetic polyethylene with sufficient structural

integrity for mechanical testing. Key processing factor in this is to keep the die swell sufficiently low. The Poisson's ratio in the radial direction of the desired material quality was measured under compression and was strain dependent. It started at –4 at low strains and ended close to 0 with increasing strain. With cylindrical extrudate of sufficient structural integrity it was now possible to produce samples in radial and axial direction for mechanical properties testing [100]. Flexural properties, the flexure modulus, flex strength, and strain to failure are determined as a measure for the structural integrity. The flexural properties for the two-stage material are several factors lower than for the three-stage material, as was to be expected.

Recently, an extensive microstructural mapping of UHMWPE has been performed by Alderson et al. to gain a better understanding of the mechanism on fibril formation [101]. This was done by analysing pre-extrudate and post-extrudate samples by SEM at several stages during the extrusion. Previously it was believed that for this fabrication method all fibrillation occurred under the shear deformation in the die [98]. Interestingly however, now it was found that the pre-extrudate material can already have enough fibrils to exhibit auxetic behaviour even though they are short and relatively few in number. The microscopy showed surface molten particles bound together by thick necks of the molten material. Apparently, when the plunger moves towards the die, the interparticle movement inside the barrel is sufficient to draw fibrils from the molten surfaces. The microstructure observed in the post-extrudate did show the influence of the die as it was much higher fibrillated and more open than the pre-extrudate. The fibrils are found to be formed in all directions, but predominantly in the axial direction because of observed anisotropy in the UHMWPE.

2.4.2.3 Two-stage method: compaction and (multiple) sintering

Another variation made on the fabrication method for UHMWPE was published in two parts in 2005 [102] and 2008 [103]. This time the extrusion step is omitted and the fabrication method now consists of a compaction stage, followed by a multistep sintering stage. A big advantage would be the possibility of more complex geometries then only cylindrical rods or other by extrusion constrained shapes. The best results in terms of auxeticity are obtained with two sintering steps with a Poisson's ratio of –0.32 and auxetic behaviour up to 5% strain. Less than two steps produce insufficient fibrillation and more than two steps result in a product that is too compact to behave auxetic. In the fabrication methods using extrusion, the fibrils are drawn from the node's transition zone by shear forces during extrusion [98]. In this fabrication method, without the extrusion step, it is believed the drawing occurs

because of movement of the nodes respective of each other due to thermal contraction and expansion between two sintering steps. These movements are relatively small, so a compact structure is obtained with a large node-fibril angle. This inhibits large auxetic behaviour and the value of $\nu = -0.32$ is indeed not as low as for the UHMWPE fabricated through the other two- and three-stage fabrication methods [102]. The change in flexural properties (flexural strength, flex modulus and strain to failure) is found to be large after the first sintering step, but after this they remain almost constant [103]. The magnitude of the flexural properties however is still lower than for the three stage fabrication method.

2.4.3 Auxetic fibres

The main drawback of auxetic polymers fabricated by either the two-stage or the three-stage process is their heterogenic microstructure. Also their appearance as low aspect ratio cylindrical rods limits application possibilities. For these reasons a new production technique is introduced in 2000 by using a screw extruder and a melt-spinning technique to produce auxetic PP fibres and Poisson's ratios of -0.60 ± 0.05 were reached [104,105]. Fibres are a much more useful form of auxetic polymer and can be used in applications like textiles and composites.

Later on, also other auxetic fibres were produced from polyester and polyamide polymers using the same technique [106,107]. Optimum process parameters are determined for these three auxetic fibre products and their Poisson's ratios are measured. In addition to PP, the polyester and polyamide fibres showed Poisson's ratios of -0.72 ± 0.05 and -0.20 ± 0.05 respectively.

Recently a much more extensive study has been conducted on the process parameters for the PP, polyester and polyamide fibres in an effort to tailor the values for the Poisson's ratio [108]. Besides the narrow temperature range being the key parameter to obtain auxetic behaviour in the first place, also the take-off speed, screw speed and the hole diameters in the spinneret die plate are varied. These latter three parameters are found to influence the percentage of auxetic fibres formed, their homogeneity, fibre diameter and Young's modulus. Therefore better control over obtaining fibres with a desired diameter, stiffness and Poisson's ratio is possible. It should be noted that the obtained amount of auxetic fibres in PP is only 18–26%, depending on the processing parameters. The remainder of the fibres have a positive Poisson's ratio, measured up to even +4.7. The polyester and polyamide fibres the other hand can be produced to exhibit respectively full and almost full auxetic behaviour.

A particular benefit of auxetic fibres could be their resistance towards pull-out from a matrix in a composite material. The negative Poison's ratio will cause the fibres to radially expand and anchor themselves in the matrix when pulled. With the conventional, positive Poisson's ratio fibres, the opposite occurs because they radially contract. This property was investigated by Simkins et al. in 2005, where single auxetic and conventional PP fibres were subjected to a pull-out test from a modified cold-cure epoxy resin [109]. The epoxy resin needed to be modified to ensure the temperature during cure stays well below the processing temperature of 159 °C for the auxetic PP fibres. It was found that the total energy required to pull out an auxetic PP fibre is more than 3 times higher than for a conventional PP fibre. A mechanism is proposed as well in order to illustrate what is happening during the fibre pull-out test. The auxetic behaviour basically retards the initiation and propagation steps of the debonding of the fibre-matrix interface. The outer surface of the fibres constantly pushes itself against the matrix, while for a conventional fibre it tends to pull away. So, the beneficial effect of auxetic behaviour on fibre pull-out is confirmed.

Besides making auxetic fibres from one intrinsically auxetic behaving material, auxeticity can also be reached by the construction of the fibre. By wrapping a much stiffer filament around a low stiffness core, the resulting fibre will show auxetic behaviour when deformed [110]. This principle is more clearly shown by Miller et al. where auxetic yarns are made from stiff UHMWPE filament (E = 6 GPa) wrapped around a much softer polyurethane core (E = 53 MPa) [111]. Negative Poisson's ratios around –2.1 are observed using this construction. The advantage of fabricating auxetic fibres or yarns through this technique is that no special equipment is required.

The auxetic fibres or yarns can be used as is, or be woven into fabrics and used as the reinforcement material of composites.

2.4.4 Auxetic films

Next produced auxetic product was in the form of PP film [106,112]. In order to produce the film the spinneret die plate in the extruder used for melt-spinning the fibres, was obviously replaced by a plate having a thin slit orifice (0.38 mm). The auxetic PP film was found to be somewhat anisotropic, having a Poisson's ratio in the extrusion direction of –1.12 ± 0.06 and –0.77 ± 0.01 in the transverse direction. The films are auxetic only at low strains. At around 1% tensile strain there is a transition in the Poisson's ratio from negative to positive, eventually going up to the

value of +0.4 for conventional PP film [112]. Tensile tests on PP film with a tear showed widening of the tear for conventional, but the tear width decreased in the auxetic film [106]. This is a clear demonstration of the auxetic effect.
More recently [113], a similar approach to the fabrication is conducted on the PP film as for the fibres. Again the processing temperature was found to be the key in obtaining auxetic properties and here even 100% auxeticity is found at 159 °C. Surprisingly, also partly auxetic behaviour is found at higher processing temperatures of 161–165 and even at 190 °C. When increasing the take-off speed three times, 100% auxeticity is also found at 180 °C. This means that surface melting of the particles may not be the only mechanism to provide auxetic behaviour. Since 180 and 190 °C are well beyond the melting peak of the used PP another mechanism must come into play, but it is yet unknown which. Pulling the film somewhat more from the extruder die by increasing take-off speed makes the film more auxetic. So, some drawing to align the microstructure seems beneficial as it will not destroy the auxetic character of the film, but makes it better.

2.4.5 Indentation resistance and ultrasonic absorption

The indentation resistance of ultrahigh molecular weight polyethylene is further investigated by using three different fabrication techniques to produce auxetic, sintered and compression moulded UHMWPE [114]. The auxetic polyethylene is very heterogeneous and has a strain dependent Poisson's ratio. Consequently a large range of indentation resistances is obtained. Nevertheless as a general observation, the auxetic polyethylene is found to be several factors (up to 8x) more difficult to indent at low loads than the other two. At higher loads the auxeticity diminishes and the result for all three is similar. Instantaneous or elastic recovery from indentation is also determined. Here is also observed that the auxetic polyethylene is the most elastic at low loads. Increasing load causes loss of auxeticity and more plastic deformation. Observation of the samples after one month revealed however that the viscoelastic recovery was highest for the auxetic polyethylene with no indent visible anymore up to higher loads than was the case for the sintered and compression moulded polyethylene. It is suggested that the fibrils coil around the node upon indentation deformation pulling the nodes together. The fibrils can uncoil when the load is released and returns the microstructure close to its original configuration.

Also, for auxetic materials specifically interesting, the indentation resistance and the ultrasonic attenuation coefficient are determined [100]. The indentation resistance

however was improved, but only at low loads. This indicates that not only the amount of auxetic behaviour is important to increase the indentation resistance, but structural integrity is also required. The ultrasonic absorption is better, but it is unclear whether this is due to increased porosity or increased auxeticity.

2.5 Liquid crystalline polymers

Another approach to design auxetic polymer materials is done using liquid crystalline polymers. When upon stretching the material parts of the polymer main chain are to rotate in a direction normal to the main chain, these parts may push neighbouring polymer chains away and cause the material to widen in the direction perpendicular to the stretching direction. Liquid crystalline polymers are very suitable for this approach. These polymers consist of molecular blocks or rods (mesogens), generally connected with alkyl chains. Normally these mesogens are built in the polymer chain through end-to-end connections. However, a part of these mesogens can also be attached to the polymer chain through lateral connections. In the nematic phase of the undeformed material all mesogens lie disordered, but along and parallel to polymer main chain. After applying a tensile load, the polymer chain stretches to a point where the attached lateral rods will reorientate to a position normal to the direction of tensile load (see Figure 2.6). On this approach was the work of Griffin and co-workers based and published in 1998 [115]. They experimentally verified this idea by synthesising such a liquid crystalline polymer and by X-ray scattering they could confirm an increase in interchain distance.

The structure of the lateral attached mesogen is of course of main influence on the increase of interchain distance. Especially the length and the rotation angle will contribute to this. Where first a para-terphenyl block was used [115], later studies synthesised liquid crystalline polymers with other laterally attached mesogen structures based on para-quaterphenyl blocks [116], para-pentaphenyl blocks [117] and bis-para-alkoxybenzoyloxy hydroquinone blocks [118] (see Figure 2.6). They all showed the interchain distance increase, possibly resulting in auxeticity. However, when actually measuring stress-strain data on the liquid crystalline polymer material with the para-pentaphenyl mesogens, unexpected Poisson's ratios of ν_{xy} = +0.43, ν_{xz} = +0.54 were found [117]. Reasons for this behaviour could be that room temperature, at which the test was conducted, is too low to allow the mesogens to rotate. Also the material could have tensile slip of the polymer chains past each other, effectively nullify any effect of the rotating mesogens.

Recent dynamic simulations have shown that rather long mesogen lengths are required to actually reach auxetic behaviour [119]. Under optimal conditions the tensile response was studied of a liquid crystalline polymer, using a hypothetical mesogen and a 1:1 ratio between end-to-end and lateral attached mesogens. This

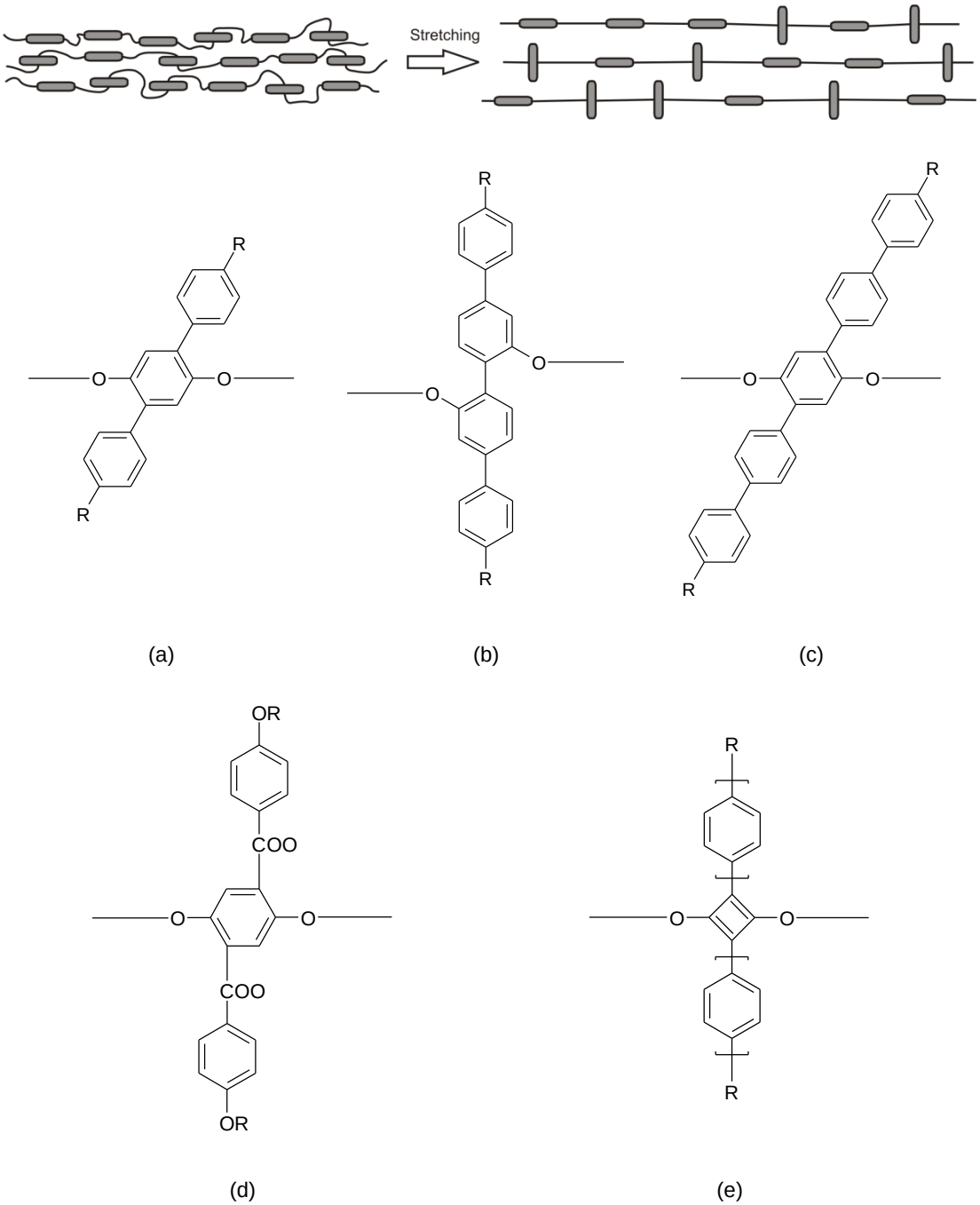

Figure 2.6: A schematic view of the increase of interchain distance by stretching a liquid crystalline polymer with laterally attached mesogens. Examples of these mesogens are shown as well: (a) para-terphenyl [115], (b) para-quaterphenyl [116], (c) para-pentaphenyl [117], (d) bis-para-alkoxybenzoyloxy hydroquinone [118] and (e) hypothetical cyclobutadiene structure [119].

mesogen (Figure 2.6 (e)) allows an approximate 90° rotation to maximise the lateral push on the neighbouring chains. This mesogen may however be difficult to synthesise or be chemically unstable. Also it will be likely that more than half of the mesogens need to be in the end-to-end configuration to ensure the right alignment. The simulations showed that the mesogen length was indeed the main determining factor in possible auxeticity. Only at a length of 7 cyclic units a clear negative value of –0.60 for the Poisson's ratio was found. Shorter mesogen lengths were lowering the Poisson's ratio, but not down to negative values. Combining this outcome with the unexpected experimental data from [117], which uses only 5 cyclic units in the mesogens, there is quite a challenge left in designing a liquid crystalline polymer that will exhibit auxetic behaviour in real applications. A more recent study focuses on crosslinked liquid crystalline elastomers in the smectic phase. Lower values for the Poisson's ratio, down to approximately 0 are found experimentally. However not negative, the lower values are maintained over the entire (elastomeric) strain range [120].

2.6 Composites

Composites is a broad term for materials consisting of two (or more) components where the combination of these components result in more superior properties than each of the individual components have. In composites hard or stiff materials are often embedded in a softer material, called the matrix. The hard or stiff materials provide strength to the composite while the matrix adds some sort of flexibility. Actually, many materials around us are composites because nature uses the concept of composite structures a lot, like in wood or bone. Beside natural, there are nowadays also many artificial composites around us: in construction, aircrafts, cars, etc. Generally, most composite materials show anisotropy. This is because the reinforcing component of the composite is often fibrous (a high aspect ratio). It is therefore important to load a composite material in the right way, i.e. in the direction of the fibres. Design of a composite product must take this into account [121].
Here the focus will be on engineered composites, viz. laminates, sandwich structures and matrix with inclusions. Especially the possibilities regarding auxetic composites are reviewed.

2.6.1 Laminates

It is well known that the directional properties of fibre reinforced composites can be influenced by the orientation of the fibres. Especially using stacks of thin layers of

fibre reinforced material (plies) the composite can be designed to desired properties, simply by laying-up the plies under certain angles (θ). Such a composite is called a laminate.

Also the Poisson's ratio can be influenced in the three orthogonal directions by the fibre angles in each layer of the laminate. This said, it should therefore also be possible to incorporate auxeticity in the composite. In the next two sections the Poisson's ratios are discussed for a laminate in the in-plane and the through-the-thickness direction respectively with a specific focus on the negative values.

2.6.1.1 In-plane Poisson's ratio

With angle-ply laminates the in-plane Poisson's ratio can be influenced dramatically. In 2007, Peel predicts from simulations it is possible to make laminates with extreme values for the Poisson's ratios ranging from –60 up to +100 [122]. The key here is a high stiffness ratio between the fibre and the matrix. Using carbon or glass fibre in an elastomer matrix can give stiffness ratios of 10^4, whereas these fibres in for instance epoxy only give a stiffness ratio of around 10. The upper values of the Poisson's ratio can be reached by balanced laminates, but the lower values require unbalanced laminates because of the high shear deformation. To some extent (in a range of $-0.4 \leq \nu \leq +1.5$) this was already shown by Miki and Murotsu in 1989 when they investigated "peculiar" behaviour of carbon-epoxy laminates [123]. Also here was observed that the higher values of the Poisson's ratio were found with balanced laminates and, however the balanced laminates came close, the lower values were found with the unbalanced laminates.

The fact that stiffness ratio is involved in the laminate's Poisson's ratio was also seen before by Zhang et al. in 1999 [124]. They investigated 2-angle ply fibre-epoxy laminates and found lower (more negative) values in laminates with increasing difference in modulus between the fibre and the matrix. Interestingly they also found that the lowest Poisson's ratios (or maximum transverse strain) were around ply orientations of $[70°/20°]_s$. Random-oriented composite laminates were also investigated by the same researchers [125]. Using a statistical analysis they found that with at least 40 plies an isotropic character of the laminate is reached. With variation of the in-plane lamina parameters E_2/E_1, G_{12}/E_1 and ν_{12}, their influence on the in-plane Poisson's ratio of the laminate is investigated. The extreme values found were $\nu_{max} = +0.7000$ and $\nu_{min} = -0.4183$.

Computer aided modelling, as for instance done by Evans et al. [126] shows that the properties of fibre reinforced laminates can be predicted accurately. Agreement with

experimental results is excellent and the model is even sensitive enough to predict the outcome of small variations in input parameters on the mechanical properties.

2.6.1.2 Through-the-thickness Poisson's ratio

Herakovich was in 1984 the first to study the through-the-thickness Poisson's ratio (ν_{xz}) of laminates with a focus on the negative values [46]. Modelling a graphite-epoxy cross-ply laminate, negative ν_{xz} were found between ply angles of 15° and 40° with a minimum value of –0.21 at 25°. Not only the $[\pm\theta]_s$ laminates were found to exhibit the negative ν_{xz}, but also combinations with 0° and/or 90° plies can have the same result. The negative ν_{xz} in the laminates is caused by a high normal-shear coupling and the constraining influence of the adjacent layers.
Similar results were found a decade later in symmetrical balanced angle-ply laminates [127,128], but here negative Poisson's ratios were only found between 15° and 30° ply angles. A consequence of a negative trough-the-thickness Poisson's ratio in these laminates is a (large, >1) positive Poisson's ratio in the in-plane direction. Extreme values of the Poisson's ratio tend to get higher when using stiffer fibres or by increasing the fibre volume fraction, i.e. increasing the anisotropy. That anisotropy is a key factor for obtaining negative through-the-thickness Poisson's is confirmed in a recent modelling study by Harkati et al. where various orientations of glass, carbon and Kevlar fibres in epoxy resin was investigated [129].

Yeh and Yeh did extensive research on the through-the-thickness Poisson's ratio and dilatation in random-oriented [130,131] and angle ply [132,133] composite laminates. With the aid of a dimensionless mathematical model general guidelines are provided about the behaviour of the through-the-thickness Poisson's ratio and the dilatation of the laminate in relation to the dimensionless lamina material parameters E_2/E_1, E_3/E_1, G_{12}/E_1, ν_{12}, ν_{31} and ν_{32}. They limited their research on positive Poisson's ratios of the laminae, resulting in positive Poisson's ratios for the laminate only. It does however show that the through-the-thickness Poisson's ratio of the laminate can be strongly influenced by the laminae properties and will likely do so as well for auxetic laminae.

Recently another approach to achieve a negative through-the-thickness or out-of-plane Poisson's ratio has been described by researchers from the University of Toledo, USA [134,135]. This involves the use of fibre networks which are then compressed. At first finite element modelling is done to get insight in the parameters influencing the out-of-plane Poisson's ratio [134]. They found that the amount of compression and the network anisotropy were the most critical factors. That

increasing compression lowers the Poisson’s ratio is explained by the idea that straight fibres will bend over each other at their contact points. Then the network of the now kinked fibres becomes analogous to a re-entrant honeycomb network as seen before in foams. Stretching this network will cause the fibres to straighten, pushing neighbouring fibres aside and the network will expand in the thickness direction. Since compression gives the fibres a displacement in the thickness direction, the amount of compression is important in how much the out-of-plane Poisson's ratio is influenced. Low compressions only have effect on the surface, but higher compressions also more into the bulk of the network.

To see this behaviour in practice sintered stainless steel fibre mats are tested of various porosities and levels of anisotropy [135]. After compression the networks indeed showed a negative through-the-thickness Poisson's ratio, with a lowest value of −18.6. To see whether this behaviour remains in a composite, the steel fibre mats are infused with polydimethylsiloxane (PDMS) and cured. It was found they still showed auxetic behaviour through-the-thickness albeit not as much as for the "empty" mats. Because of the high stiffness difference, the deformation behaviour is still mainly governed by the steel reinforcement and the PDMS can only constrain this to a minor extent.

Additionally, polymer nanocomposites were produced by mixing (functionalised) carbon nanofibres into PDMS. The mixture was then sheeted between a two-roll mill and cured. Through-the-thickness auxetic behaviour was observed on the resulting composites as well. The carbon nanofibres in the PDMS form a network, providing they are well distributed in the matrix. The compression between the rollers of the mill then seemed to be sufficient to let the carbon nanofibre network become auxetic similarly to the steel fibre mats. Here the stiffness difference between the carbon fibre and the PDMS is also sufficiently high to keep the resulting composite auxetic.

A few years earlier it was derived that auxetic behaviour in carbon nanotubes is principally possible [181]. Modelling single wall nanotubes with the zigzag and armchair wall configurations has shown that the Poisson’s ratio and therefore also auxetic behaviour is dependent on the chirality of the nanotube. Using these nanotubes could also produce an auxetic composite when mixed into a matrix material.

2.6.2 Sandwich structures

In structural applications sandwich panels are extensively used. Sandwich structures normally consist of a core material sandwiched between faces of a strong and stiff material. These outside layers, which can be thin fibre composite laminates,

provide the structure with in-plane stiffness and carry the loads in-plane as well as in bending. The core is a light and open structure and can be in the form of a foam, honeycomb, web, or truss core (see Figure 2.7) and also combinations are possible. The main purposes of the core are to resist the transverse shear loads and to keep the structure light [136].

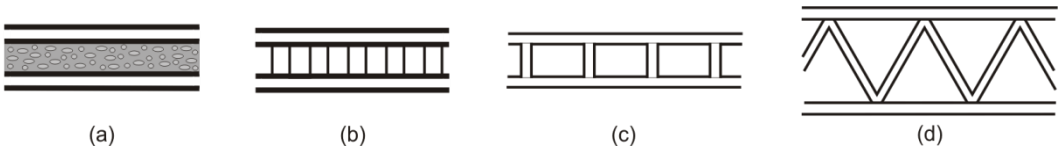

Figure 2.7: Examples of sandwich structures with a foam (a), honeycomb (b), web (c) or truss (d) core.

A disadvantage of common sandwich composite structures can be their reaction towards bending especially when they have a single curvature. Such a plate or beam will deform by in-plane bending when subjected to an out-of-plane moment. This will cause the sandwich plate or beam curvature to become anticlastic (concave or saddle-shaped). Synclastic (convex or dome-shaped) doubly-curved surfaces will then be difficult to produce without local collapse and buckling within the core of the sandwich structure. This is all a direct result of the positive Poisson's ratio of the common sandwich composite materials. After Evans [56] proved the idea suggested by Lakes [44] to use an auxetic core this disadvantage could be solved and synclastic doubly-curved shapes can be produced naturally (see Figure 2.8).

The easiest way to produce the auxetic core is with the re-entrant cellular foams mentioned before (section 2.3). Using such an auxetic core may have the benefit of producing synclastic doubly-curved surfaces, but it will come at the expense of something else. Whitty et al. have predicted there is a difference between these re-entrant and conventional honeycomb foam core structures in crack propagation under thermal or mechanical stress build-up [137]. The results of their simulations show that thermal stress build-up will be minimised in the auxetic structure, but hydrostatic stress build-up will be higher than for conventional honeycombs. So the auxetic re-entrant foam sandwich panels will be less resistant towards in-plane hydrostatic stresses than their conventional counterparts.

Besides the ability to shape them into synclastic doubly-curved plates or beams, the auxetic core sandwich structures can also have enhanced out-of-plane mechanical properties. With the right cell geometry in the core, properties like increased bending stiffness and lower natural frequencies can be obtained [138]. The latter property

can be used to obtain wave attenuation or vibration reduction in sandwich structures [139].

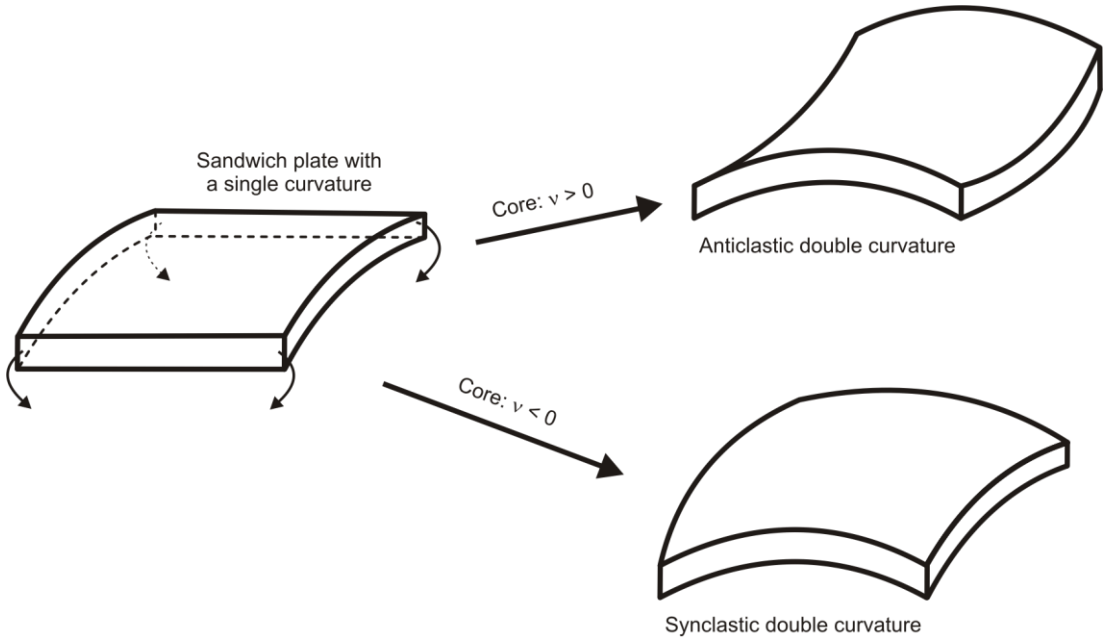

Figure 2.8: Schematic representation of bending a single curved sandwich plate to produce a double curvature. A conventional, positive Poisson's ratio, core will produce an anticlastic shape, where an (in-plane) auxetic core will produce a synclastic shape.

2.6.3 Matrix with inclusions

Another way to produce auxetic composite materials is by using a matrix material with inclusions of auxetic domains, a two-phase disordered composite. This is extensively studied by Wei and Edwards [140-143]. They had the expectancy there are intervals of the inclusion volume fraction and the Young's modulus ratio of inclusion to matrix, inside which auxeticity will be exhibited by the composite.

The first analysis, using the main-field theory of effective elastic moduli and corrected by two and three body interaction approximations where appropriate, is done on spherical auxetic ($\nu = -1$) inclusions in a positive Poisson's ratio matrix [140]. The minimum volume fraction of spherical inclusions to give the onset to auxeticity depends on the Poisson's ratio of the matrix: less volume fraction is required for lower ν_{matrix} in the range [0, ½]. Secondly, it also depends on the Young's modulus ratio $E_{inclusion}$ / E_{matrix}: a higher volume fraction is required for a higher ratio. For example in a rubber matrix ($\nu_{matrix} = ½$) the volume fraction of inclusions needs to be around 42% for the onset of auxeticity when the Young's modulus ratio is low (<0.1). Increasing the Young's modulus ratio to 20, an inclusions volume fraction of 82% is required to start auxeticity.

Besides spheres there can also be other shapes with a higher aspect ratio. The analysis has been extended to these other shapes (2-dimensional discs and blades; 3-dimensional disks and needles) [141-143]. A complete set of equations is derived to link the composite's effective Poisson's ratio with the other parameters, e.g. Young's modulus ratio, the volume fraction of inclusions and the Poisson's ratio of the matrix valid for all the above mentioned shapes [143]. From derived auxeticity windows it is shown that it is always possible to achieve an auxetic composite from auxetic inclusions in a non-auxetic matrix, regardless of the inclusion shape. It is also found that (for a certain volume fraction of inclusions at a given Young's modulus ratio) for all shapes there is a maximum effective Young's modulus of the composite [141,142].

2.7 Auxetic (micro)structures

Because of the deformation mechanism, auxetic structures are independent of size and the Poisson's ratio of such a structure is always the same whether it is on a macro-, micro- or nanoscale. Study of the deformation mechanism can therefore be done analytically and experimentally verified on a convenient large scale. Because of this property it is interesting to look at a variety of shapes that can give auxetic behaviour.

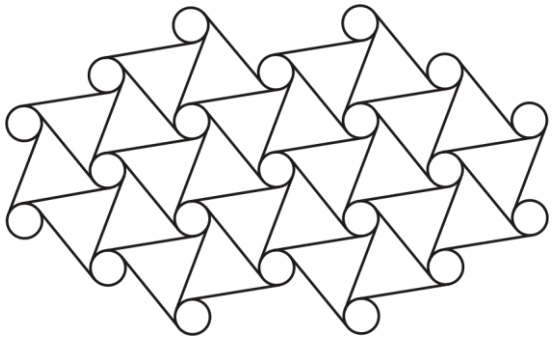

Figure 2.9: The chiral honeycomb structure.

Early auxetic structures were based on the re-entrant honeycomb shape. New structural ideas came based on the honeycomb structure. Examples are the chiral honeycombs [144,145] (see Figure 2.9) and the "connected swastikas" [146].

Advantage of the chiral honeycombs is their in-plane hexagonal structure, which gives in-plane isotropic behaviour and a Poisson's ratio of –1 [144]. It is also shown that the buckling behaviour under planar compression is much better for this chiral structure when compared to conventional and re-entrant honeycombs [145].

In the past decade and especially in recent years, interest grew towards regular geometrical shapes able to rotate into a two-dimensional tessellating auxetic

structure. Squares were the first shapes studied [147] and this structure has a Poisson's ratio of –1 as becomes clear from Figure 2.10. The squares are connected by hinges on their vertices providing the ability to rotate. Perfect tessellation can only occur when there is no shear, so the sides must be infinitely rigid. In following studies the geometrical shapes that give auxetic structures are extended with triangles [148-150], rectangles [148,151], rhombi and parallelograms [152]; see Figure 2.10 for examples and conformations of these auxetic structures.

As already mentioned, the Poisson's ratio for the rotating rigid squares is –1, what essentially means that the structure will maintain its aspect ratio upon deformation. The same is the case for the rotating rigid (equilateral) triangles [148-150]. The rigid rectangles structures can be built in two different ways. In the Type I structure, the open spaces between the rectangles form rhombi with dimensions of the side lengths of the rectangles. In the case of Type II structures the open spaces form equal sized parallelograms [151]. Each type exhibits very different properties. Type I structures are anisotropic and show strain dependent properties depending on the size and shape of the rectangles.

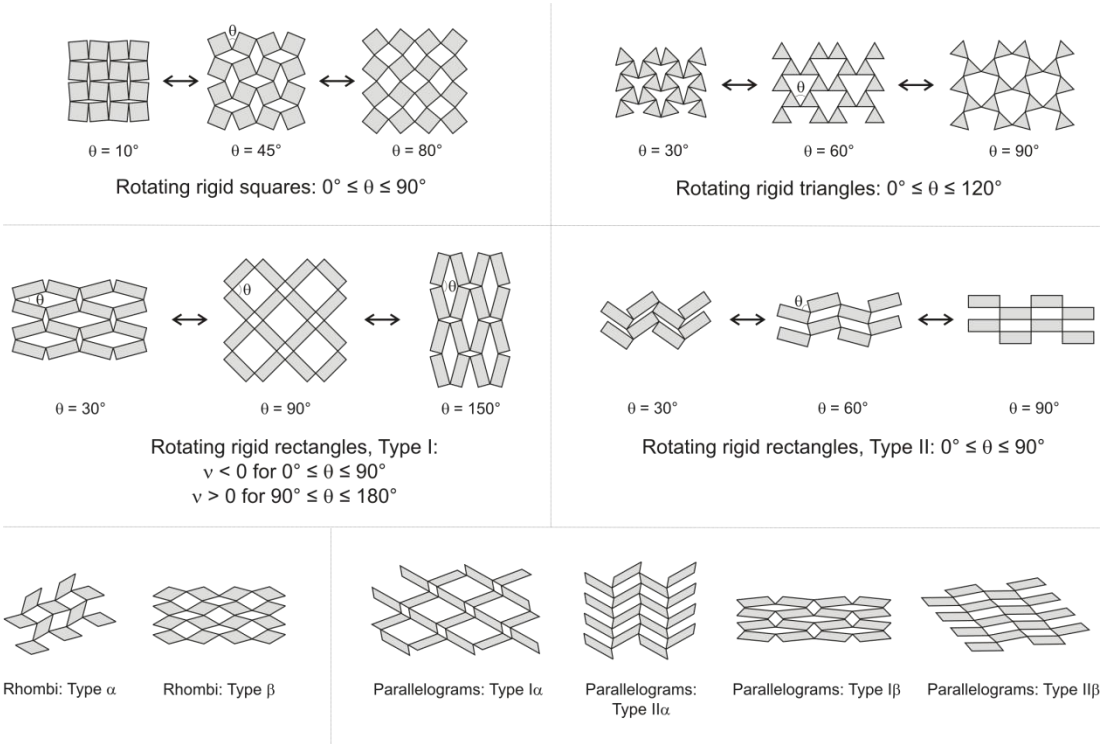

Figure 2.10: Auxetic structures from various rotating rigid shapes.

As shown in Figure 2.10, the Poisson's ratio of these structures can be positive and negative, depending on the starting configuration [148]. Type II structures on the

other hand are isotropic and the Poisson's ratio will always be negative with a value of –1 [151]. Basically, squares are special cases of rectangles, which are in turn special cases of rhombi or parallelograms. The structures for squares and rectangles can therefore be generalised. A first start has recently been made by Grima et al. in 2008 [152] to model the behaviour of Type IIα rotating rhombi and parallelograms.

With use of these rotating rigid structures as a model for "real materials", it is found that their deformation behaviour can often be treated as if they are constructed from these structures. This can be useful to have an alternative way to explain or predict auxetic behaviour in certain materials. Examples are the auxetic planes in α-cristobalite where the Type II rotating rectangle structure can be identified [151], or certain KH_2PO_4 crystals with a rotating structure similar to squares [153]. Also the process to turn conventional foams into auxetic ones can be considered as either a rotating squares [148] or triangles [154] structure.

Continued modelling of rotating structures included the incorporation of simultaneous stretching in the case of rotating squares [155]. The structure remains auxetic, but the magnitude will depend on the relative magnitude of the stretching and hinging constants, the dimensions of the square and the angle between the squares. Other modelling involved different sizes of squares or rectangles within the same structure [156]. For these structures Poisson's ratios can be isotropic and strain-independent, but also Poisson's ratio's that are dependent on the shape and relative size of the rectangles, the angle between the rectangles and the direction of loading. With this model properties of very different "real" systems can be described, from silicates and zeolites to liquid-crystalline polymers.

2.8 Concluding remarks

In the research area of auxetic materials a lot has been done on the modelling side. Plenty of ideas are mentioned in the literature and this gives a rather clear view on the possibilities of these materials. The manufacturing of auxetic materials however seems to be limited to a relative small number of applications even though the possibilities could be great. The research area of auxetic materials is of course still very young (about 2.5 decades), so the application range is likely to grow in due time. Considering this, there is a vast open field to study relevant material properties for peristaltic tubing, such as mechanical and dynamic properties as well as fatigue and crack growth characteristics.

The next chapter narrows down on the possibilities for auxetic materials in relation to peristaltic pump tubing. Starting off with STA-PURE™, it further describes the considerations and choices made to come to the selection of the material, how it can be manufactured and what its properties and behaviour should be.

3 Methods and approach

3.1 STA-PURE™

Most of what is known about STA-PURE™ tubing comes from the patents [38,39] and to some extent from meetings between Watson-Marlow and W.L. Gore. The material is silicone elastomer reinforced with continuous phase of microporous expanded PTFE (ePTFE). The starting material is an ePTFE membrane which is impregnated and coated with liquid silicone elastomer by a gravure coating process. This is wound on a mandrel like a Swiss roll and compression moulded to the final tube.

A 55x magnified part of the cross-section of a 3.2 x 1.6 mm STA-PURE™ tube is shown in Figure 3.1. The distortion of the mould split can be clearly seen on the outside and silicone flow during the curing step has caused a local distortion in the structure. The wall thickness of 1.6 mm is built-up of circa 32 layers (or wrappings) of coated and impregnated ePTFE. This gives an average combined thickness of the ePTFE plus coating layer of 50 μm. According to the patents, the tubes have an elastomer content of around 90%. The membranes used have a density 0.4 or 0.44 g/cm^3. With the density of PTFE being 2.2 g/cm^3, this means a porosity of the membranes of 80-82%.

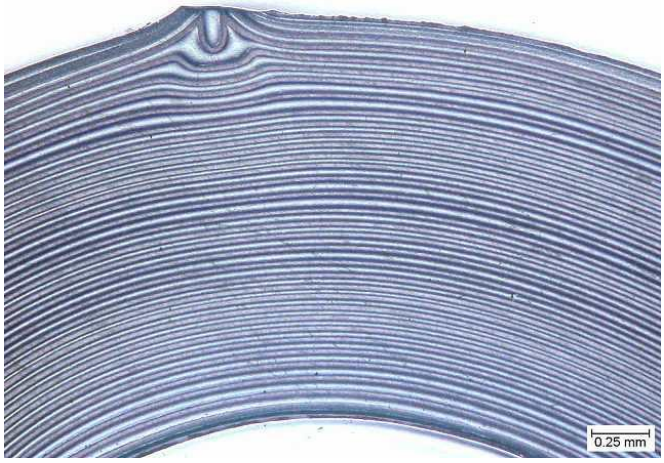

Figure 3.1: Optical microscopy image of a part of the cross-section of a 3.2 x 1.6 mm STA-PURE™ tube.

The reinforcing microstructure in ePTFE of nodes interconnected by fibrils can transfer and distribute the stresses on a molecular level. The very good flexure endurance of this composite material is attributed to this microstructure.

3.2 Establishing a baseline

In order to know what basic properties a new tube needs to have, a number of current tube materials have been tested. Naturally, STA-PURE™ is investigated

more elaborately by testing different tube sizes. Other tube materials that will be characterised are Bioprene®[1] in 73 and 80 Shore A hardness and two more recent developments of W.L. Gore: a fluoro-elastomer (FKM) reinforced with ePTFE and a high-pressure variety of STA-PURE™. The ePTFE/FKM tube is fabricated by a tape wrapping process as described in Example 10 of the patent [39].

The characterisation of these peristaltic tube materials will be done by determining their mechanical properties in the circumferential and, where possible, the axial direction of the tube. The compression or occlusion behaviour is also determined by compressing a tube section between two flat plates. From one size STA-PURE™ and Bioprene® tube a strain map of the cross-section is determined. This is done by applying a speckle pattern on the tube's cross-section and then follow the occlusion with two high-speed cameras. Movement of the dots in the speckle pattern can be recognised by the camera equipment's software and a strain map can be computed. By using two cameras a stereo image can be constructed, so also the out-of-plane movements can be monitored.
The mechanical properties and especially the Young's modulus can also be determined by free vibration experiments as they are related to the natural frequencies of the material. These vibration tests are attempted to cross-check the results from the tensile testing machine.

With the results from the tests mentioned above a baseline can be established. They give a guideline for some approximate basic (mechanical) properties as a starting point for the new tube material.

3.3 Possible routes to new laminate constructions for tubing

There are in principle two ways to construct a composite laminate, namely using fibres or microstructured membranes as the reinforcement. Using fibres (single ones or woven into a fabric) is a standard technique for laminates, but the use of membranes is not. Auxetic behaviour to balance deformation in a certain direction can then be achieved through the orientation of the reinforcement or by giving the reinforcement material intrinsic auxetic properties. Both can of course also be combined. This results in the following possible routes to make an auxetically balanced laminate as an alternative to STA-PURE™:

1. Fibres in an elastomer matrix

[1] Bioprene® is a registered trademark of Watson-Marlow Ltd. The material is a thermoplastic vulcanisate (TPV) of polypropylene and EPDM rubber.

- Conventional fibres
- Fibres where either the fibre material is auxetic [105,107,108] or the fibre's construction is auxetic [111]

2. Membranes in an elastomer matrix
   - Anisotropic membranes, i.e. uni-directional stretched to form a node-fibril structure oriented in just one direction
   - Custom membrane designs using re-entrant honeycombs or other auxetic cell shapes as the "pores" of the membrane [157-160].
3. A combination: nanofibre networks in an elastomer matrix after [134] and [135]

A fourth possibility is not a laminate, but is a composite material using auxetic inclusions in an elastomer matrix as described by Wei and Edwards [140-143]. The inclusions could be made from finely chopped auxetic fibres or finely grated auxetic foams.

For reasons of direct comparability with STA-PURE™, (liquid) silicone rubber will be chosen as the matrix material and preferably in the same viscosity and hardness range. An obvious alternative to silicone rubber is polyurethane rubber as this is also available in large range of viscosities. Other (liquid) elastomers may be suitable as well depending on the application and the type of reinforcement that will be used.
The reinforcement can be basically any thermoplastic polymer, but it should be kept in mind that the laminate construction can be deformed easily. Too stiff and rigid reinforcement materials are therefore less suitable.

In order to choose from the above described possible routes to make a laminate for peristaltic pump tubing, it is necessary to look at some constraining factors. The two obvious ones are dimensions and the availability of the reinforcement material.

The smallest peristaltic pump tubing of Watson-Marlow has a wall thickness of only 1.6 mm. This means the thickness dimension of the reinforcement must be quite thin (say < 0.1 mm) in order to get a decent number of laminate layers in a tube wall of this size.
This size constraint will make the use of fibres difficult as most of them have a thickness of at least several tenths of a millimetre [108,111] and the use of fibres may only be viable for tubes or hoses with larger wall thicknesses. Also, the development of the auxetic fibres made by melt-spinning extrusion is still in a laboratory stage as became clear after a meeting with someone from Auxetic Technologies Ltd., assignee of the patent [161] on this technique (04/09/2009).

The option of auxetic inclusions in an elastomer matrix suffers from similar issues. The inclusions need to be small enough what may be acceptable from chopping the thinnest auxetic fibres of 0.170 mm [108], but as mentioned before, they are not available yet on an industrial scale. Another requirement of the inclusions is a relative high auxeticity to make the whole composite behaving auxetic at a reasonable volume fraction of inclusions [142]. To use grated foams as the inclusion material it would require microcellular foams to start with and turn them auxetic by the triaxial compression technique. However, this technique becomes less successful with smaller cell sizes of the conventional starting foam and the level of auxeticity that can be obtained is limited [79]. So, high auxetic inclusions that are sufficiently small cannot be made from microcellular foams for the thinnest tube wall. For thicker walls larger cell foams may however still be a possibility.

Membranes will fulfil the constraining factor of size. Their thickness is generally well below 0.1 mm. Anisotropic membranes like Celgard® are used as battery separators and have a typical thickness of 25 μm [162]. Designing and making custom structures can be done by femtosecond laser ablation [158], but for larger areas lithographic techniques [157,163-166] are more suitable. Self-designed auxetic membrane structures also open up the possible use for a wide variety of materials including thermoplastic elastomers. Especially lower hardness range of co-polyetheresters (TPE-E) may have the right properties to act as the reinforcement material. TPE-E has a relative high stiffness and exhibits good creep properties to give a peristaltic tube resistance to internal pressure. It is also flexible and has good fatigue properties that make it suitable for the dynamic load on the tube.

Some membranes used for air filtration may be able to function as nanofibre networks mentioned as laminate possibility 3 above. The membranes in question are produced by electrospinning. With this technique large areas can be covered with long fibres with a thickness in the submicrometer range. The materials choice for electrospinning is large. The material has to be able to melt or dissolve in a quickly evaporating solvent to get it to a viscosity that makes the spinning possible.

3.4 Design and manufacture of the reinforcement

The initial approach for the reinforcement has been the route of a self-designed membrane structure. A custom design will eventually have the largest possibilities to tune the reinforcement to the desired properties. The manufacturing route for this is the embossing technique from soft lithography. The general process is that at first the membrane structure is made from a thin metal sheet (~ 25 μm) by a

photochemical etching process. This metal structure (the template) is then overmoulded with polydimethylsiloxane (PDMS, a silicone rubber) to create a stamp holding the negative of this structure. Pressing this stamp in molten polymer and letting it solidify, a positive of the membrane structure is produced. By stamping into a molten polymer it is likely a very thin film forms over the pores in the structure. This film needs to be removed to open up the pores. Reactive-ion etching is a possibility to remove the film [164], but the size of the structure is likely to be too large. An alternative is a short heat treatment at the melting temperature of the polymer, short enough to allow surface melting only. This may break open the film and the material will be pulled towards the cell ribs with the release of the surface tension. Once the pores are open the polymer membrane layers can be impregnated with liquid elastomer and stacked to the required thickness. Curing of the liquid elastomer will then produce the laminate.

3.4.1 Design of the membrane structure

As a first design for the reinforcement the re-entrant honeycomb or bowtie shape will be used. Most is known of this shape's behaviour and is therefore a logical choice to start with. Figure 3.2 shows the chosen dimensions for this structure.

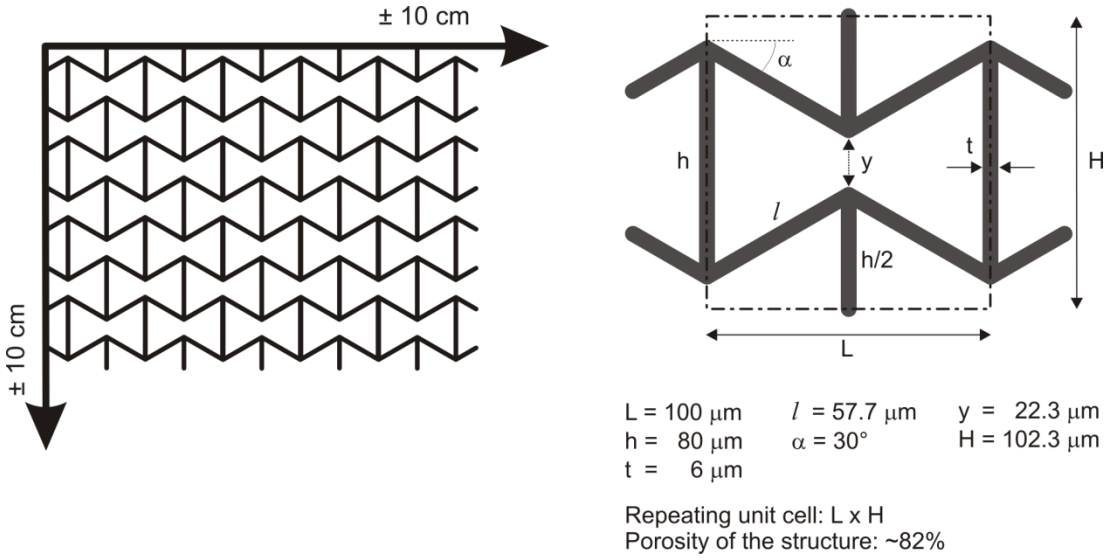

Figure 3.2: Dimensions of the re-entrant honeycomb structure as reinforcement in the laminate for first experiments.

The membrane, or grid structure, needs to have a total surface area of at least 10 x 10 cm. This to be able to die-cut the required size test samples from the final laminates to do the tensile testing. The geometry of the re-entrant cells is somewhat arbitrary, so the length of the cell is chosen as 0.1 mm to ensure a sufficient number of cells in the width (4 mm) of the test pieces. A complete rigid re-entrant structure

allows approximately 30% of deformation and it will therefore be important to choose the re-entrant angle in such a way that there can be sufficient compression and stretch in the structure. Here the angle is set at 30°, which allows about 15% compression and 15% stretch in the structure. The reinforcement materials used in this laminate will not be rigid, so bending and stretching of the ribs will occur. This will make the amount of possible deformation larger.

3.4.2 Manufacturing of the membrane structures

The template structure is ordered from and supplied by Tecan Ltd., Weymouth, United Kingdom. The template is made of hard electroformed nickel structures on a brass substrate. The liquid silicone rubber used to make the stamp is RTV615 from Momentive Performance Materials Inc., Leverkusen, Germany. This is an easily pourable two-component liquid silicone rubber with a viscosity of 4,300 mPa·s. After mixing the two components and degassing the mixture in vacuum, it is carefully poured in a mould containing the template and then cured for 1 hour in an oven at 100 °C. The cured silicone rubber can then be removed from the template and the stamp is ready for use. The thickness of the stamp is approximately 4 mm.

Two grades of TPE-E, Arnitel® EM460 and EL550, are supplied as granulates by DSM Engineering Plastics, Geleen, The Netherlands. It has been tried to melt the granulates and press them into a thin sheet. The obtained sheets however had a thickness in the order of 150-200 μm, too thick for the stamp to transfer the structure through the sheet. Nevertheless, the pattern has transferred very well from the silicone rubber stamp into the TPE-E as can be seen in the optical microscope image of Figure 3.3.
To solve the film making problem, DSM supplied extruded film of Arnitel® EM550 with a nominal thickness of 30 μm. Still slightly too thick, but a new template structure is made to so address this problem. Increasing the height of the template structure also means a scale-up of the unit cell sizes, because of aspect ratio limits in the electrodeposition technique used to make the structure. All length dimensions from Figure 3.2 are now increased by a factor 4.

With this new thinner film it was found that the film had some holes across its surface. A likely cause for this lies in the use of a PTFE release layer in the manufacturing process. Apparently, in the melt the polymer doesn't wet the PTFE release layer sufficiently causing holes to be drawn in the film. Instead of using PTFE, glass is chosen as release layer for the TPE-E film. This functions well and

the holes are gone. Unfortunately the resulting film with the imprinted structure turned out to be too fragile to be removed from the glass without tearing.

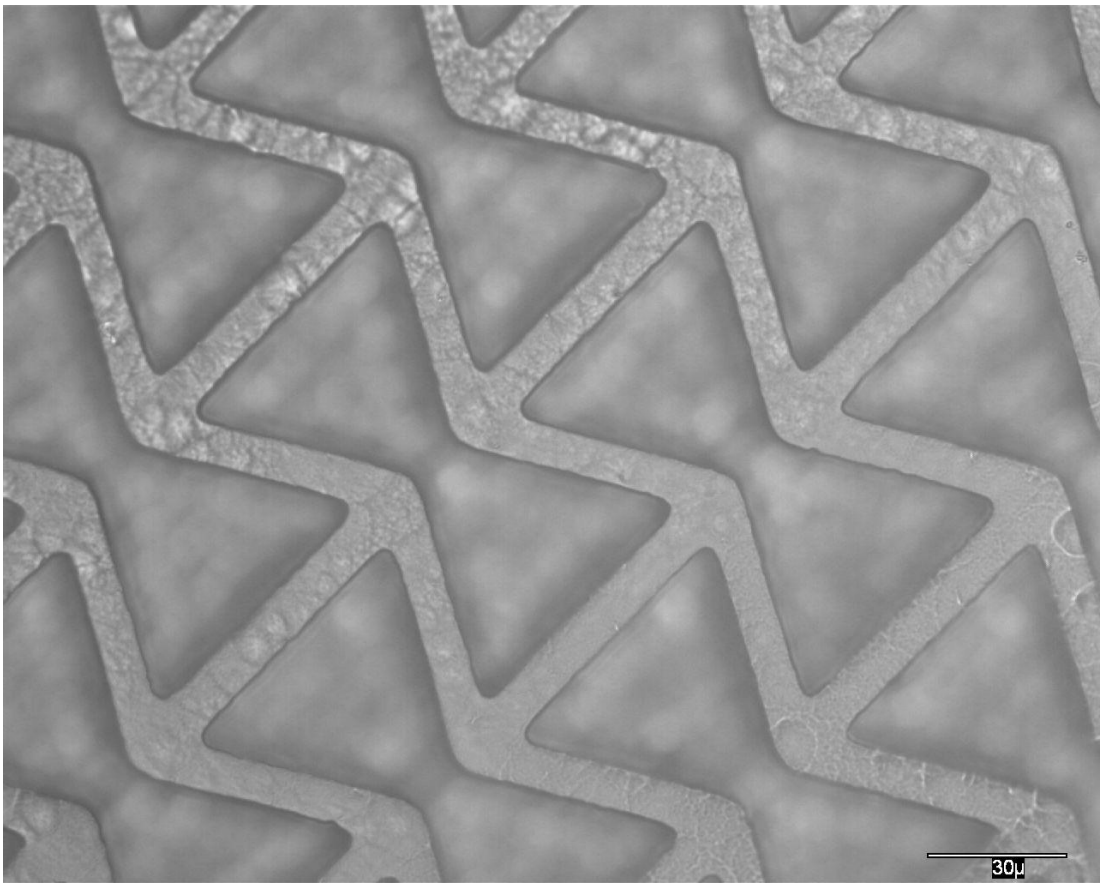

Figure 3.3: Optical microscope image of the re-entrant honeycomb structure in TPE-E (Arnitel® EM460) using soft lithography.

After a critical review of this soft lithography technique it must be concluded that it is not a feasible route to manufacture the reinforcement structures for the laminate. An alternative route to manufacture is required. This alternative should produce the reinforcement structure preferably in one step.

3.4.3 Alternative approaches for reinforcement manufacturing

Various other routes have been considered to manufacture the reinforcement layers with the re-entrant honeycomb structure. Initially these route still used the TPE-E film for this purpose. One approach could be chemical etching in for instance concentrated sulphuric acid. A mask can be made in a similar way as the template structure for the soft lithography described in the previous section, but then without the brass substrate. The hard nickel should have sufficient chemical resistance towards the acid to survive several hundreds or thousands of etching steps [167]. However, besides working with an aggressive chemical there are also some other

disadvantages in this process. The acid will not only eat away the film in the thickness direction, but also sideways leaving the struts in a somewhat trapezoid shape. Secondly, the mask has to be perfectly flat and cover the film well. Obviously, if the acid can come underneath the mask the resulting structure will be locally damaged. A mask produced with electrodeposition of nickel will be to fragile to ensure this. Another way to produce the mask could be by laser micromachining the structure from a thin sheet of stainless steel. Still the sheet has to fairly thin for the acid to fully enter the apertures in the mask's structure and reach the TPE-E film. Also here a perfectly flat mask cannot be guaranteed.

Laser micromachining on the other hand can also be used to directly machine the structure into the TPE-E film. Initial trials done by Laser Micromachining Ltd., St. Asaph, United Kingdom, have shown that the required accuracy can be reached without damaging the film between the apertures (see Figure 3.4). Although laser micromachining is a promising technique to produce the reinforcement structure the cost is too high to continue. The estimated cost for such a fine and detailed structure would currently be in the order of £2,000 per layer.

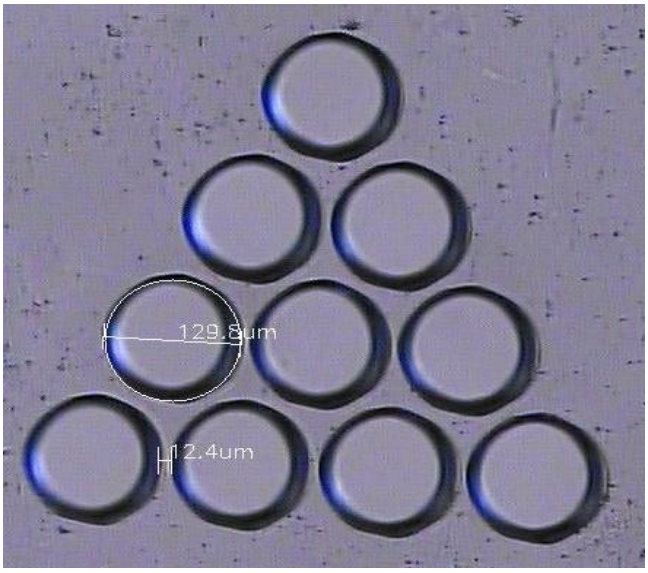

Figure 3.4: Microscopy image of the laser micromachining trial on Arnitel® EL550 film.

Leaving the use of a TPE-E film, other approaches have been investigated to manufacture the reinforcement structure. This is done in the area of rapid prototyping and manufacturing. Many techniques are available here, like Stereolithography, Selective Laser Sintering (SLS) and 3D Printing. They basically all building an object layer by layer by either selectively fusing powder particles or depositing droplets of UV curable polymer (resin). A laser will do the fusing or the curing and the spot size of the laser is the main limit in the accuracy of the various techniques. Most of these techniques have typical build size steps in the order of 100 μm, which is too large for the reinforcement structure. Only 3D Printing comes close to the required resolution. Currently the most advanced commercially available machines like the Objet Connex500 can reach a build resolution in length and width

of 42 μm (600 dpi) with a layer thickness of 16 μm [168]. But there is a lot of research done on increasing the accuracy of 3D printing, especially in the field of medical implants. It is therefore likely that in the near future it is possible to manufacture the reinforcement structure from Figure 3.2 as a 3D print.

3.4.4 Final approach

For the final approach of the reinforcement in the tubing laminate is stepped away from the custom self-designed membrane structure. It turned out that manufacturing techniques were either not feasible or current techniques are simply not yet developed far enough. Therefore normal available membranes will be used to build the laminates. The fibre network morphology looks to be an interesting starting point. Also through-the-thickness is the main direction of interest for a negative Poisson's ratio when considering tube occlusion in the peristaltic pump. Nanofibre membranes are the materials of choice as reinforcement in the laminates.

Summarising, the next chapters are firstly about the baseline. Typical properties are identified of current peristaltic tubes in use, with a special attention towards STA-PURE™. Thereafter a modelling chapter shows the effects of the Poisson's ratio on an occluding tube. This also gives an idea of how much the Poisson's ratio has to be lowered and if overall auxeticity is really necessary. The next chapter is about the actual manufacturing, testing and characterisation of flat sheet laminates made with the nanofibre membrane reinforcement. Finally tubes are made with this laminate structure and put to test in a peristaltic pump in order to see how it performs in the actual application.

4 Determination of the baseline

In this chapter the results are presented of the baseline tests on existing tube materials as described in the previous chapter (Section 3.2). An overview of the tests conducted on which tube is given in Table 4.1.

	Tensile tests			**Occlusion behaviour**		**Vibration**
	Circumferential	Axial		Without cameras	With cameras	
	θ-x direction	x-θ direction	x-r direction			
STA-PURE™ 4.8 x 2.4 mm	**X**			**X**		
STA-PURE™ 9.6 x 2.4 mm	**X**			**X**		
STA-PURE™ 12.7 x 4.8 mm	**X**	**X**			**X**	
STA-PURE™ "high pressure" 6.4 x 2.54 mm	**X**			**X**		**X**
W.L. Gore ePTFE/FKM 4.8 x 2.4 mm	**X**	**X**		**X**		
Bioprene® 73 Shore A 12.7 x 4.8 mm			**X***)		**X**	
Bioprene® 80 Shore A 12.7 x 4.8 mm			**X***)		**X**	
*) Earlier tests (2005) on 40 x 12.75 mm tubing.						

Table 4.1: Overview of the baseline tests conducted for which tube size and material.

The circumferential direction is chosen because the mechanical behaviour in this direction determines the pressure resistance of the tube. The occlusion tests with cameras mean that for these tubes the strain maps of the cross-section are determined.

4.1 Tensile tests

Samples for the tensile tests are prepared in the form of strips. They were cut from the tube with a sharp knife in the directions to those mentioned in Table 4.1 and defined according to Figure 4.1. Obviously by preparing samples from finished products in this way, the geometry of the samples will not follow the ones described in the standard ISO 37. Especially the requirement of flat parallel opposing surfaces is nearly impossible to fulfil. Because only approximate property values are necessary is this not really an issue, even though the results may be somewhat affected. The narrowest part of the sample strips is taken as the cross-sectional area. The tests are done using an Instron 3369 tensile machine equipped with a 1 kN load cell using a crosshead speed of 100 mm/min. The tests on each tube are repeated at least in threefold. Average results of all the tensile tests are shown in Figure 4.3 and Figure 4.4; the data is summarised in Table 4.2. A complete overview of the tensile test results is given in the Appendix (Figures A1 − A6).

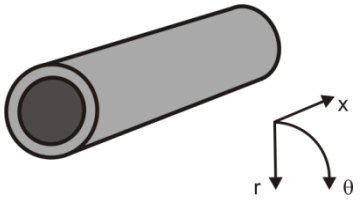

Figure 4.1: Definition of the directions of the tensile test samples cut from the tubes.

A few difficulties were seen during the tensile tests. The surfaces of the STA-PURE™ samples were very slippery and sand paper in the clamps along with strong clamping compression was required to prevent slip. The consequence was that nearly all samples failed at the location of one of the clamps. This suggests that the ultimate properties in reality are somewhat higher than these measurements show. The second difficulty involved mounting the circumferential test pieces of the smallest diameter (4.8 mm) between the clamps of the tensile machine as is schematically shown in Figure 4.2. In some occasions the sample was not completely stretched yet, causing a slight shift of the curve to higher elongations (see curves 2 and 4 in Figure 4.3). This has been taken into account for determining the Young's modulus.

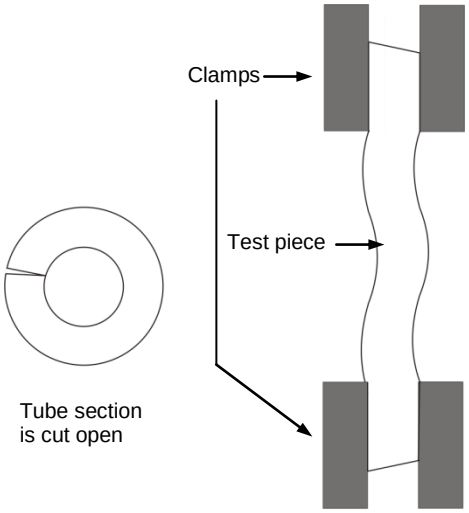

Figure 4.2: Schematic drawing of the mounting of the circumferential test pieces. Smaller diameter tubes give more curvature in the test piece.

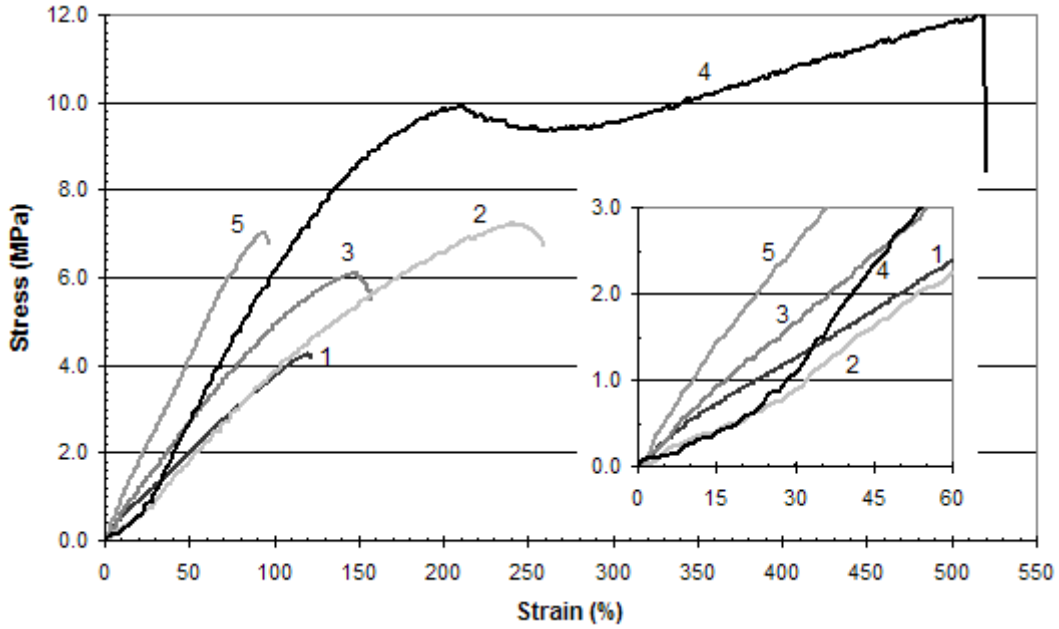

Figure 4.3: Average tensile curves of five tube materials and sizes in the circumferential (θ-x) direction. Curve labels correspond with: 1. STA-PURE™ 12.7 x 4.8 mm; 2. STA-PURE™ 4.8 x 2.4 mm; 3. STA-PURE™ 9.6 x 2.4 mm; 4. ePTFE/FKM 4.8 x 2.4 mm; 5. STA-PURE™ "high pressure" 6.4 x 2.54 mm.

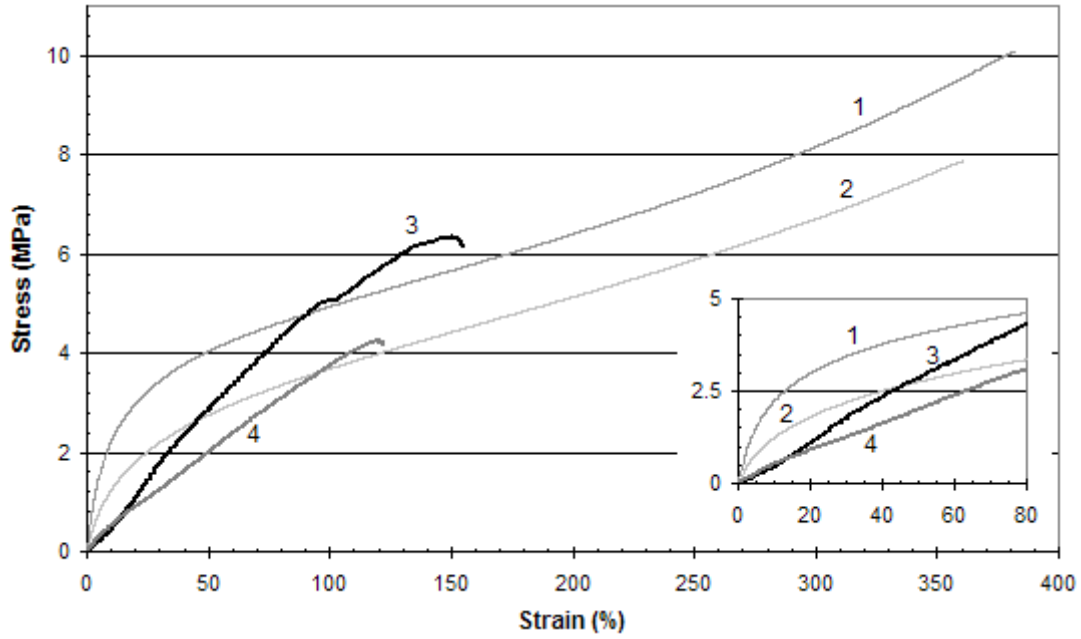

Figure 4.4: Average tensile curves for Bioprene® in the axial (x-r) direction and for STA-PURE™ 12.7 x 4.8 mm in axial (x-θ) and circumferential (θ-x) direction. Curve labels correspond with: 1. Bioprene® 80 Shore A; 2. Bioprene® 73 Shore A; 3. STA-PURE™ 12.7 x 4.8 mm in x-θ direction; 4. STA-PURE™ 12.7 x 4.8 mm in θ-x direction.

Tensile tests on the two Bioprene® grades of 73 and 80 Shore A hardness have been done previously (in 2005) for Watson-Marlow Bredel. These tests were done in a Zwick Z020 tensile machine (1 kN load cell) with extensometers according to the

standard ISO 37 using Type 2 dumbbell samples. The only deficiency was a slightly irregular thickness of the samples since they were also cut from a tube, albeit a much larger one (40 x 12.75 mm). Also the crosshead speed of 100 mm/min is lower than the standard prescribes.

Property	**STA-PURE™ 4.8 x 2.4 mm**	**STA-PURE™ 9.6 x 2.4 mm**	**STA-PURE™ 12.7 x 4.8 mm**	
[MPa]	n = 3	n = 3	*Circ.*, n = 4	*Axial*, n = 3
Young's modulus	3.85 ± 0.27	5.76 ± 0.52	4.80 ± 0.33	5.95 ± 1.34
Modulus @ 10%	0.28 ± 0.06	0.59 ± 0.06	0.54 ± 0.02	0.39 ± 0.08
Modulus @ 50%	1.10 ± 0.52	2.63 ± 0.31	2.11 ± 0.08	2.67 ± 0.46
Modulus @ 100%	2.90 ± 0.73	3.42 ± 0.64	3.42 ± 0.64	4.84 ± 0.66
Tensile strength	7.3 ± 0.7	6.6 ± 0.8	3.7 ± 0.5	6.8 ± 0.7
Strain at break [%]	310 ± 66	183 ± 30	104 ± 14	192 ± 33

Property	**STA-PURE™ "high press." 6.4 x 2.54 mm**	**ePTFE/FKM 4.8 x 2.4 mm**		**Bioprene® 73 Shore A**	**Bioprene® 80 Shore A**
[MPa]	n = 4	*Circ.*, n = 3	*Axial*, n = 4	n = 3	n = 3
Young's modulus	10.39 ± 1.49	8.08 ± 0.42	7.02 ± 0.48	24.7 ± 1.0	52.1 ± 4.6
Modulus @ 10%	0.77 ± 0.45	0.40 ± 0.15	0.62 ± 0.14	1.20 ± 0.04	2.28 ± 0.25
Modulus @ 50%	4.05 ± 0.43	3.19 ± 0.42	2.63 ± 0.12	2.68 ± 0.12	4.12 ± 0.41
Modulus @ 100%	---	6.41 ± 0.34	4.22 ± 0.17	3.59 ± 0.17	5.02 ± 0.46
Tensile strength	6.2 ± 1.0	10.9 ± 1.3	8.2 ± 0.8	7.7 ± 0.1	10.5 ± 0.7
Strain at break [%]	99 ± 8	481 ± 42 *)	378 ± 62	364 ± 15	398 ± 12

*) Average of two samples (n = 2); the third sample failed at 225%.

Table 4.2: Overview of the mechanical properties of various peristaltic tube materials and sizes.

A striking result for the materials with ePTFE reinforcement is the long nearly linear response of stress with approximately the first 50% strain and then slightly deviates

to non-linearity. This opposed to Bioprene® which shows strong non-linear behaviour already at low strain. It seems that the ePTFE structure can take a large part of the strain by a re-ordering mechanism, like straightening and hinging of the fibrils. Support for a microstructural rearrangement can be found in a number of curves where “knee-points” can be observed (Appendix: Figures A3 and A5).The (gradual) transition to non-linearity could be caused by plastic deformation of the fibrils until they break. At some point, insufficient fibrils are left to support the stress and the sample fractures. This stress-strain behaviour is probably the reason for the good pressure performance and the low flow-drop over life of STA-PURE™ tubing.

Peculiar behaviour is shown by the ePTFE/FKM material (curve 4 in Figure 4.3). An elongation at break around 500% cannot be explained when looking at ePTFE and FKM separately. Both materials would have failed long before that amount of elongation. Somehow the different manufacturing route of tape wrapping must play a role allowing the material to elongate beyond its normal limits. On the other hand, the STA-PURE™ material could have shown similar behaviour, but this is not observed due to premature failure of the samples as discussed above.

From the tests on tube material in both axial and circumferential direction can be seen that there is anisotropy (see Figure 4.4 and Appendix: Figures A3 and A5). The measurements show that for STA-PURE™ the stress-strain properties are higher in the axial direction. For ePTFE/FKM the opposite is the case and the properties in the circumferential direction are higher. This difference must also have to do with the two distinctive fabrication methods. The tape wrapping process will place the anisotropic ePTFE membrane under an angle what may well be the cause for the change in directional properties.

4.2 Occlusion behaviour

The occlusion behaviour is monitored by compressing a tube section between two flat plates. It should be noted that in the real application of the tube in the peristaltic pump the occlusion is between two curved surfaces, namely the roller and the pump casing. In practice the required compression load for occlusion is higher than the value measured between flat plates. However for reasons of simplicity, compression between flat plates will give a good indication and comparable results with respect to each other.

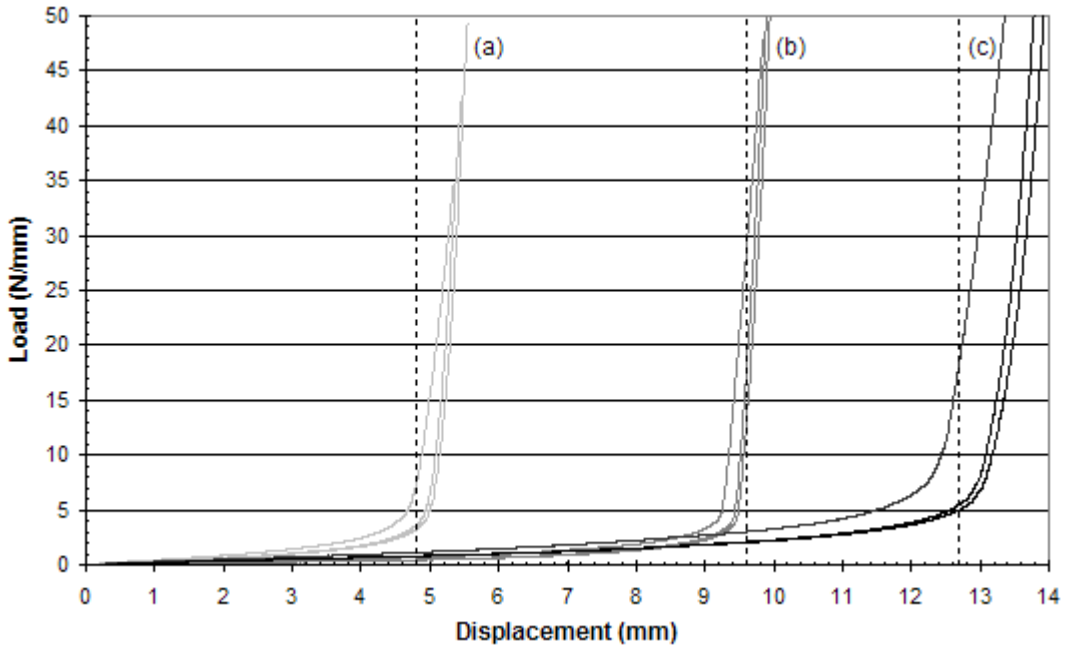

Figure 4.5: Occlusion curves for the three STA-PURE™ tube sizes 4.8 x 2.4 mm (a), 9.6 x 2.4 mm (b) and 12.7 x 4.8 mm (c). The dashed lines denote the inner diameter of the respective tubes.

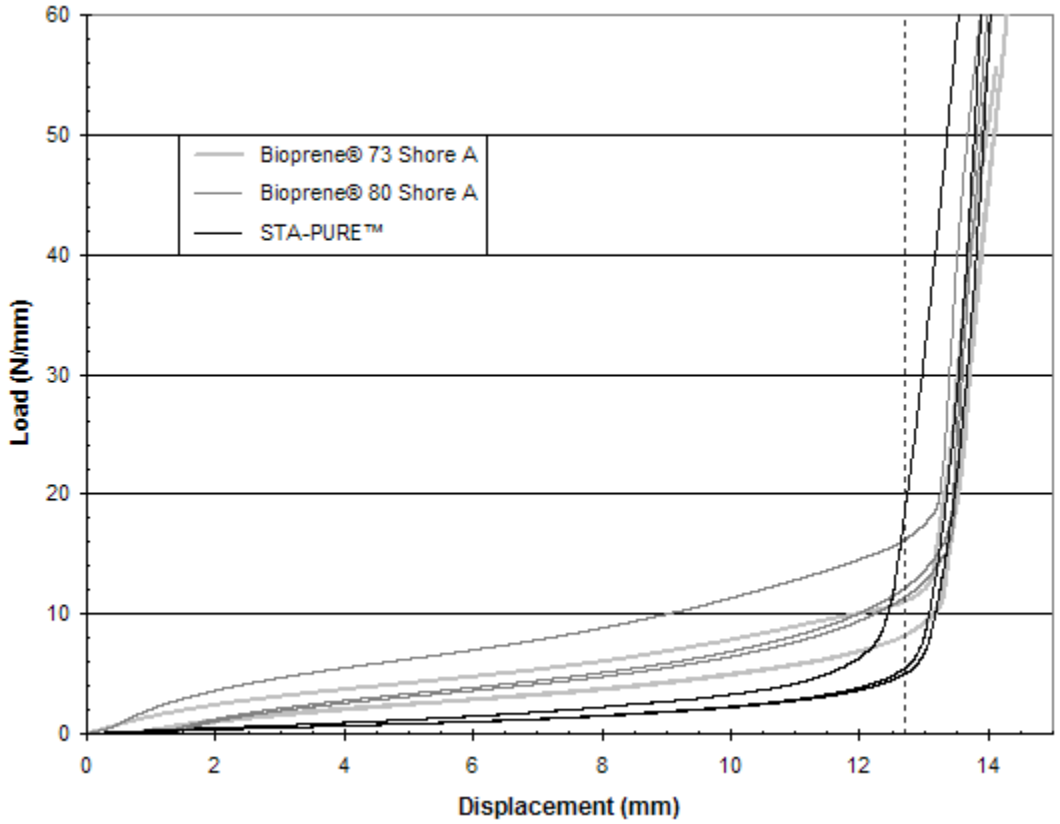

Figure 4.6: Occlusion curves for Bioprene® and STA-PURE™ of tube size 12.7 x 4.8 mm. The dashed line denotes the inner diameter of the tubes.

The tube occlusion tests were done using the same machine as for the tensile tests (Instron 3369). The crosshead speed was set at 10 mm/min. Each tube section has been occluded three times in order to see the effect of permanent deformation. The length of the tube sections was approximately 25 mm, except for the 12.7 x 4.8 mm sections; they were approximately 45 mm long. The compressive load required to occlude the tube is divided by the section lengths in order to obtain an in between comparable value for the load per millimetre length. Results for the various sizes of STA-PURE™ tubing are shown in Figure 4.5.

The results for the 12.7 x 4.8 mm tubes of Bioprene® and STA-PURE™ are shown in Figure 4.6. The data obtained from the occlusion curves is summarised in Table 4.3. A complete overview of the test results is given in the Appendix (Figures A7 − A13).

For all tubes irrespective of material or size the first occlusion requires the most force. After this first occlusion a softening effect causes the subsequent occlusions to require less force. The softening is generally attributed to rearrangements in the microstructure. In STA-PURE™ the fibrils may hinge with respect to the nodes, but also some buckling will occur. The buckled fibrils cannot support compressive load anymore and the occlusion load decreases. In the 2.4 mm walls this effect is not so large, but at 4.8 mm wall thickness it becomes significant. Permanent strain (plastic) deformation is also small as can be seen from Table 4.3. This is also a reason for the very good flow stability of the STA-PURE™ tubes in a peristaltic pump. Bioprene® on the other hand shows a complete different behaviour. High non-linear and viscoelastic behaviour show a significant softening effect and plastic deformation.

Another remarkable difference between STA-PURE™ and Bioprene® is the behaviour of the first occlusion. The sharp increase in occlusion load starts for STA-PURE™ already before the dashed lines denoting the tube's inner diameter. Only for the 9.6 x 2.4 mm and the "high pressure" tube this behaviour remains in the subsequent occlusions.

To look closer to the occlusion behaviour of the tubes, the strain distribution on the cross-section of the tube is mapped with use of two synchronised high-speed cameras and specific software. On the cross-sections of the 12.7 x 4.8 mm tube sections, a speckle pattern is applied by spraying black paint from a toothbrush onto the surface. Photos are taken with the two cameras (Photron Fastcam S3) during the occlusion test of the tube sections. The software (Vic-3D®, Correlated Solutions

Inc.) analyses the photos and can track the movement of the speckle pattern which it uses to calculate various parameters. Because two synchronised cameras are used, the software can create a stereo image and is able to determine the movement of the speckle pattern in 3D (i.e. in-plane and out-of-plane).

	bore : wall ratio	**Occlusion load** [N/mm]		**Occl. displ.** (estimated at n^{th} occl.) [mm]	**Permanent plastic strain** [mm]	
					After 1^{st} occl.	After 2^{nd} occl.
STA-PURE™ 4.8 x 2.4 mm	2 : 1	11.5		5.21	0.14	0.14
STA-PURE™ 9.6 x 2.4 mm	4 : 1	23.0		9.85	0.15	0.21
STA-PURE™ 12.7 x 4.8 mm	8 : 3 (= 2.66 : 1)	31.5		14.00	0.07	0.10
STA-PURE™ “high pressure” 6.4 x 2.54 mm	5 : 2 (= 2.5 : 1)	20.7		6.65	0.20	0.24
W.L. Gore ePTFE/FKM 4.8 x 2.4 mm	2 : 1	12.3		5.25	0.20	0.24
Bioprene® 73 Shore A 12.7 x 4.8 mm	8 : 3 (= 2.66 : 1)	17.4 (1^{st} occl.)	12.3 (2^{nd} & 3^{rd} occl.)	13.50	0.70	0.77
Bioprene® 80 Shore A 12.7 x 4.8 mm	8 : 3 (= 2.66 : 1)	22.7 (1^{st} occl.)	17.2 (2^{nd} & 3^{rd} occl.)	13.50	0.96	1.11

Table 4.3: Overview of the data obtained from the occlusion measurements. The occlusion displacement is estimated by extrapolation of the first three curves.

Figure 4.7 to Figure 4.9 show some pictures of the strain maps of the three tubes at displacements close to full occlusion. The blank parts in the cross-section are areas where the software has lost track of the movement of the speckles. This occurs especially at the edges of the sample and at higher deformations in regions with a lot of out-of-plane movement (e.g. the cusp region). The maximum values for the

tensile and compressive strains are listed in Table 4.4.The range of mechanical properties used in occluding the tubes is globally between –30% and +70%. This range can become somewhat larger with different bore to wall ratios. The more elastic deforming STA-PURE™ shows a wider strain field for the occlusion than the viscoelastic and more plastic deforming Bioprene®. This strain range is used for the occlusion of the tubes and needs to be the focus for the new laminates. The remainder of the tensile curve, beyond +70%, is of course also important in terms of tube life: crack growth is governed by the ultimate properties locally around the crack tip.

Interesting behaviour is observed with both the Bioprene® tubes. As can be seen from Figure 4.8 and Figure 4.9 the tubes lift somewhat from the bottom plate. This is in contrast to STA-PURE™ where the tube remains in contact with the bottom plate.

Whether this is a thinning effect caused by the Poisson's ratio is not completely clear. What can be seen from the test results is a stronger out-of-plane deformation for the Bioprene® tubes. During the occlusion the cusp area moves forwards (out of the paper), while the middle area (around the bore) moves inwards enough to lift the outer edge of the tube. This is much less seen for the STA-PURE™, suggesting less incompressibility and therefore a lower Poisson's ratio.

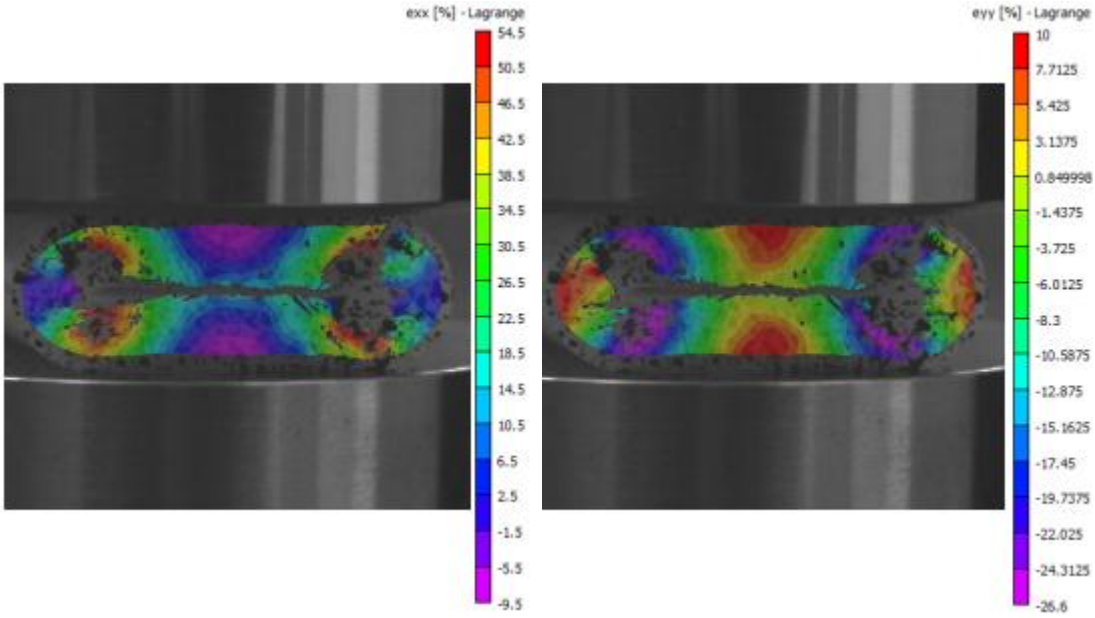

Figure 4.7: Strain map of the first occlusion of STA-PURE™ 12.7 x 4.8 mm tubing at 12.01 mm displacement. The left picture shows the strain in horizontal direction; the right picture shows the strain in vertical direction.

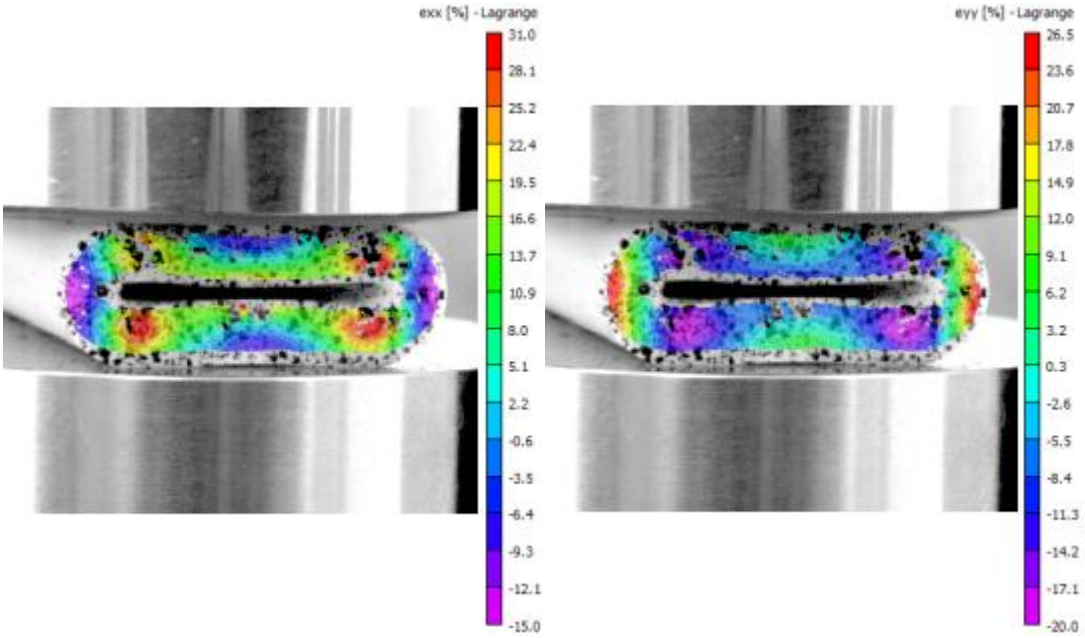

Figure 4.8: Strain map of the first occlusion of 73 Shore A Bioprene® 12.7 x 4.8 mm tubing at 11.30 mm displacement. The left picture shows the strain in horizontal direction; the right picture shows the strain in vertical direction.

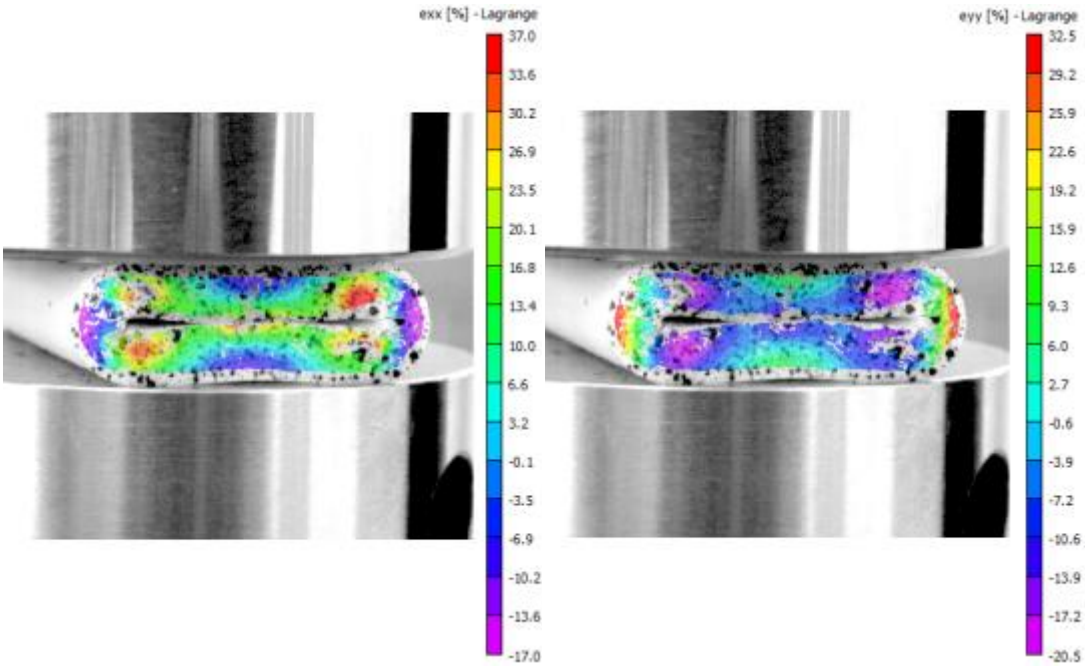

Figure 4.9: Strain map of the first occlusion of 80 Shore A Bioprene® 12.7 x 4.8 mm tubing at 12.75 mm displacement. The left picture shows the strain in horizontal direction; the right picture shows the strain in vertical direction.

Tube material	Max. tensile strain (%)		Max. compressive strain (%)	
	Horizontal	Vertical	Horizontal	Vertical
STA-PURE™	66	21	–10	–27
Bioprene® 73 Shore A	35	27	–15	–20
Bioprene® 80 Shore A	40	33	–18	–21

Table 4.4: Maximum tensile and compressive strains in the occlusion of various 12.7 x 4.8 mm tubes.

4.3 Vibration measurements

A small number of vibration measurements have been done on the STA-PURE™ 12.7 x 4.8 mm tube to determine the elastic properties. The tests were limited to transverse or flexural vibration, which only gives the Young's modulus. The relationship between the natural frequencies and the Young's modulus for tubes is given by [169]:

$$f_i = \frac{\lambda_i^2}{8\pi L^2}\left(\frac{E\left(D_o^2 + D_{in}^2\right)}{\mu}\right)^{1/2} \quad \text{or} \quad E = \frac{64\pi^2 L^4 \mu}{\lambda_i^4\left(D_o^2 + D_{in}^2\right)} f_i^{\,2} \qquad (4.1)$$

With f_i the natural frequency for mode i, E the Young's modulus, L is the span length, μ is the mass density and D_o and D_{in} are the outer and inner diameter of the tube respectively. λ_i is a dimensionless parameter of which the value depends on the boundary conditions and the mode shape of the natural frequency.

Because of the low stiffness of the STA-PURE™ material also low natural frequencies are expected. This may interfere with the excitation frequency which is also low. The tube pieces should therefore be short to increase the natural frequencies.

A 164 mm long STA-PURE™ 12.7 x 4.8 mm tube section is clamped on a standard on one side with the other end free (clamped-free boundary condition). An accelerometer (Brüel & Kjær) is stuck to the outside of the tube with double-sided tape and connected to a four channel oscilloscope (Tektronic TDS 3014). Matlab is used for the signal processing. Two methods of excitation are used: a hit with a metal rod and bending the tube a little downwards with a finger and releasing it. The resulting Young's moduli from these experiments are listed in Table 4.5.

Excitation method	**Natural frequency** [Hz]		**Young's modulus, E** [MPa]	
	f_1	f_2	**from** f_1	**from** f_2
Metal rod	11	101	7.5	5.0
Finger	13	120	10.5	7.1

Table 4.5: Results for the natural frequencies and Young's moduli from vibration tests.

The mode 1 natural frequencies were still difficult to identify. Only with the prior knowledge that a natural frequency should be somewhere in the signal in the range of 8–15 Hz gave the ability of finding it.

The use of even a shorter tube section might have resulted in identifying the first natural frequency more easily. This was not pursued any further since the results from tensile testing were consistently clear. Also the effect of dampening is unsure. As a non-destructive test it can be useful to determine the Young's modulus. But when destructive testing is not an issue, results can be quicker obtained using conventional tensile testing methods.

4.4 Conclusions

A number of ideal characteristics for the new laminate for peristaltic tubing can be derived from the baseline test results:

– A (in circumferential direction) Young's modulus around 10 MPa and a stress at 100% strain between 5 and 10 MPa.

– The stress-strain response should be as linear as possible in the range of –30% to +70% strain.

– From the patents on STA-PURE™ [38,39]: The elastomer content of the laminate should be around 90% (see also section 3.1).

5 Modelling of the effect of the Poisson's ratio

Using an auxetic material for peristaltic tubing seems to be a sensible and logical thing to do. But the question is by how much the Poisson's ratio actually needs to be lowered. In order to get an idea of the influence of the Poisson's ratio on the occlusion behaviour of a peristaltic tube a finite element model is set up. In this model the principal stresses and strains in the cross-section of the tube are calculated at certain levels of occlusion for various Poisson's ratios between +0.5 and –1. This will verify the idea whether a lower or negative Poisson's ratio indeed is beneficial. It will also show around which value of the Poisson's ratio gives the best properties for the peristaltic tube, i.e. lowest stress state during occlusion within reasonable strains.

5.1 Model approach

5.1.1 Geometry

A tube is modelled using a 2D plain strain model in Abaqus 6.10-1. Because the tube is symmetric only one half of the tube is modelled. The inner diameter of the tube is 12.7 mm and the wall thickness is 4.8 mm. In the model the tube is occluded between two plates, where the bottom plate is fixed and the top plate moves downwards.

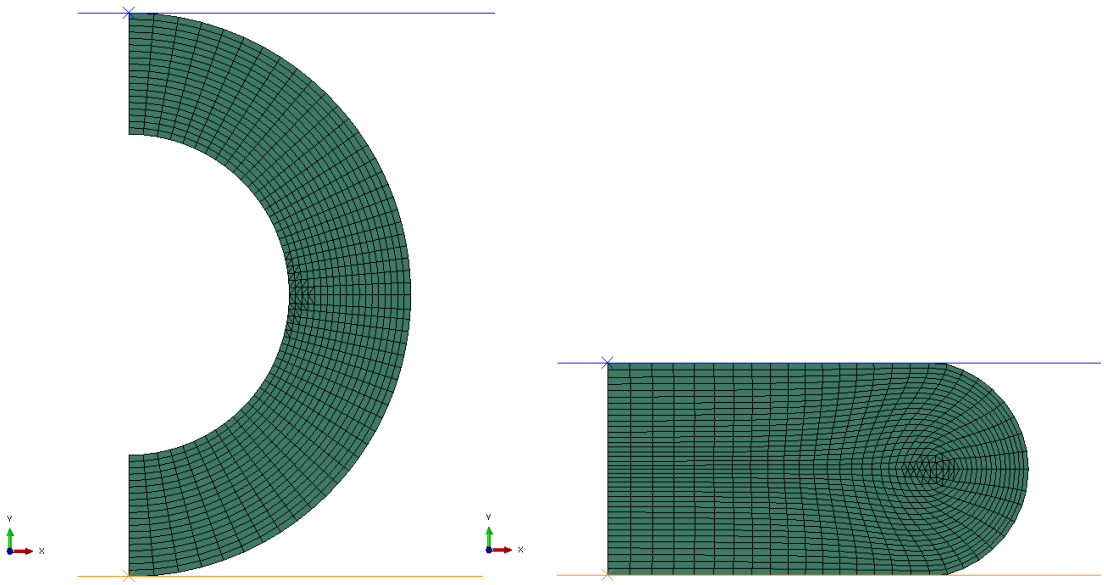

Figure 5.1: The geometry of the tube in the model. Left is the undeformed state and right the fully deformed (occluded) state.

5.1.2 Material model

The material used in the model is isotropic and is linear elastic. The stress at 100% strain is set at 10 MPa, towards the upper end of the STA-PURE™ properties as determined in Chapter 4. The investigated Poisson's ratios are +0.5, +0.25, +0.1, 0, –0.1, –0.25, –0.5 and –1.

It is difficult to find a good material model that is able to cope with the large element deformations during occlusion of the tube in the complete range of Poisson's ratios between +0.5 and –1. A neo-hookean material model for instance, can cope with the element deformations, but should only be used for Poisson's ratios of +0.45 and above. Eventually it is found that a hyperfoam model gives the best approach. It can cope with large element deformations and can be used over a wide range of Poisson's ratios as it allows for compressibility. To check the robustness of this model a simple one-element tensile test is run on a 100x100x100 mm cube. Figure 5.2 shows the results of this one-element tensile test. It can be seen that the Poisson's ratios from the results deviate somewhat from the input values.

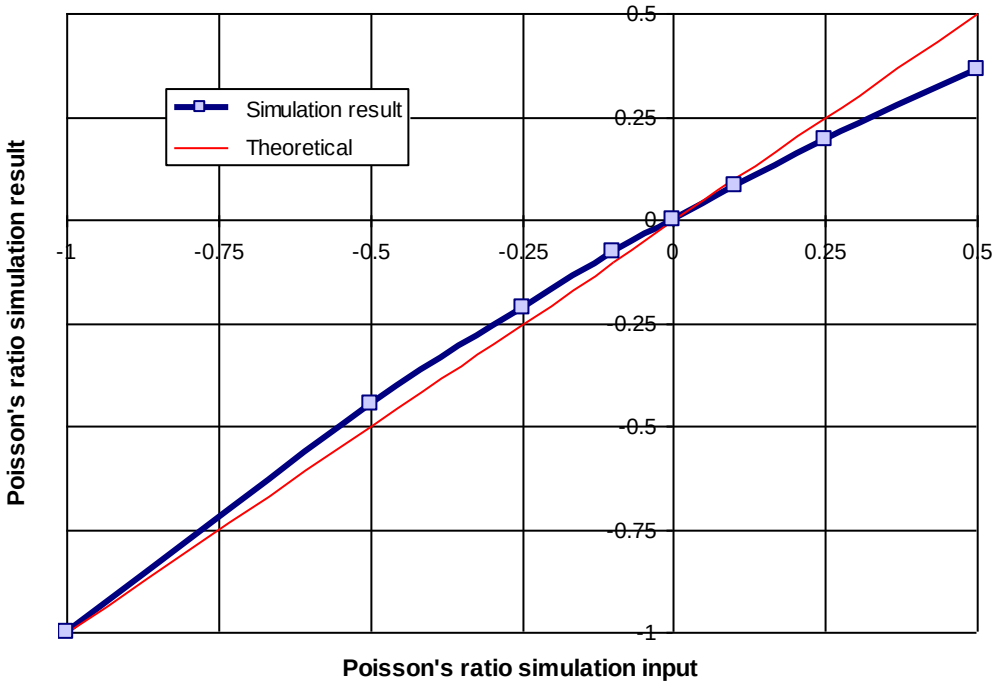

Figure 5.2: Model check on the Poisson's ratio with a one-element tensile test on a 100x100x100 mm cube.

In this one-element tensile test the force-strain curves are also recorded up to strains of 50% as shown in Figure 5.3. From these curves can be seen that for Poisson's ratios ranging from +0.5 down to –0.25 the force deviation is within 5% of the desired 5 MPa stiffness at 50% strain for this material (note that the 50 kN on

the y-axis equals 5 MPa for the geometry in this one-element tensile test). The stiffness deviation with a Poisson's ratio of –0.5 is about 20% while for a Poisson's ratio of –1 there is hardly any force response. Because of these large deviations (or errors) the stress and strain distributions in occluding tubes with a Poisson's ratio of –0.5 and –1 are not investigated, so the analyses are limited to the Poisson's ratio range of +0.5 to –0.25.

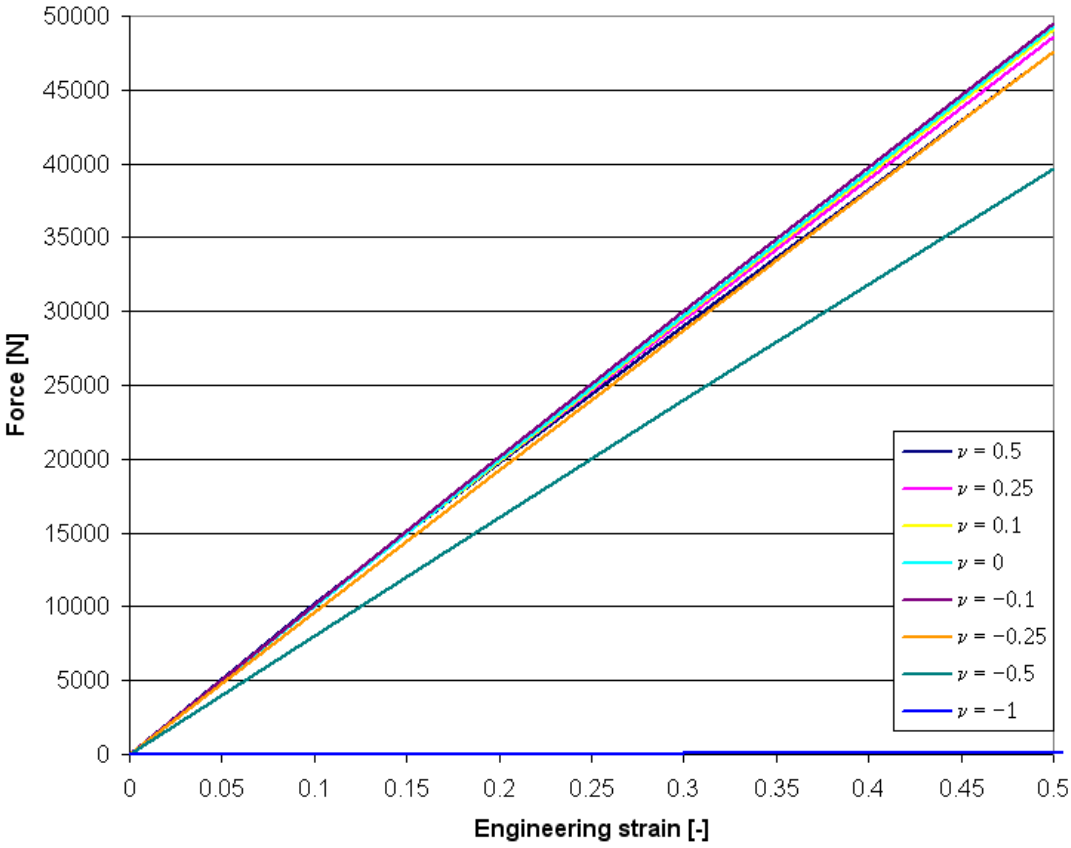

Figure 5.3: Force-strain curves for the one-element tensile test on a 100x100x100 mm cube with a material having various Poisson's ratios.

In the further analyses the Poisson's ratio of +0.5 is slightly lowered to +0.495 to avoid possible convergence issues in the model and to better reflect the real elastomeric or rubber materials used in peristaltic pump tubing.

5.2 Modelling results

The results are calculated for the following levels of occlusion: 10%, 50%, 90%, 100% and 110%. An occlusion of 100% means that the distance between the top and bottom plate is twice the wall thickness of the tube. Therefore 110% means an over-occlusion of 10%, an amount typically needed in a running peristaltic pump.

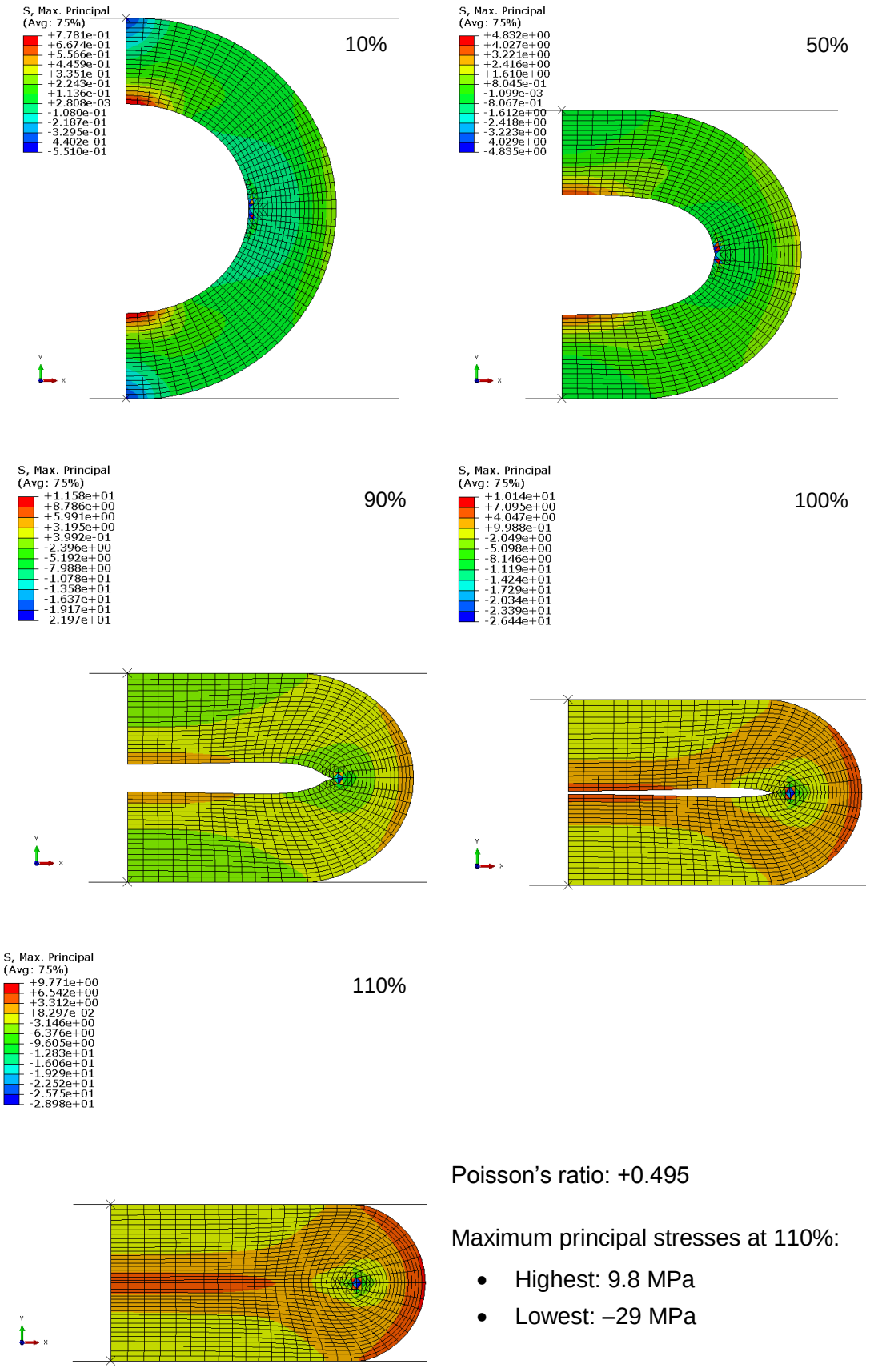

Poisson's ratio: +0.495

Maximum principal stresses at 110%:

- Highest: 9.8 MPa
- Lowest: –29 MPa

Figure 5.4: Maximum principal stress distribution in the cross-section of a tube with increasing levels of occlusion. The Poisson's ratio is +0.495.

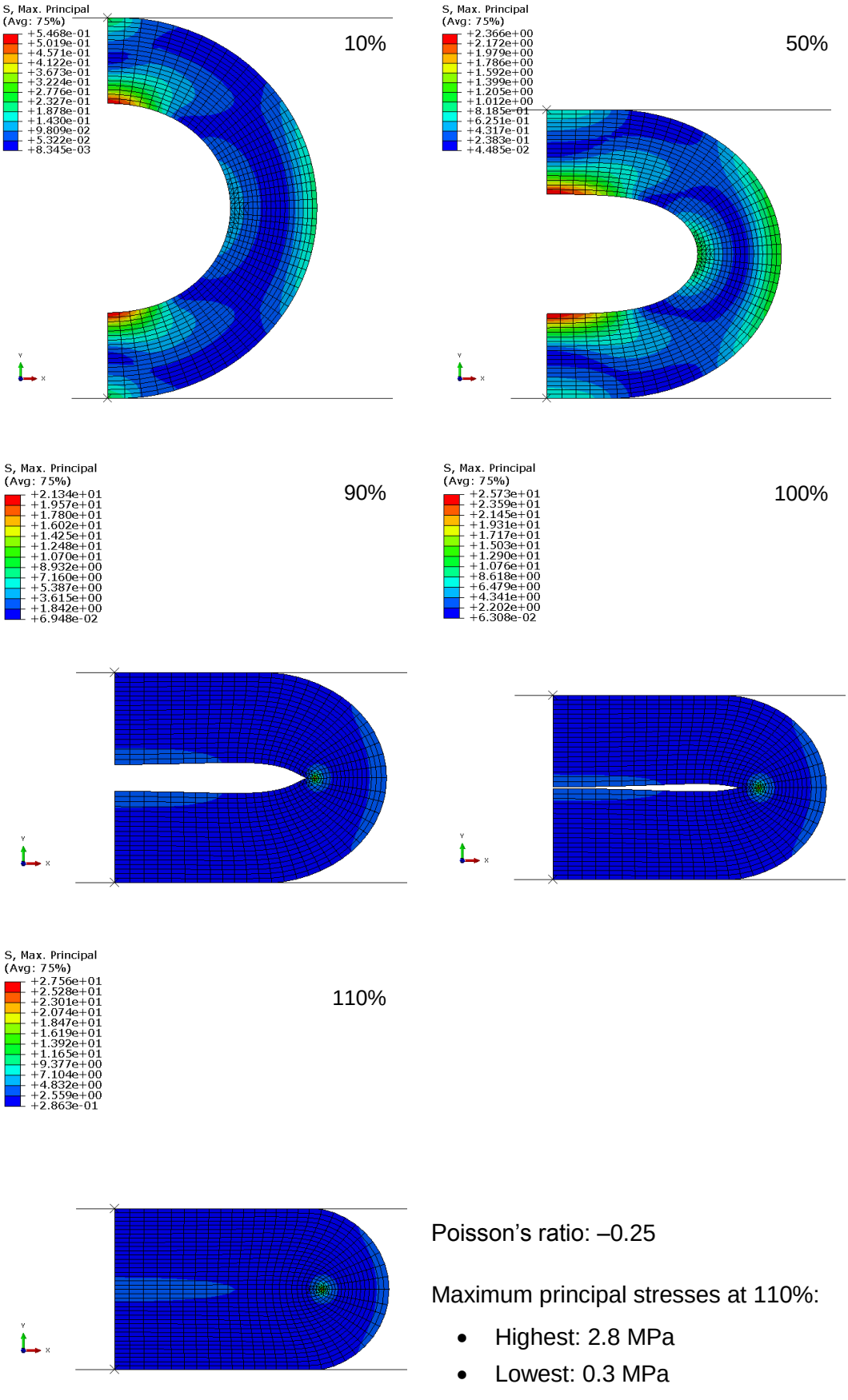

Figure 5.5: Maximum principal stress distribution in the cross-section of a tube with increasing levels of occlusion. The Poisson's ratio is –0.25.

As an example of the modelling results, Figure 5.4 and Figure 5.5 show the maximum principal stresses in the tube's cross-section at several occlusion levels for a Poisson's ratio of +0.495 and –0.25 respectively. It is clear that the maximum principal stress levels drop dramatically going from the positive to the negative value for the Poisson's ratio. Besides the maximum principal stresses, also the minimum principal stresses, and the maximum and minimum principal strains are calculated for all the above mentioned situations. The results for this are summarised and analysed in the next section.

5.3 Analysis of the results

The results of the calculations are assessed by analysing four points in the cross-section of the tube as depicted in Figure 5.6. They are located at the inside and outside of the cusp and at the inside and outside in the middle of the tube. These points are chosen at the locations that normally show the highest stresses and strains in tube occlusion. These are also the locations where tube failure can occur. Note that point 1 is chosen somewhat away from the inner surface of the cusp. This is done because the mesh deforms heavily at the higher levels of occlusion resulting in highly unreliable values for the elements at the inside of the cusp. For each of the four points the values for the maximum and minimum principal stresses and principal strains are retrieved from the model at the different levels of occlusion and for the different Poisson's ratios. The relation between the stress or strain with the level of occlusion and the Poisson's ratio is then shown graphically in a 3D plot. For reasons of clarity, the figures for point 1 are shown in the text, whilst the figures for the other three points can be found in the appendix.

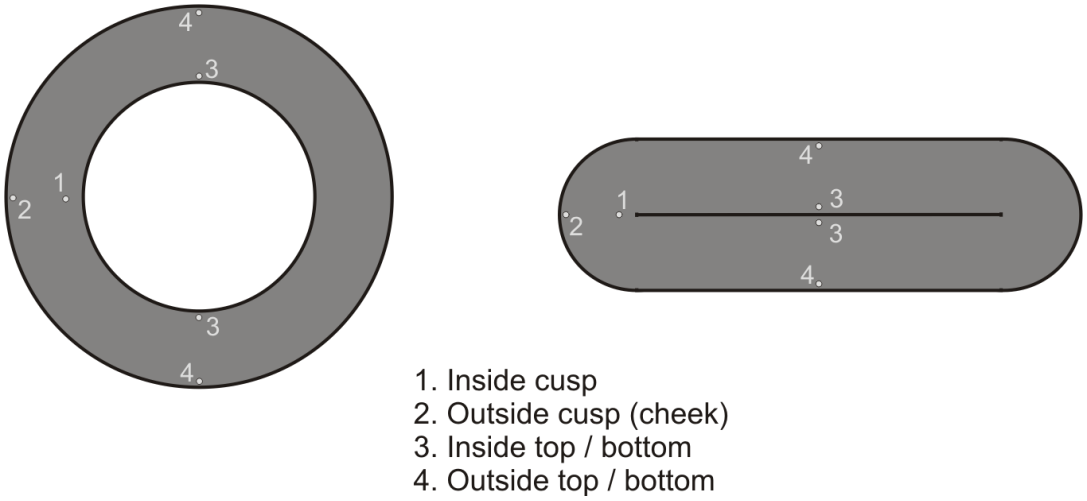

Figure 5.6: The location of the 4 points on the cross-section of a tube for the modelling results analysis.

5.3.1 Maximum principal stress

For the peristaltic tube the stress level under occlusion should be as low as possible as this would increase lifetime. With less stress required for occluding the tube, less energy is required for the occlusion and less energy is available for crack initiation and propagation.

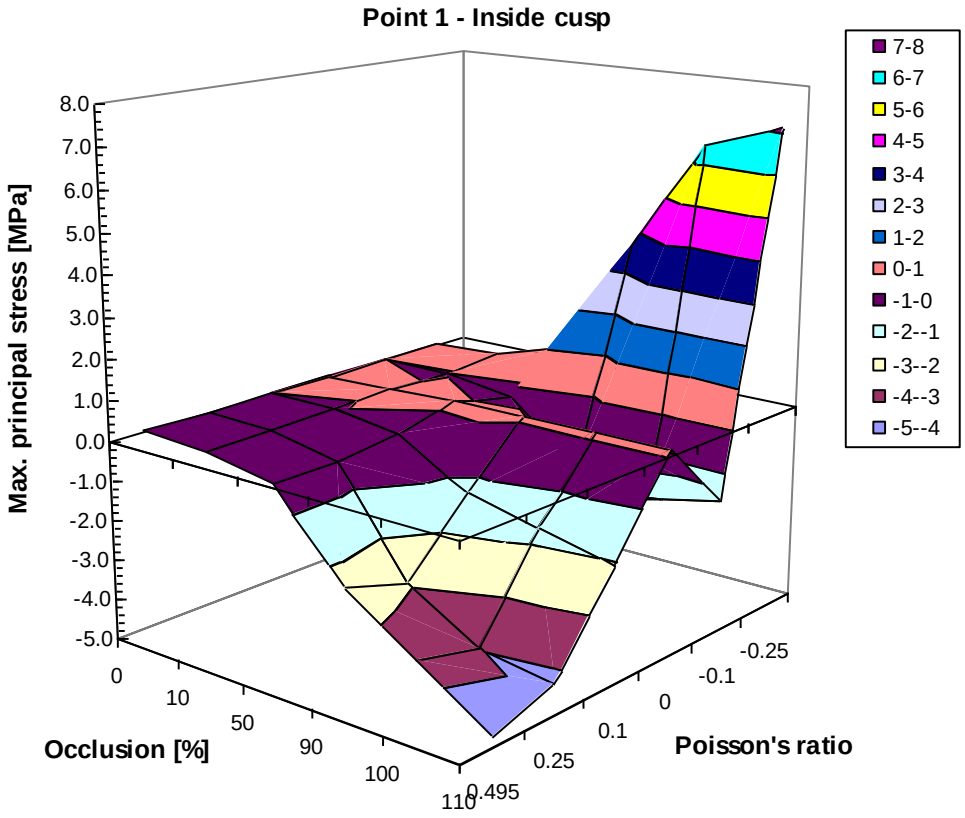

Figure 5.7: Maximum principal stresses in the inside cusp (point 1) related to the level of occlusion and the Poisson's ratio.

Figure 5.7 shows the maximum principal stresses in the inside cusp (point 1) in relation to the level of occlusion and the Poisson's ratio (ν). Similar figures of the other three points can be found in the Appendix (Figures A14, A18 and A22). From these figures can be seen that for full occlusion (110%):

- Inside cusp: optimum results for $\nu = 0$; worst results for $\nu = +0.495$ and $\nu = -0.25$
- Outside cusp: optimum results for $\nu \leq +0.25$; worst results for $\nu = +0.495$
- Inside top/bottom: optimum results for $\nu \leq +0.25$; worst results for $\nu = +0.495$
- Outside top/bottom: optimum results for $\nu = 0$; worst results for $\nu \geq +0.25$ and $\nu = -0.25$

In this situation, the auxetic effect can most clearly be seen in point 1 (inside cusp) and point 4 (outside top/bottom). These areas are in full compression for a tube with

a conventional rubberlike material (ν = +0.495) as the maximum principal stress is negative. With an auxetic (ν = –0.25) material however tensile stresses appear as well. The material in these points pulls at the surrounding material when it densifies under the overall compression during occlusion. That there is still compression at these points will become clear from the minimal principal stresses shown in the next section.

5.3.2 Minimum principal stress

Figure 5.8 shows the minimum principal stresses in the inside cusp (point 1) in relation to the level of occlusion and the Poisson's ratio. Similar figures of the other three points can be found in the appendix (Figures A15, A19 and A23). In here it can be seen that for full occlusion (110%):

- Inside cusp: optimum results for ν = –0.1 and ν = +0.1; worst results for ν = +0.495
- Outside cusp: optimum results for ν = +0.495; worst results for ν = –0.25
- Inside top/bottom: optimum results for ν = 0; worst results for ν = +0.495
- Outside top/bottom: optimum results for ν = 0; worst results for ν = +0.495

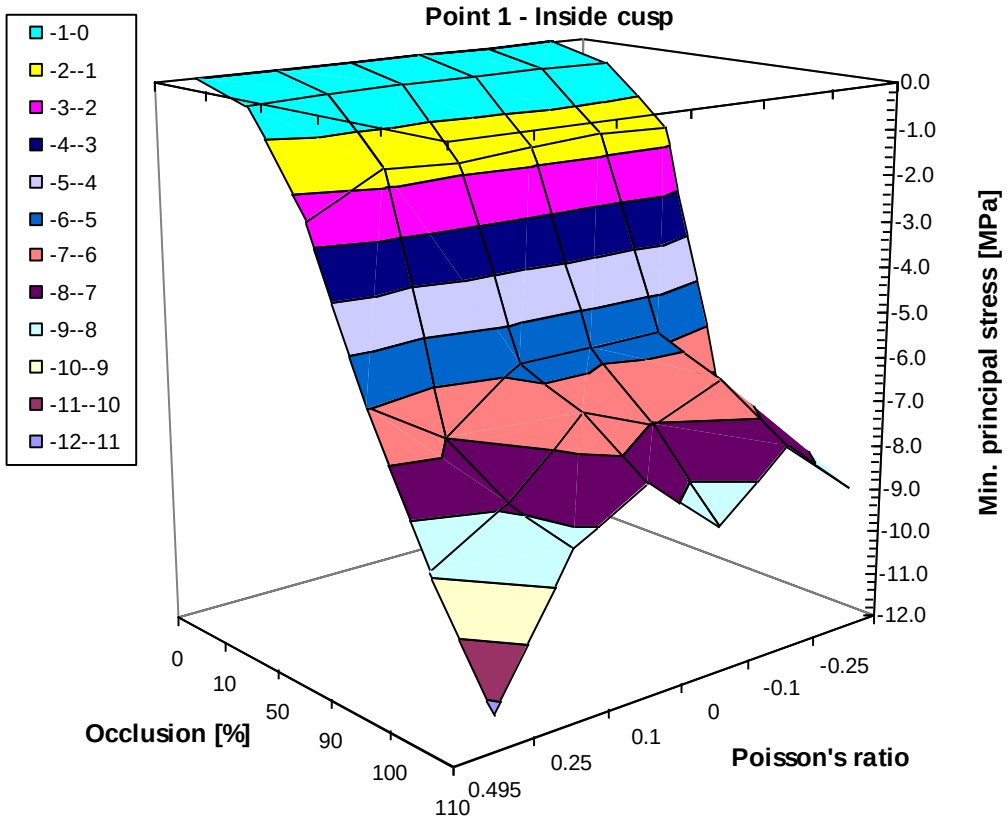

Figure 5.8: Minimum principal stresses in the inside cusp (point 1) related to the level of occlusion and the Poisson's ratio.

It can be seen that compression is present for these 4 points. It is then interesting to see what the absolute difference is between the maximum and minimum principal stress for each point, which is shown in Figure 5.9. As a general trend the difference becomes smaller or remains the same with decreasing Poisson's ratio. As already mentioned in the previous section, in point 1 and 4 there is a sign change in the maximum principle stress causing the difference to go up dramatically. This sign change, where the stresses partially change from compression to tension should be avoided. Depending on the direction of the stresses this may cause extra shear in the material making it more susceptible to crack propagation.

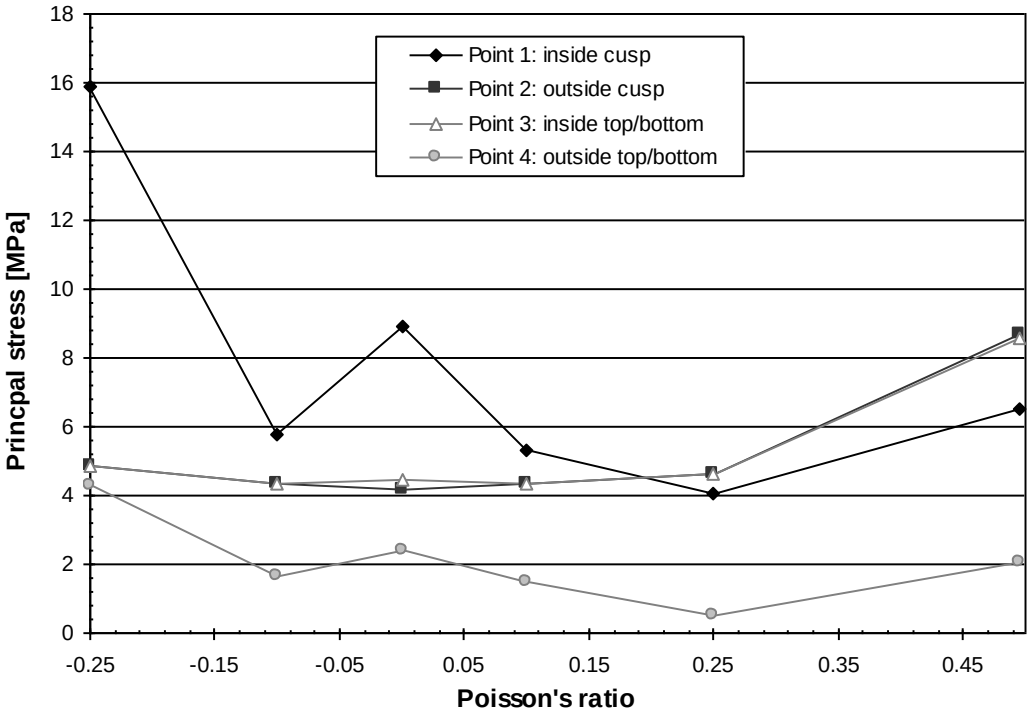

Figure 5.9: Difference between maximum and minimum principal stress for the four points in the cross-section of the peristaltic tube.

5.3.3 Maximum principal strain

Just like for the stresses, also the strains in the cross-section of a peristaltic tube should be as low as possible. A lower strain in the material under the same deformation means a lower strain energy density. This is important in fatigue resistance of the material as a lower strain energy density will lower crack propagation. Figure 5.10 shows the maximum principal strains in the inside cusp (point 1) in relation to the level of occlusion and the Poisson's ratio. Similar figures of the other three points can be found in the appendix (Figures A16, A20 and A24). In here it can be seen that for full occlusion (110%):

– Inside cusp: optimum results for $\nu \leq +0.1$; worst results for $\nu = +0.495$

– Outside cusp: optimum results for $\nu \leq +0.1$; worst results for $\nu = +0.495$
– Inside top/bottom: optimum results for $\nu \leq +0.1$; worst results for $\nu = +0.495$
– Outside top/bottom: optimum results for $\nu \leq +0.25$; worst results for $\nu = +0.495$

In terms of the maximum principal strain the conventional rubberlike material is shows the worst behaviour in all four points. Lowering the Poisson's ratio quickly brings the maximum principal strains to a much lower level.

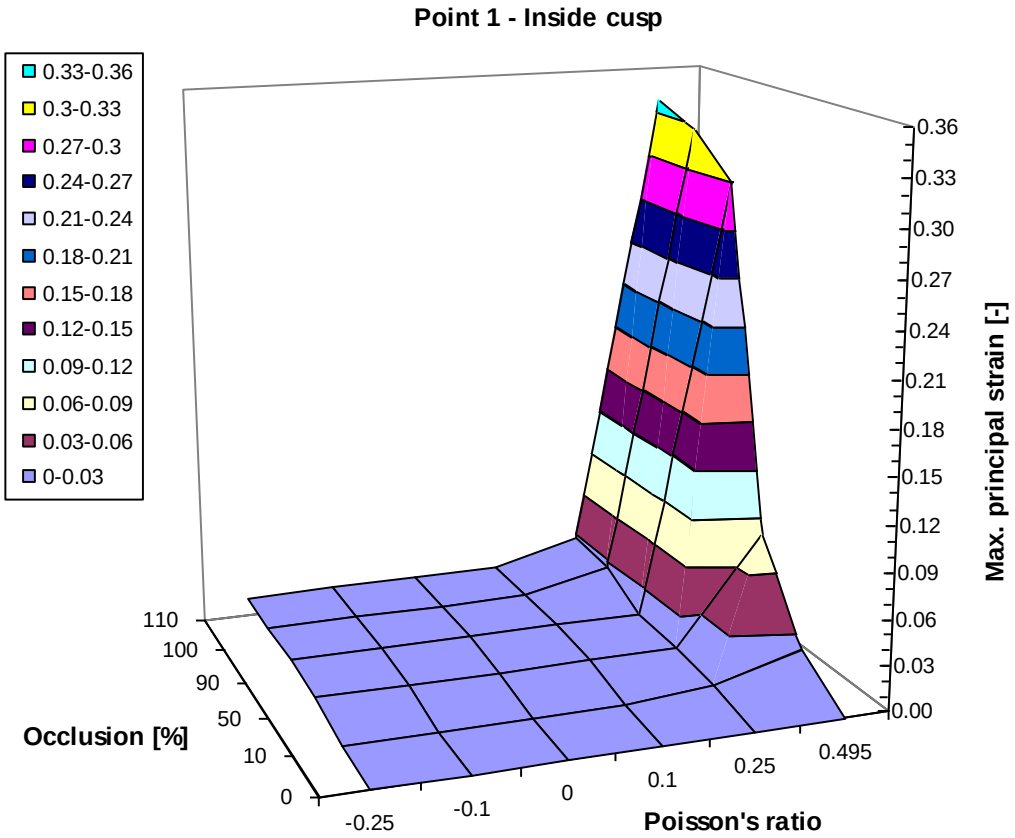

Figure 5.10: Maximum principal strains in the inside cusp (point 1) related to the level of occlusion and the Poisson's ratio.

5.3.4 Minimum principal strain

Figure 5.11 shows the minimum principal strains in the inside cusp (point 1) in relation to the level of occlusion and the Poisson's ratio. Similar figures of the other three points can be found in the appendix (Figures A17, A21 and A25). In here it can be seen that for full occlusion (110%):

– Inside cusp: optimum results for $\nu = +0.495$; worst results for $\nu = -0.25$
– Outside cusp: optimum results for $\nu \leq +0.1$; worst results for $\nu = +0.495$
– Inside top/bottom: optimum results for $\nu = -0.25$; worst results for $\nu = +0.495$

– Outside top/bottom: optimum results for $\nu \leq +0.495$; worst results for $\nu \leq +0.25$

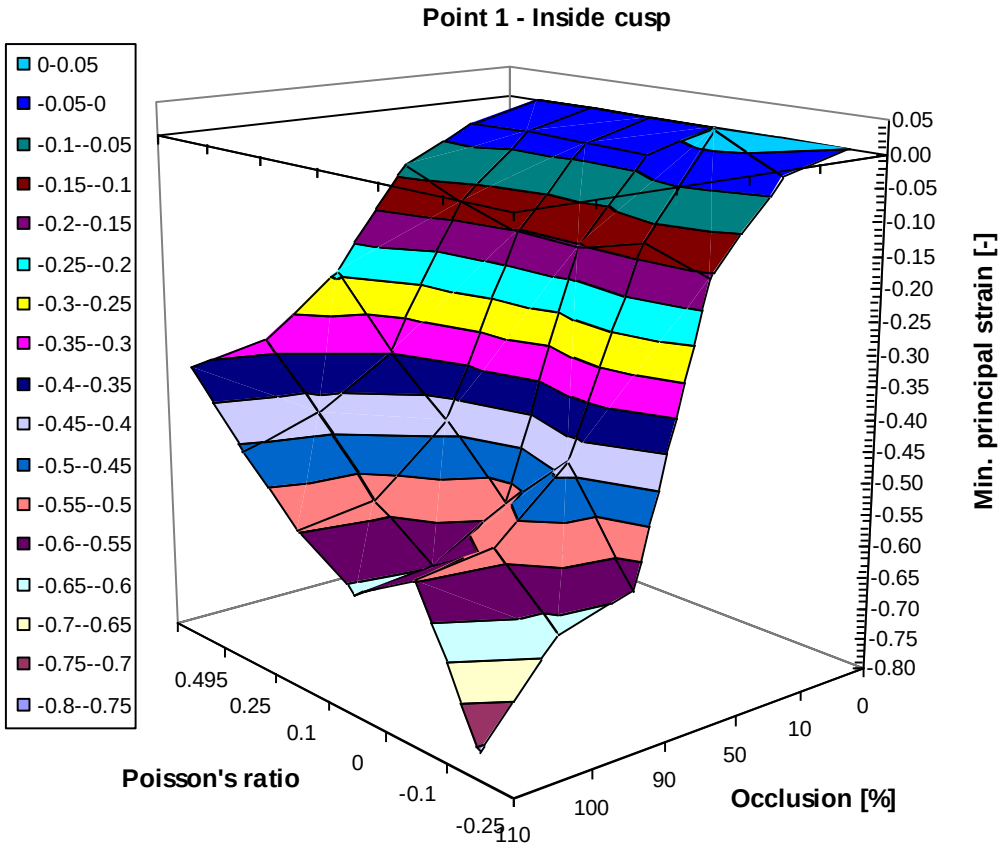

Figure 5.11: Minimum principal stresses in the inside cusp (point 1) related to the level of occlusion and the Poisson's ratio.

For the minimum principal strains the picture is less clear as for the maximum principal strains. When lowering the Poisson's ratio the minimum principal strains increase at points 1 and 4, while the opposite is the case for points 2 and 3.

To clarify the situation for the strains, a similar picture as above for the principal stresses is shown for the difference in maximum and minimum principal strains in Figure 5.12. The general trend here is also that the difference lowers of remains the same when lowering the Poisson's ratio. Only point 1 goes through a low between the extreme values of +0.495 and –0.25.

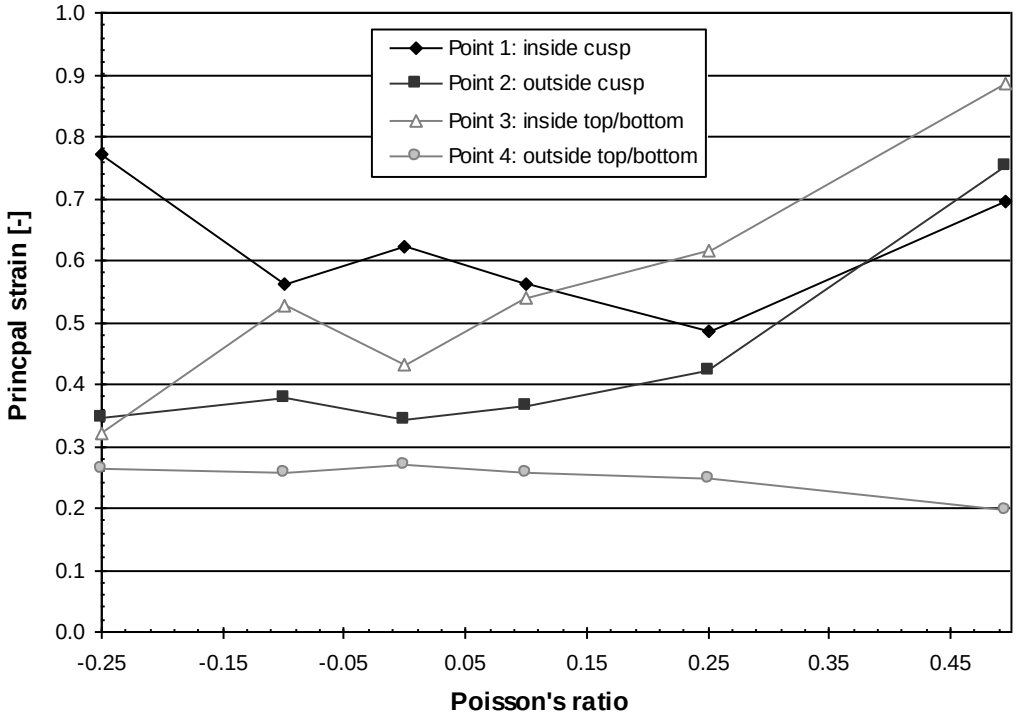

Figure 5.12: Difference between maximum and minimum principal stress for the four points in the cross-section of the peristaltic tube.

5.3.5 Conclusions

Lowering the Poisson's ratio of a peristaltic tube material has a great effect on the stress and strain levels in a peristaltic tube. Already a small decrease shows positive effects on the overall stress and strain levels in the cross-section of the tube. However, lowering the Poisson's ratio too much (i.e. too negative) will cause several benefits to diminish or make it even worse. The best results are obtained for a material with a Poisson's ratio between –0.1 and +0.1, with a preferable value of 0.

Based on this significant improvements are expected when a peristaltic tube is manufactured from a material with a lower Poisson's ratio than the conventional elastomers. However, rubberlike materials will still be necessary for peristaltic tubing because of the recovering properties after occlusion. In order to lower the Poisson's ratio of the peristaltic tube material an auxetic component has to be added.

6 Flat sheet laminate structures

This chapter describes the materials and the manufacturing process used for the production of flat sheet samples. Flat sheets are chosen first as this is the easiest geometry to produce laminates by simply stacking layers up to a desired thickness. This gives the opportunity to learn and get some skill in the lamination process before attempting to produce tubular samples. Besides this, flat sheets are also more useful to cut specimens from for characterisation and testing. This characterisation and testing for the determination of several material properties of the flat sheet samples is discussed in the final section of this chapter.

6.1 Materials

Electrospun nylon6 nanofibre membranes are purchased from eSpin Technologies, Inc. (Chattanooga, TN, USA) in two thicknesses, 25 µm and 50 µm. They were supplied on silicone release paper in sheets of 30.5 x 101.6 cm (12" x 40").
Figure 6.1 shows Scanning Electron Microscopy (SEM) images of the electrospun nylon6 nanofibres. These, and all other SEM images in this chapter, are made with a Field Emission Scanning Electron Microscope (JEOL, JSM6301F) using samples sputter coated with gold in order to minimise surface charging. From the images can be derived that the typical fibre thickness is between 100 nm and to 1 µm and pore sizes are up to around 2 µm.

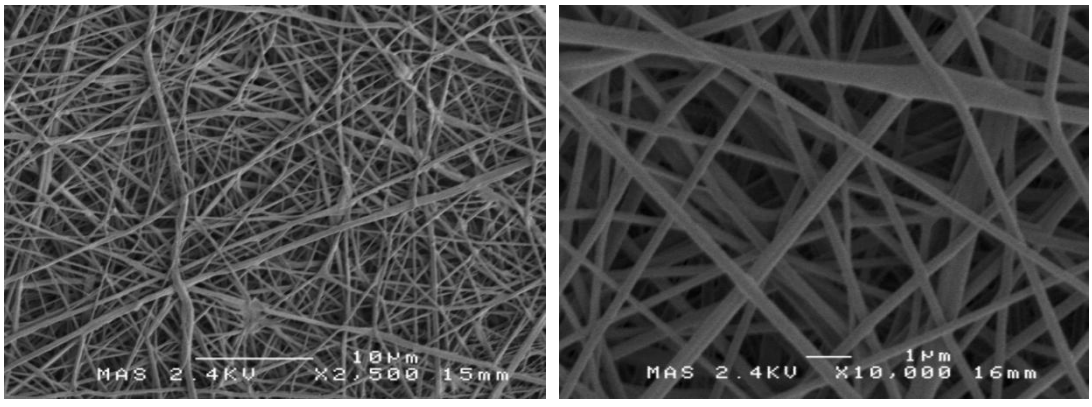

Figure 6.1: Scanning Electron Microscopy images of the used electrospun nylon6 nanofibres.

Platinum curing liquid silicone rubber Elastosil® LR 3043-50 is obtained from Wacker Silicones (Munich, Germany). This liquid silicone rubber is supplied in two components, A and B, which have to be mixed in a 1:1 ratio to get the curable compound. The LR 3043-50 is a shear thinning paste-like substance (dynamic

viscosity, η = 1,200 Pa·s at shear rate 0.9 s^{-1}; η = 0.43 Pa·s at shear rate 10 s^{-1}) and it cures to a hardness of 50 Shore A [170].

6.2 Manufacturing of flat sheets

6.2.1 Preparation

For the manufacturing a steel compression mould is made to produce flat sheets with dimensions of 14 x 14 cm and a height of 2 mm. The total mould consists of five components and is designed in such a way that it ensures convenient handling, no premature scorch and/or curing of the silicone rubber, but also with the possibility to keep the overall temperature of the compression mould as close to the curing temperature. A schematic view of the compression mould is given in Figure 6.2.

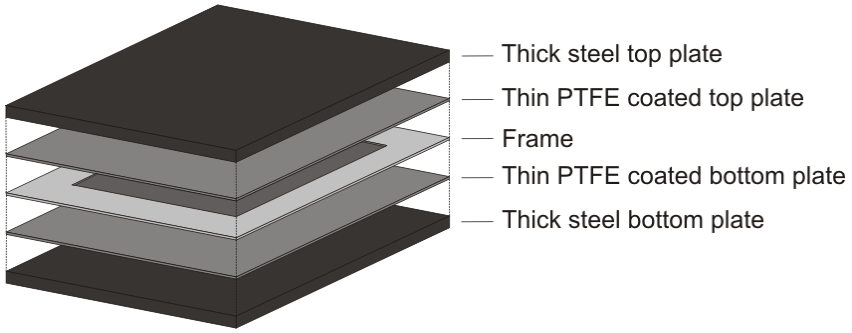

Figure 6.2: Schematic view of the five component compression mould used to manufacture the flat sheet materials.

The sheets of the electrospun nylon6 were cut along their length in two strips of 14 cm wide, to be of the same width as the frame in the mould.

The liquid silicone rubber compound is prepared by thoroughly mixing equal amounts of the components A and B in a plastic container for about 10 minutes using a spatula. The entrapped air, visible as air bubbles in the rubber mixture, is then removed through degassing under vacuum.

6.2.2 Fabrication of the flat sheet laminate

The thick steel top and bottom plate are put in a hydraulic press (Moore, Birmingham, England) and the press is closed to heat up to the curing temperature. On the thin PTFE covered bottom plate some of the silicone rubber was dropped and rolled out to an area of 14 x 14 cm in the centre of the plate. This is done to also have silicone rubber as the bottom layer, because the nylon6 will only be coated at one side. Then the frame was put on this thin bottom plate.

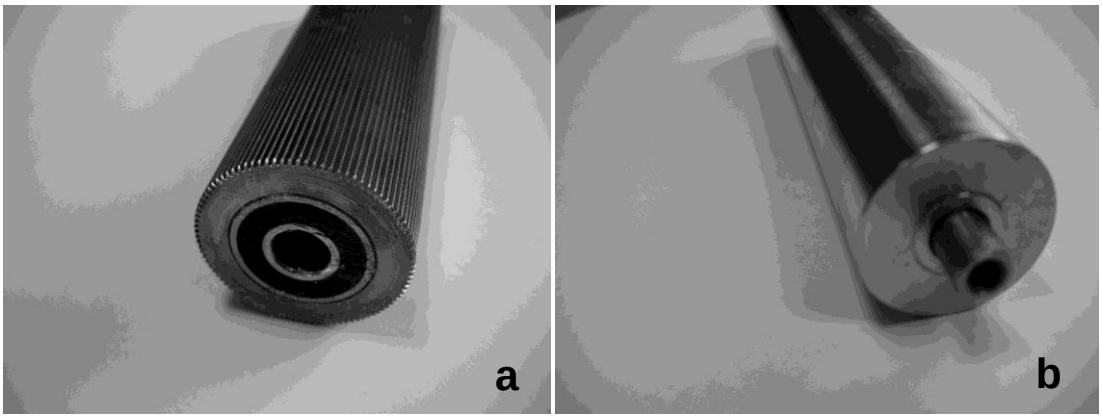

Figure 6.3: The gravure roller (a) and smooth roller (b) used for laminating the electrospun nylon6 with silicone rubber.

The electrospun nylon6 was removed from the release paper and laid on non-sticky paper for the laminating process. The silicone rubber was applied to the electrospun nylon6 by a variety of gravure coating. A gravure roller (see Figure 6.3a) was covered in the silicone rubber and this was manually rolled on the nylon. A smooth roller (see Figure 6.3b) was subsequently used to even out the silicone rubber on the surface. This laminating process has to be done carefully and not applying too much shear in the silicone rubber, i.e. push the roller too much into the membrane when rolling. When this happens it will cause the nylon6 to contract dramatically when the silicone chains relax back to their unstretched state.

An example of how this looks like is shown in Figure 6.4. Additionally, it also turned out that it was only possible to produce laminates with the 50 µm thick nylon6 membranes. The thinner membranes with a thickness of 25 µm were not strong enough to handle the application of the highly viscous silicone rubber. The now coated electrospun nylon6 strips are cut in pieces of around 14 cm and are then stacked on top of each other in the frame of the compression mould. After 14 layers of silicone rubber coated nylon6 the frame was full. The thin PTFE covered top plate was put on the frame and all was put in the hydraulic press between the preheated thick plates for curing. Curing was done for 5 minutes at 165 °C and a pressure of

Figure 6.4: Contraction of the electrospun nylon6 due to relaxation of the silicone rubber polymer chains after applying the silicone rubber with too much shear.

10 MPa. After curing the nylon6 – silicone rubber laminate was removed from the mould and put in an oven for post-curing.

Recommended post-curing conditions from the supplier are 4 hours at 200 °C. This temperature however is very close to the melting temperature for nylon6. Therefore the post-curing temperature is lowered to 175 °C. However, when removing the laminate from the oven its colour had changed from white to brown indicating strong degradation of the nylon6. For this reason the post-curing conditions have been lowered further to 2 hours at 150 °C. This resulted in a laminate with a slightly yellowish colour. This may still indicate that a little degradation has taken place, but the integrity of the laminate looked good. Whether there is degradation and if this amount really is an issue to the laminate's performance has to be taken into account when interpreting test results. For both post-curing conditions also a plate of pure silicone rubber is made as a reference material for the tests described in section 6.3. So in total, four flat sheets have been produced and they are coded as follows (see also Figure 6.5):

- B50-175: Laminate with 50 µm nylon6, sheet B, post-cured at 175 °C
- 0-175: Silicone rubber LR 3043-50, post-cured at 175 °C
- C50-150: Laminate with 50 µm nylon6, sheet C, post-cured at 150 °C
- 0-150: Silicone rubber LR 3043-50, post-cured at 150 °C

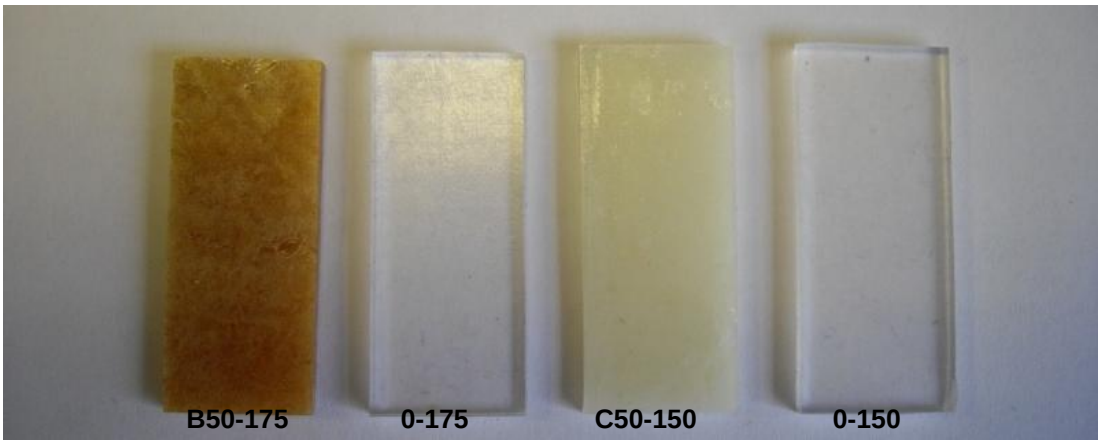

Figure 6.5: The four produced flat sheet materials, the laminates B50-175 and C50-150 and the pure silicone rubber 0-175 and 0-150.

6.3 Characterisation and testing

The flat sheets produced as described in the previous section 6.2 are subjected to several tests in order to assess their properties. First the cross-section of the laminate C50-150 is analysed by Scanning Electron Microscopy to produce a visual characterisation of the laminate. Secondly tensile tests are done on all four of the flat sheet materials and the through-the-thickness Poisson’s ratio is determined for

the laminate C50-150 as well as the silicone rubber 0-150 as comparison. Further tests involve the determination of the hardness and tear strength of all four flat sheet materials. The tearing crack surface of laminate C50-150 is further analysed with SEM. Conclusively, on the laminate C50-150 and the silicone rubber 0-150 Dynamical Mechanical Analysis is done for a more in depth analysis of the dynamic-mechanical response of these materials.

6.3.1 Scanning Electron Microscopy

Scanning Electron Microscopy (SEM) is done on a cross-section of the C50-150 laminate in order to see how the nylon6 layers are positioned and how well the bonding is between the silicone rubber and the nylon6.

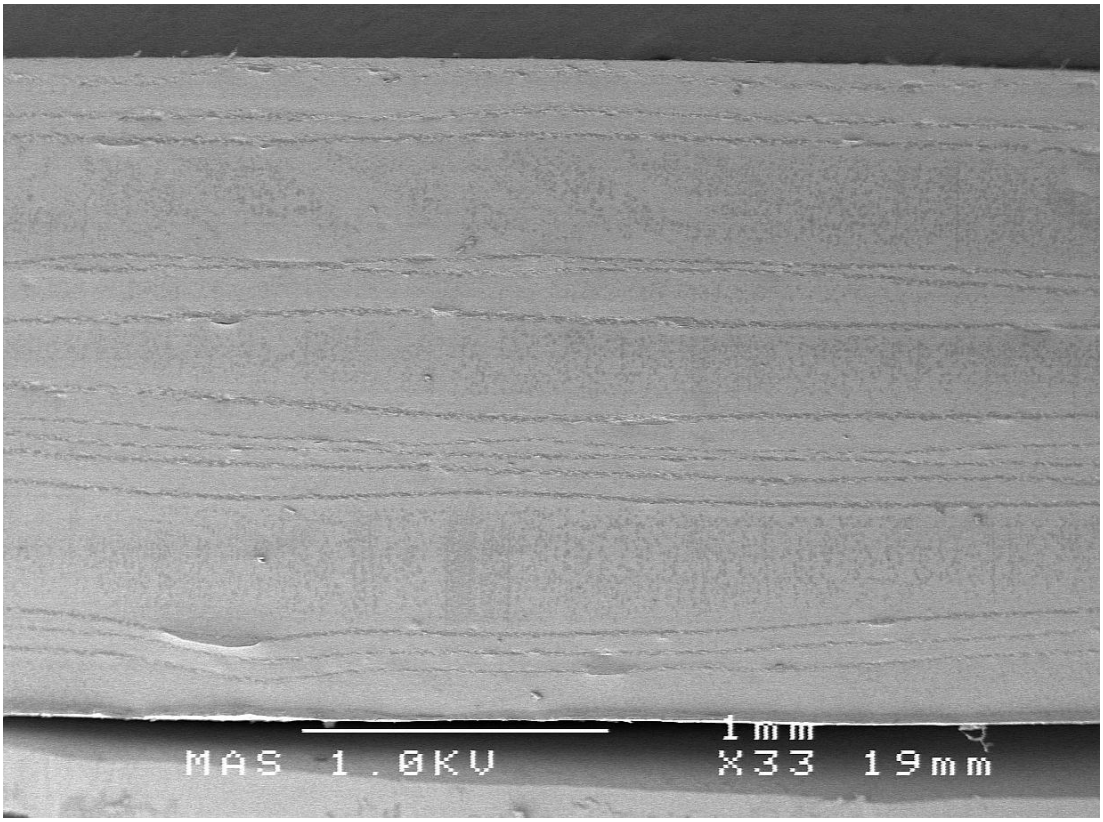

Figure 6.6: SEM image of the cross-section of the laminate C50-150.

Figure 6.6 shows a low magnification image (33x) of the cross-section. The 14 layers of electrospun nylon6 can easily be identified. It is also clear that the nylon6 layers are not uniformly distributed through the thickness of the laminate. Apparently not all nylon6 layers were coated with the same amount of silicone rubber. In the manual process described in section 6.2.2 it is indeed difficult to apply the same amount of silicone rubber to the membrane. It is likely that the nylon6 layers separated with the thicker layers of silicone rubber are the ones coated where a new

amount of silicone rubber is applied to the gravure roller. From this image and Figure 6.7a can also be derived that the thickness of the electrospun nylon6 layers are reduced to around 25-35 µm, a reduction of 30-50%.

Zooming in on the interface between the silicone rubber and nylon6 shows an intimate bonding between the two as can be seen in Figure 6.7a-c. The silicone rubber seems to wet the nylon6 nanofibres very well. More evidence for this is discussed in section 6.3.5 where the crack surface of this laminate is examined. Figure 6.7d shows the electrospun nylon6 at high magnification (90,000x) around an air bubble, which is drawn out by the degassing vacuum required for SEM sample preparation. The nylon6 fibres are strongly deformed and compressed. Whether the number of layers and the nylon6 fibre deformation are sufficient to lower the through-the-thickness Poisson's ratio will be tested and the results for this are described in section 6.3.3 below.

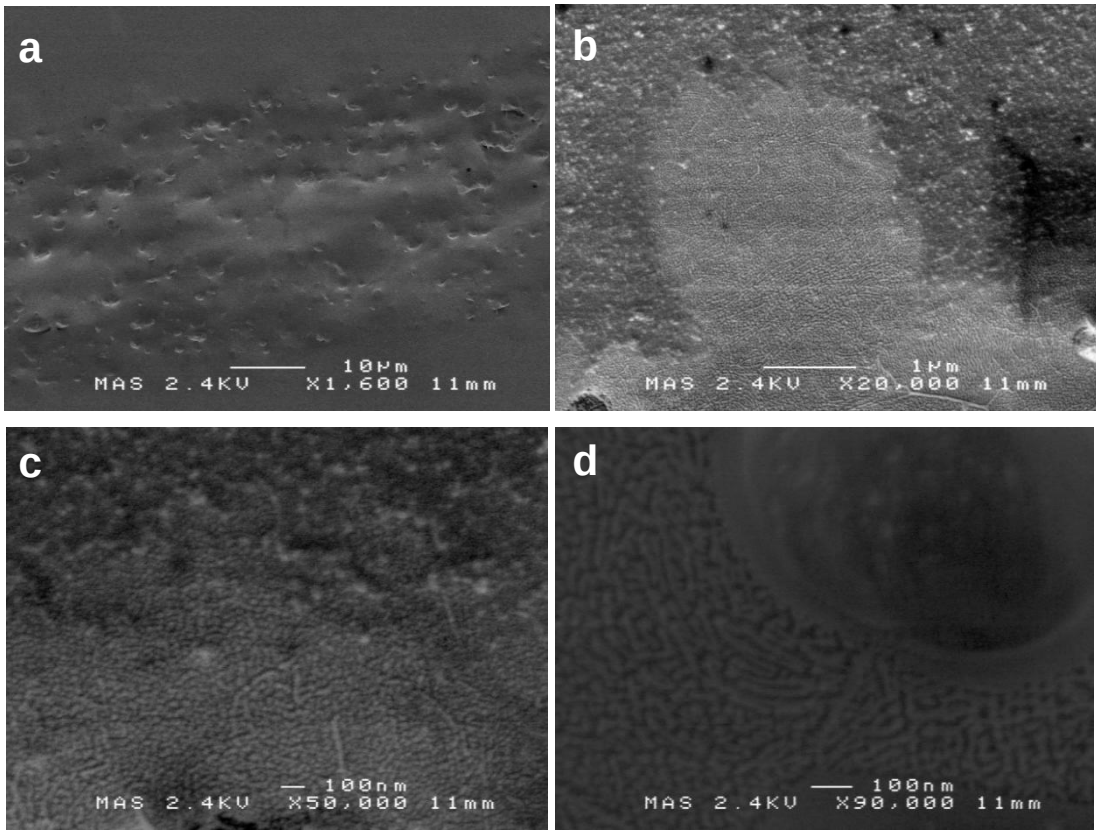

Figure 6.7: SEM images of the interface between the silicone rubber and the electrospun nylon6 (a-c) and a close up of the electrospun nylon6 surrounding an air bubble (d).

6.3.2 Mechanical properties

The mechanical properties of all four flat sheet materials are determined using an Instron 3369 tensile machine. The procedure for the tensile tests is carried out according to ISO 37 [171], using the type 2 dumbbell test pieces. The crosshead speed is 500 mm/min. Because of the combined measurement with the through-the-thickness Poisson's ratio no extensometers are used. Instead the displacement of markings on the side of each specimen is monitored by a high-speed camera and this is used to calculate the real strain in the specimen. For further details, see section 6.3.3. The results of the tensile tests are shown in Figure 6.8 for the laminate B50-175 and in Figure 6.9 for the laminate C50-150 and some of the mechanical properties are summarised in Table 6.1. For both laminates, the electrospun nylon6 layers show a reinforcing effect at lower strains.

As expected, the degraded laminate B50-175 performs significantly less than laminate C50-150, losing strength more quickly. The bonding between the layers of B50-175 is poor causing delamination and fracture of several layers before complete failure of the specimen. Laminate C50-150 however shows a reinforcing effect over a much larger strain range. The cross-over point with silicone rubber 0-150 is at around 150% strain and after this point only loses up to 10% strength until (initial) fracture. It is also clear from the scatter between the stress-strain curves

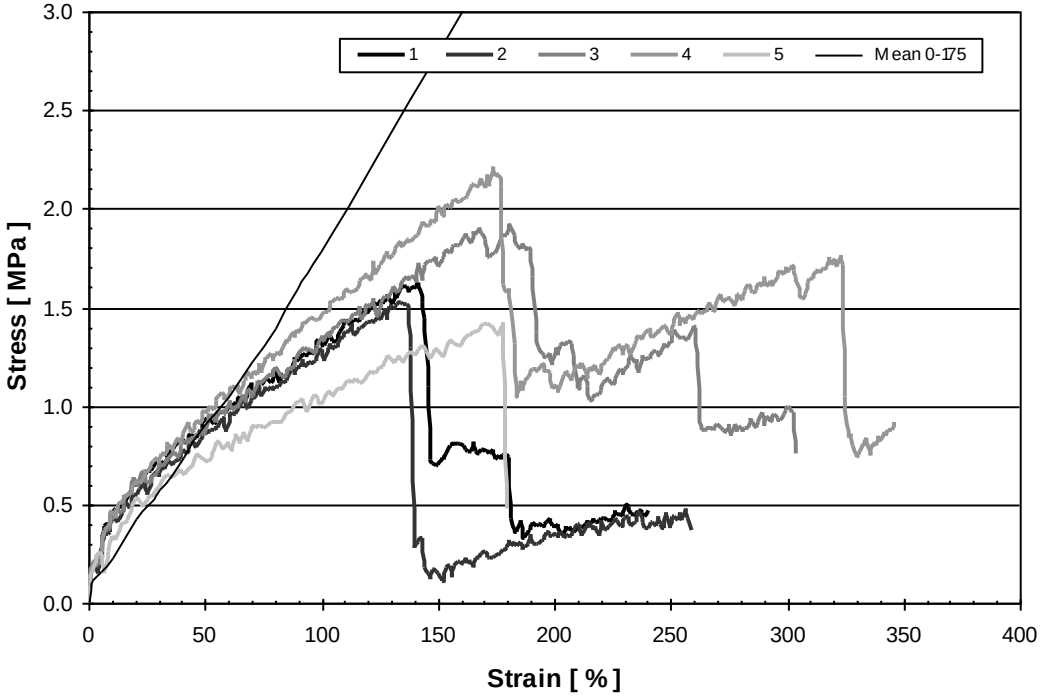

Figure 6.8: Stress-strain curves for 5 specimens of laminate B50-175. The mean curve for the pure silicone rubber material (0-175) is depicted as the thin black line.

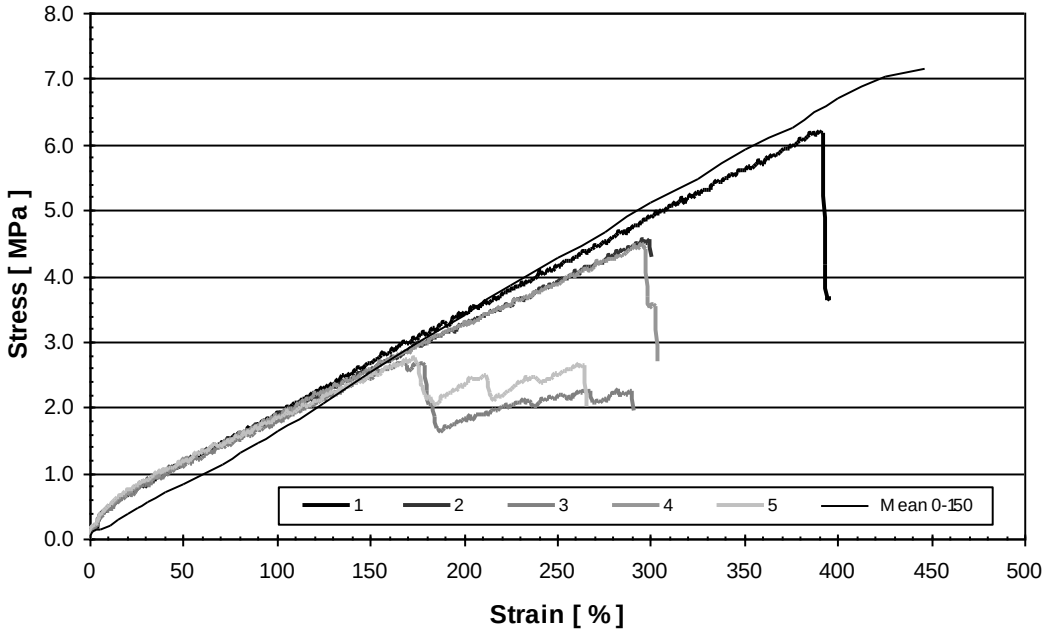

Figure 6.9: Stress-strain curves for 5 specimens of laminate C50-150. The mean curve for the pure silicone rubber material (0-150) is depicted as the thin black line.

that there are inconsistencies in the manufacturing. A likely cause is that the layer thicknesses are not constant throughout the flat sheet resulting in different stress profiles in the cross-section of the dumbbell test pieces.

Property [MPa]	**Laminate B50-175**	**Sil. rubber 0-175**	**Laminate C50-150**	**Sil. rubber 0-150**	**Data sheet LR 3043-50** [170]
Young's modulus	11	9	12	9	–
Modulus @ 10%	0.40 ± 0.02	0.23 ± 0.02	0.47 ± 0.03	0.22 ± 0.01	–
Modulus @ 50%	0.83 ± 0.05	0.90 ± 0.02	1.1 ± 0.04	0.85 ± 0.05	–
Modulus @ 100%	1.3 ± 0.10	1.8 ± 0.02	1.9 ± 0.05	1.7 ± 0.06	–
Modulus @ 300%	–	5.6 ± 0.07	4.9 ± 0.7	5.1 ± 0.12	–
Tensile strength	1.7 ± 0.3	7.9 ± 0.4	4.1 ± 1.5	7.2 ± 0.5	9.1
Strain at break [%]	158 ± 23	434 ± 23	268 ± 92	446 ± 38	470

Table 6.1: Mechanical properties of the four flat sheet materials.

For the ease of comparison, mean stress-strain curves of all four flat sheet materials are constructed and shown in Figure 6.10. Besides the influence of the electrospun nylon6 reinforcement it is also clear that the post-curing conditions affect the

mechanical properties of the silicone rubber. It is indeed a well known effect that post-curing improves several mechanical properties in silicone rubbers. Volatiles present in the rubber matrix are driven off and the silicone rubber network density is improved. This makes the silicone rubber product more elastic, improving tensile strength, compression set and tear resistance [172].

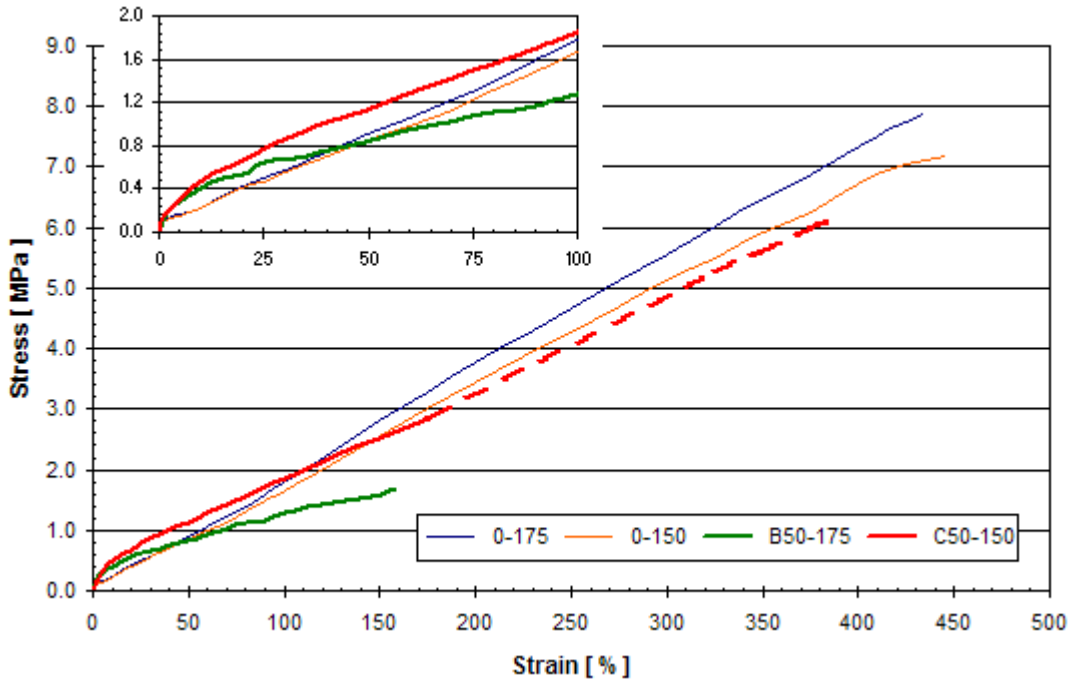

Figure 6.10: Mean stress-strain curves for the four flat sheet materials.

6.3.3 Through-the-thickness Poisson's ratio

Simultaneously with the tensile properties the change in thickness during the extension of the specimens is also measured. Displacements of dotted markings on the side of the specimens are monitored with a 1 Megapixel high speed camera (Photron Fastcam S3) at a rate of 60 frames per second. The resulting 8 bit black/white images are analysed using CorelDRAW Graphics Suite 12 software by counting the change in number pixels between the centres of the markings for the displacement in the vertical direction. For the horizontal (thickness) direction the edge-to-edge distance is taken through markings in the middle of the specimen's length. Through-the-thickness Poisson's ratios are calculated using equation (2.4) and the results are shown in Figure 6.11 as a function of the vertical strain for the laminate C50-150 and the pure silicone rubber 0-150. The data points are the individual measurements for each specimen and the solid line is the average of these data points. It must be noted that at a vertical strain of 0 there is of course no lateral deformation and the Poisson's ratio then is also 0. In Figure 6.11, for small

vertical strains, the through-the-thickness Poisson's ratio value is going to infinity. This is a consequence of the mathematical definition of the Poisson's ratio causing a singularity when limit of the vertical strain goes to 0.

A clear difference can be seen between the pure silicone rubber 0-150 and the laminate C50-150, especially at lower strains. The electrospun nylon6 reinforcement causes the through-the thickness Poisson's ratio of the laminate to lower considerably. At higher strains this effect diminishes similar to the other mechanical properties as discussed in the previous section. The other laminate, B50-175, did not show a lowering in the through-the-thickness Poisson's ratio, but followed a similar line as the silicone rubber. The degradation of the nylon6 and the lack of intimate bonding between the layers caused this laminate to lose this property. Looking at Figure 6.11 the question arises what happens at the lower strains for the laminate. From the images no change in thickness change could be seen for about the first 10% of vertical strain. This explains the many data points at zero Poisson's ratio. Obviously, the detectable change in dimensions is limited by the resolution of the camera. Higher resolution images are required to resolve these points at the zero Poisson's ratio line in more detail. This may result in negative Poisson's ratios, i.e. auxetic behaviour of this laminate.

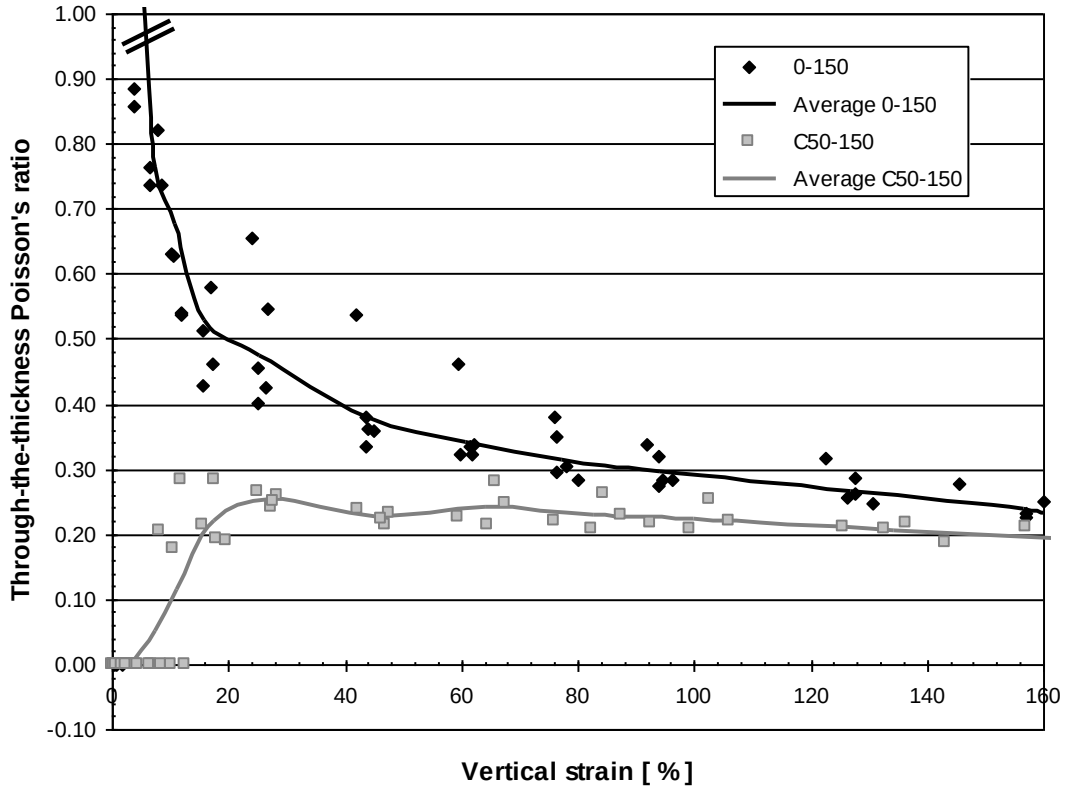

Figure 6.11: The through-the-thickness Poisson's ratio of the silicone rubber 0-150 and the laminate C50-150 as a function of the applied vertical strain.

That a non-uniform laminate as this C50-150 already shows a considerable drop in the through-the-thickness Poisson's ratio it can be expected that this effect becomes more pronounced when the layers are more evenly spaced and more layers of the electrospun nylon6 are present. Other electrospun materials could have more or less effect as well depending on their stiffness.

6.3.4 Hardness

The (indentation) hardness of a material is a measure of its resistance to penetration and is dependent on the material's Young's modulus. Besides this material property, the penetration depth is also dependent on the shape of the penetrating body and the type of loading. In order to make measuring devices for the hardness of a material that are reproducible, these two are standardised.
For rubber materials most commonly the Shore-Hardness method is used to determine the hardness. The penetrating body, the indenter, is a truncated cone which is connected to a calibrated leaf spring in the measuring device. The amount of deflection of this spring is a measure of the hardness of the material. Soft rubbers are measured with a Shore A instrument and harder rubbers with a Shore D instrument, the two differing in the detailed shape of the indenter and stiffness of the spring [173].

As mentioned in section 2.2, auxetic behaviour increases the indentation hardness [44,57]. This is due to densification of the material around the penetrating body, increasing its apparent Young's modulus. To see if the electrospun nylon6 in the manufactured laminates also produces this effect, hardness measurements are done.

The indentation hardness of all the four flat sheet materials is measured using a handheld durometer type A (Rex Gauge, Model 1600). Durometer hardness measurements require a samples thickness of at least 6 mm. Since the thickness of the flat sheets is only just over 2 mm, three samples from the flat sheet are stacked to reach the required thickness, as is allowed by the standard [174]. The results of the hardness measurements are shown in Table 6.2.

	Laminate B50-175	**Silicone rubber 0-175**	**Laminate C50-150**	**Silicone rubber 0-150**
Hardness [Shore A]	53	53	57	51

Table 6.2: Hardness of the four flat sheet materials.

No difference in indentation hardness could be found between the laminate B50-175 and the pure silicone rubber 0-175. Any effect on the hardness from the electrospun nylon6 reinforcement here is gone. For the other laminate however, a clear increase in indentation hardness is observed. It is not completely clear whether this could be just an effect of the presence of the electrospun nylon6 layers, or that these layers really cause some auxetic behaviour in the laminate C50-150. Supporting evidence for the latter comes from the tensile tests and the determination of the through-the-thickness Poisson's ratio described in the previous two sections. From these tests was found that the laminate B50-175 still shows a reinforcing effect of the electrospun nylon6, despite of it being somewhat degraded. Since the nylon6 is still contributing to the laminate B50-175's mechanical properties, it is to be expected to add to the hardness as well just due to its presence. This however is not observed in the measurements. Besides this, the through-the-thickness Poisson's ratio of the B50-175 laminate remained unchanged compared with silicone rubber. Combining the observations in these tests with the results found for the hardness measurements, is making it more likely that the increase in indentation hardness in laminate C50-150 is caused by auxetic behaviour.

6.3.5 Tear strength

Tear strength of the four flat sheet materials is determined according to ISO 34 [175] using an Instron 3369 tensile machine. From this standard, trouser test pieces (method A) are used. Deviating from the standard only three specimens of each material are tested. The results of the trouser tear tests are shown in Table 6.3. Again, the laminate C50-150 shows the best performance with the highest level of tear strength.

Trouser tear strength [N/mm]	**Laminate B50-175**	**Sil. rubber 0-175**	**Laminate C50-150**	**Sil. rubber 0-150**	**Data sheet LR 3043-50** [170]
Median	6.7	8.7	11.9	8.5	15
Range	8.5	9.1	4.8	6.5	–
Minimum	2.7	5.2	9.6	6.4	–
Maximum	11.2	14.3	14.4	12.9	–

Table 6.3: Results for the trouser tear strength on the four flat sheet materials.

In the trouser tear test the crack propagation should be straight through the middle of the sample. For the pure silicone rubber samples this was largely the case, but the laminates behaved differently. The crack propagation in laminate B50-175 immediately went sideways, tearing off a leg of the trouser sample. Bonding between the layers in this laminate is poor and is at several locations already delaminated. The crack propagation in laminate C50-150 was initially straight, but then showed similar behaviour as the other laminate. Delamination starts to occur in the sample and the crack goes sideways. The weakest link in the laminate structure therefore looks to be the bonding between the layers.

To investigate the bonding and delamination of the laminate C50-150 in more detail, the fracture surface from the tear test is further analysed with SEM. Figure 6.12 shows the fracture surface through the thickness of this laminate.

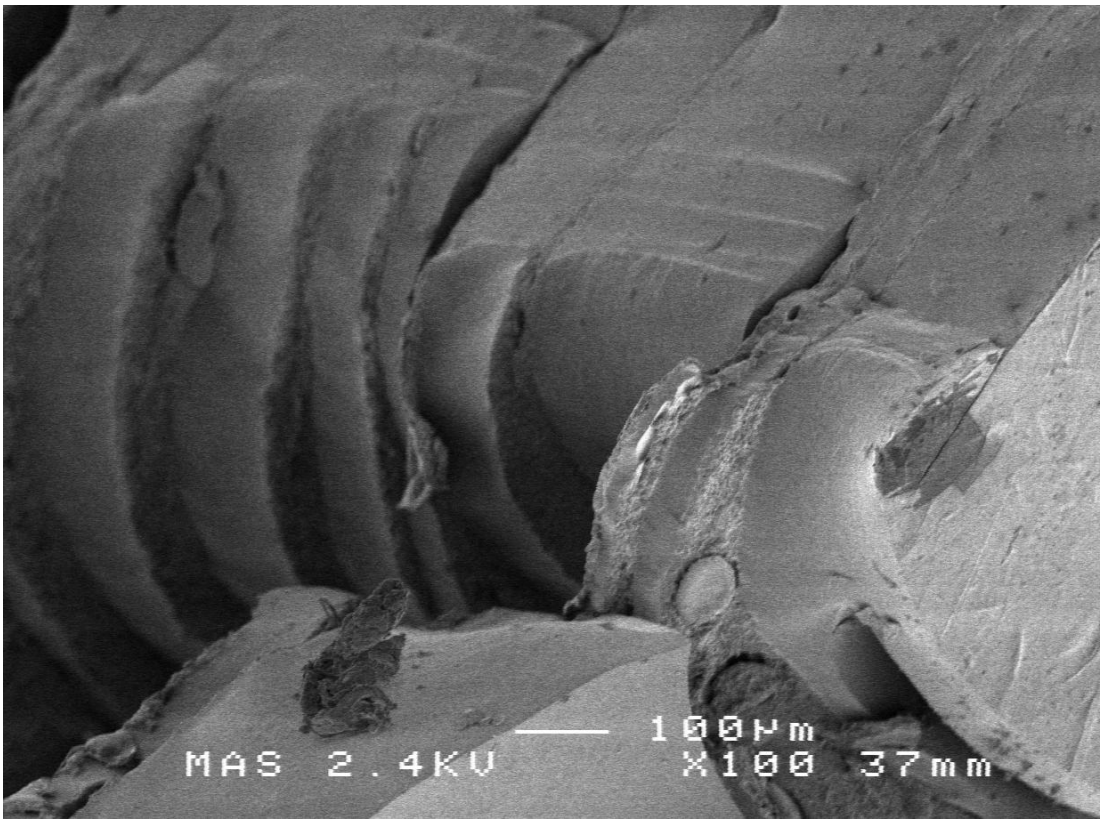

Figure 6.12: SEM image of the torn surface from the trouser tear test on the C50-150 laminate. The view is through-the-thickness clearly showing the various layers of the laminate.

A higher magnification image of this fracture surface is shown in Figure 6.13a. This part is a crack through one of the silicone rubber layers. The top left of the image shows the remains of a nylon6 reinforcement layer with nanofibres. The bottom right shows the prints of the nylon6 nanofibres in the silicone rubber. Further magnification of the top left is shown in Figure 6.13b. The nylon6 nanofibres are

indeed well covered with the silicone rubber at this location of the fracture surface. Most of the fracture surface looked like what is shown in Figure 6.13, confirming the observations from section 6.3.1: good wetting of the nylon6 nanofibres by the silicone rubber.

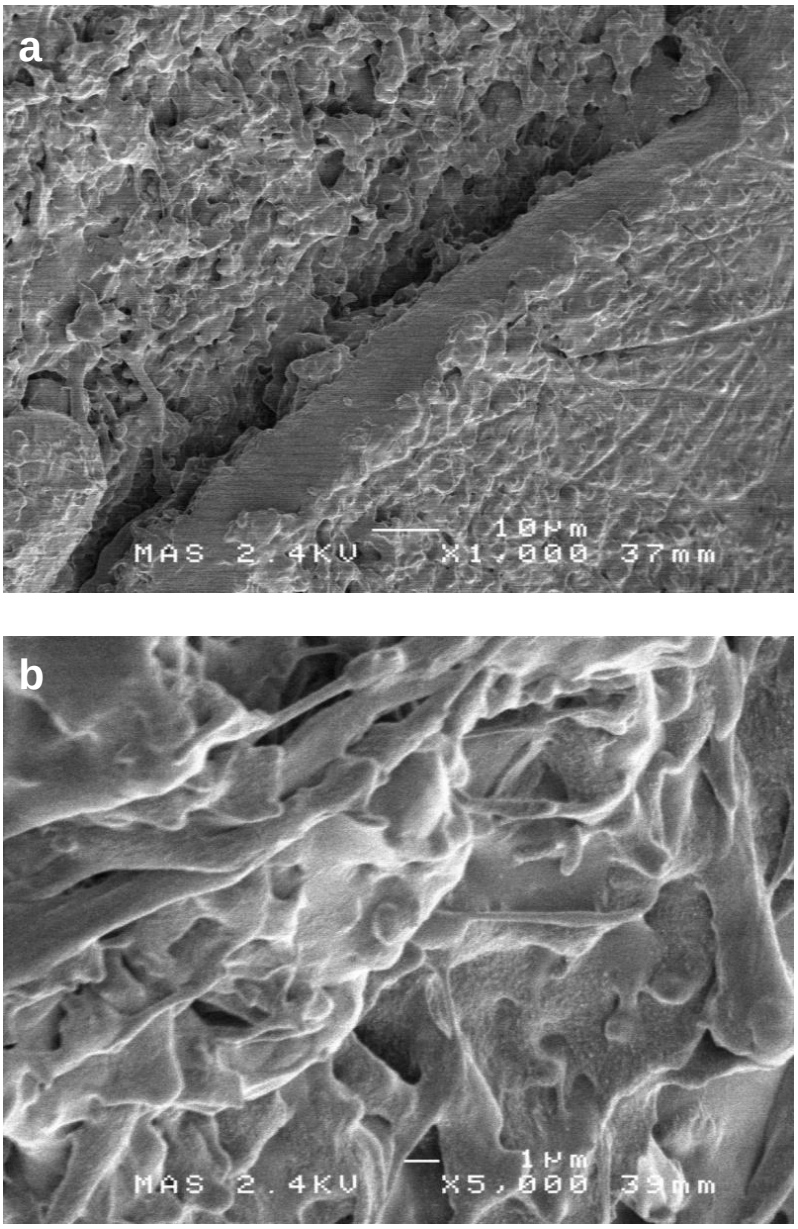

Figure 6.13: SEM images of the torn surface from the trouser tear test on the C50-150 laminate. (a) shows the fracture through a layer of the silicone rubber. In the top left and bottom right remains and prints of the nylon6 fibres are visible. (b) is a higher magnification of the fracture surface showing the nylon6 fibres coated in silicone rubber.

Where the fracture went through the nylon6 reinforcement, the nanofibres themselves are found as can be seen in Figure 6.14. These fibres look to be clean without remains of silicone rubber. Whether this is due to fibre pull-out from the silicone rubber or just lack of impregnation of the membrane is not entirely clear. What is clear, is the strong deformation of the fibres when compared to the virgin membrane (see Figure 6.1). This deformation is a prerequisite for auxetic through-the-thickness behaviour as discussed previously.

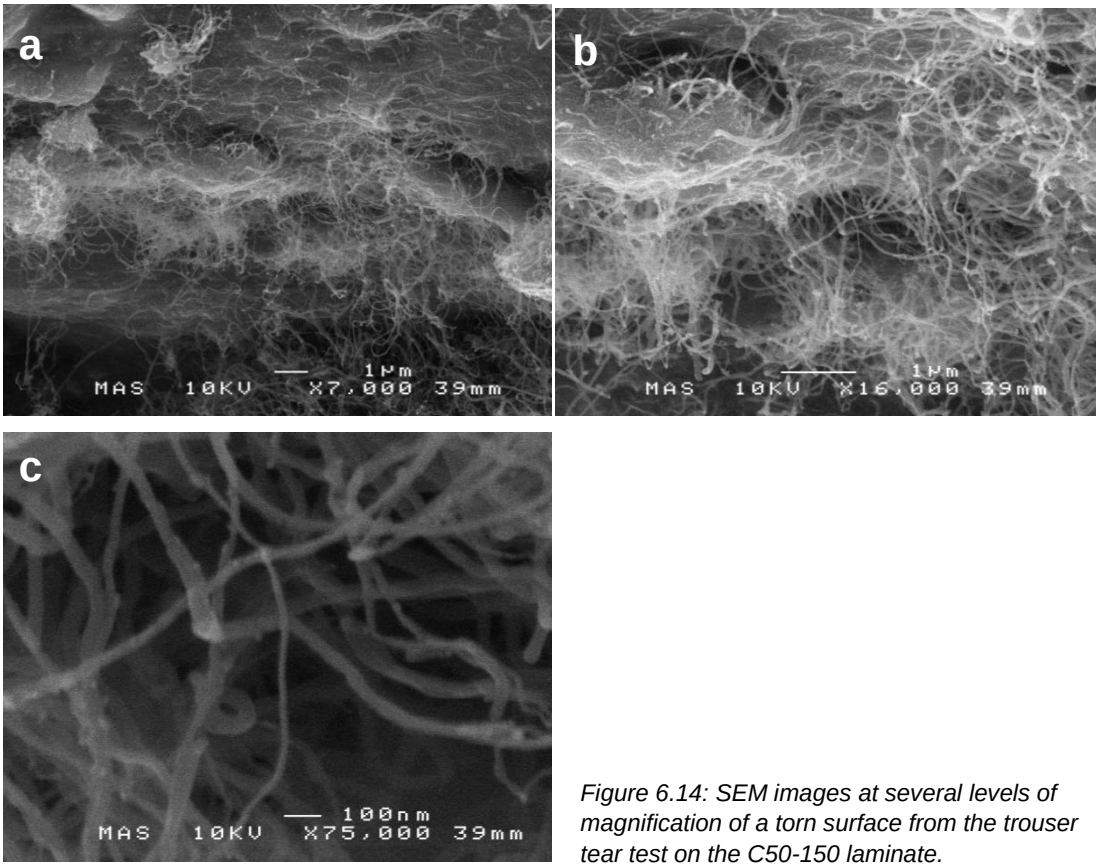

Figure 6.14: SEM images at several levels of magnification of a torn surface from the trouser tear test on the C50-150 laminate.

6.3.6 Dynamical Mechanical Analysis (DMA)

For the application in a peristaltic pump it is useful to study the dynamic properties of the laminate material. The materials used in the laminate, nylon6 and silicone rubber, are viscoelastic. This means the behaviour is between that of a full solid elastic material, obeying Hooke's law:

$$\sigma = E \cdot \gamma \qquad (6.1)$$

and that of a full liquid viscous material, obeying Newton's law:

$$\sigma = \eta \cdot \dot{\gamma} \qquad (6.2)$$

In these equations, σ is the stress, E the Young's modulus, γ the deformation, η the viscosity and $\dot{\gamma}$ the shear rate [173].

This viscoelastic behaviour is due to the nature of polymeric materials like the one used in the laminate C50-150. When a load is applied to such a viscoelastic material (segments of) the polymer chains will start to move trying to lose some of the stress in the material (relaxation). This movement however is inhibited by inter and intra

molecular forces like Vanderwaals forces, entanglements and chemical crosslinks. Sufficient energy is required to overcome these restrictions and therefore the amount of movement is dependent on the temperature, timescale and the rate of deformation. Movement of the polymer chains will influence the mechanical properties of the material. An example of the influence of the timescale on the elastic (E) or shear modulus (G) is shown in the relaxation curve in Figure 6.15.

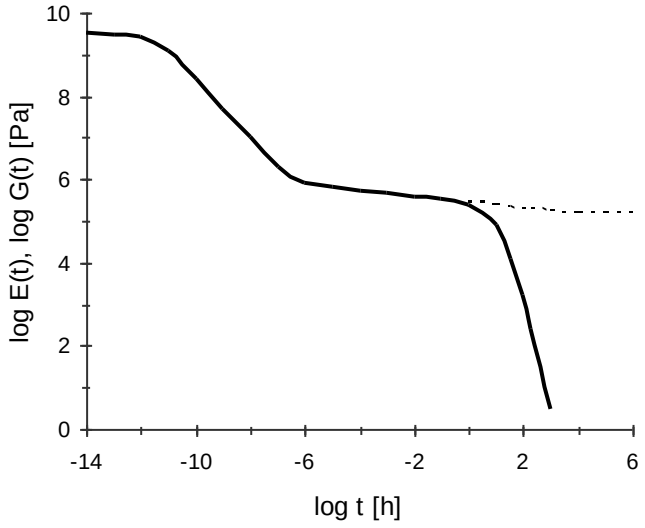

Figure 6.15: Relaxation curve for a polymeric material without (——) and with (- - - -) a permanent (chemically crosslinked) network structure [176].

Within a short time period after the deformation the stretched polymer chains did not yet have time to change their configuration. Only localised movement of small chain segments is possible as would be the case for a glassy polymer. This part of the curve is therefore called the glass plateau. After somewhat longer times a transition zone is reached. Larger chain segments are moving now and this is assumed to be the movement of chain segments between entanglements (physical crosslinks) of different polymer molecules. After this, the so-called rubber plateau is reached. Little more happens in the polymer chain movement on a molecular level than small rearrangements between (physical) crosslinks. In the final part, polymers with a permanent, chemically crosslinked network remain in the rubbery state. Polymers without chemical crosslinks however go through a rubbery-fluid end zone finally ending up in a situation that the material can be considered to be a fluid [176]. The same processes happen when going through ranges of temperature and rate of deformation.

Besides a simple (single) applied stress as described above, it is also possible to apply a periodic stress to the material. This is what is done in Dynamic Mechanical

Analysis (DMA). A sinusoidal alternating stress with a certain frequency *f* (or angular velocity, $\omega=2\pi f$) is applied to the material. Because of the viscous part in the (linear) viscoelastic behaviour of the polymeric materials, the responding strain will be sinusoidal as well, but lagging somewhat behind. The amount of which the strain is out of phase with the stress is described by the phase angle δ. The stress (with amplitude σ^0) on the material can then be written as [177]:

$$\sigma = \sigma^0 \sin(\omega t + \delta) = \sigma^0 \cos\delta \sin\omega\delta + \sigma^0 \sin\delta \cos\omega\delta \qquad (6.3)$$

Now, analogous to Hooke's law (6.1), two frequency dependent functions are defined, the storage modulus E' and the loss modulus E'':

$$E' = (\sigma^0/\gamma^0)\cos\delta \qquad (6.4)$$

$$E'' = (\sigma^0/\gamma^0)\sin\delta \qquad (6.5)$$

From (6.4) and (6.5) can be derived:

$$E''/E' = \tan\delta \qquad (6.6)$$

The sinusoidal stress can also be expressed as a complex quantity. The modulus is then also complex and is given by (see also Figure 6.16)

$$\sigma^*/\gamma^0 = E^* = E' + iE'' \qquad (6.7)$$

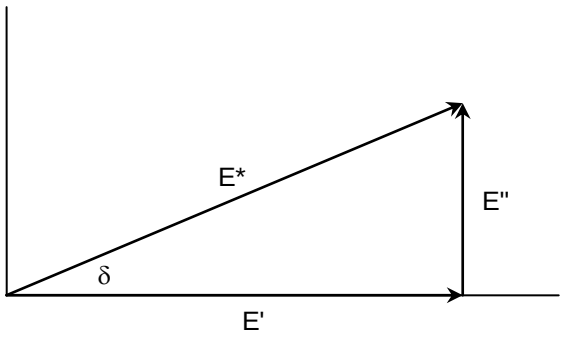

Figure 6.16: Vectorial display of the complex modulus E and its components E' and E''.*

The applied periodic stress is now expressed with a component in phase and a component out of phase. The in-phase (elastic) part is the storage modulus E' and is a measure of the energy that is reversibly stored and recovered in the material per cycle. The out-of-phase (viscous) part is the loss modulus E'' and is a measure of the dissipated or lost energy per cycle.

In the following sections the results of the DMA are presented for the laminate C50-150 and the silicone rubber 0-150. The apparatus was a Tritec 2000 DMA from Triton Technology Ltd., United Kingdom. Rectangular samples were cut and all measured in the tensile mode with free lengths of 3-5 mm. These settings gave the most stable results. As already mentioned, the dynamic properties are temperature, time and deformation dependent. Therefore measurements are done varying only one of these parameters whilst keeping the other two constant. The variation of the parameters is kept between relevant limits for the peristaltic pump application.

6.3.6.1 Temperature sweep

A temperature sweep is made on the laminate C50-150 and the silicone rubber 0-150 from −25 up to 125 °C. The frequency is set at 1 Hz and the strain at around 1%, both expected to be on the rubber plateau over this temperature range. The results are shown in Figure 6.17. The difference between the two measured materials can be attributed to the nylon6 nanofibre reinforcement. At low temperatures, the storage modulus of the laminate is approximately an order of magnitude higher than the one of the silicone rubber alone. The nylon6 here is still in a glassy state. At the upper end of the measured temperatures this is difference is about halved.

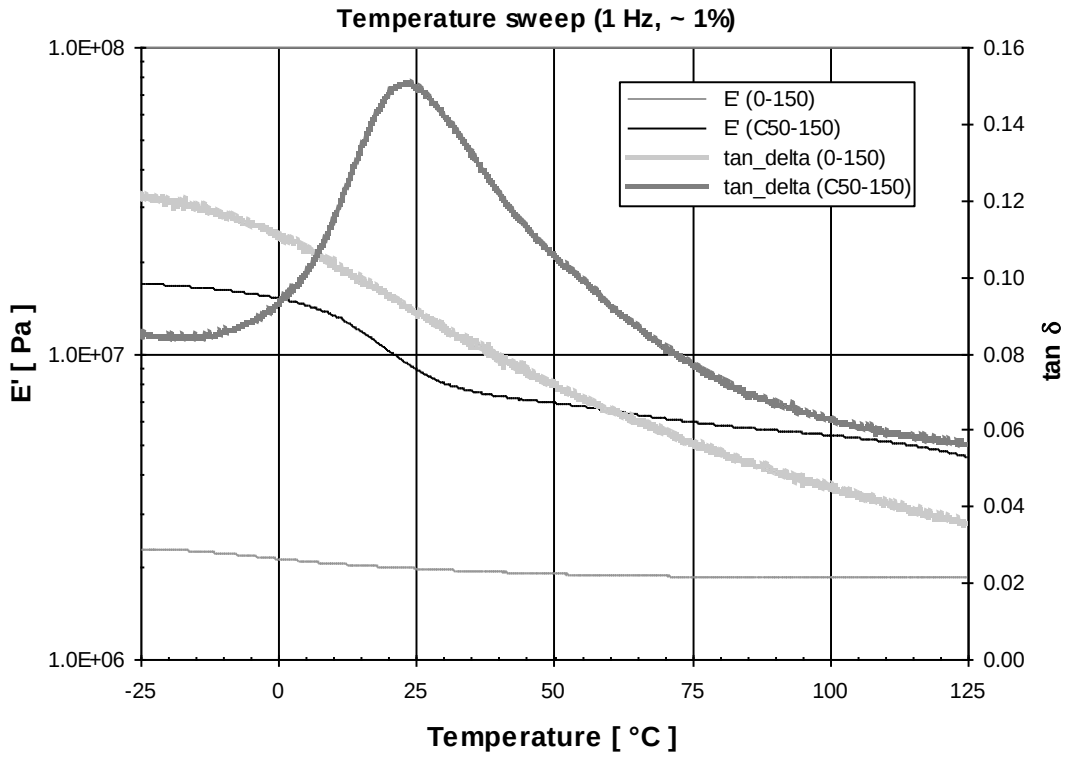

Figure 6.17: Temperature sweep on the laminate C50-150 and the pure silicone rubber 0-150.

In between the nylon6 goes from the glassy to the rubbery state and a peak is observed in the tanδ of the laminate. The temperature at the top of this peak is the glass transition temperature, T_g, and is just under 25 °C for the nylon6 in the laminate. This is lower than the expected 47-57 °C [178] indicating that indeed the nylon6 has somewhat degraded during post-curing of the laminate as was already suspected from the colour change (see section 6.2.2).

6.3.6.2 Frequency sweep

The occlusion frequency in peristaltic pump can roughly range between 0.025 and 25 Hz, but will mostly be between 0.5 and 5 Hz. Therefore the frequency sweep of the laminate and the silicone rubber is set between 10^{-2} and 10^{2} Hz, covering 4 decades. The strain again is set at 1%. The frequency sweeps are conducted at four different temperatures, 25, 50, 75 and 100 °C. The results are shown in Figure 6.18. At this strain the materials are on their rubber plateau for all four temperatures. The course of all the curves for E', E'' and tanδ is as expected. There is a slight increase over the frequency range for all three parameters and at each increasing temperature, the value of the dynamic properties is lower. Some irregularities show up on the high frequency side, close to 100 Hz. These seem to be caused by limits of the DMA apparatus by being not fully capable of reaching the 1% strain towards the higher frequencies.

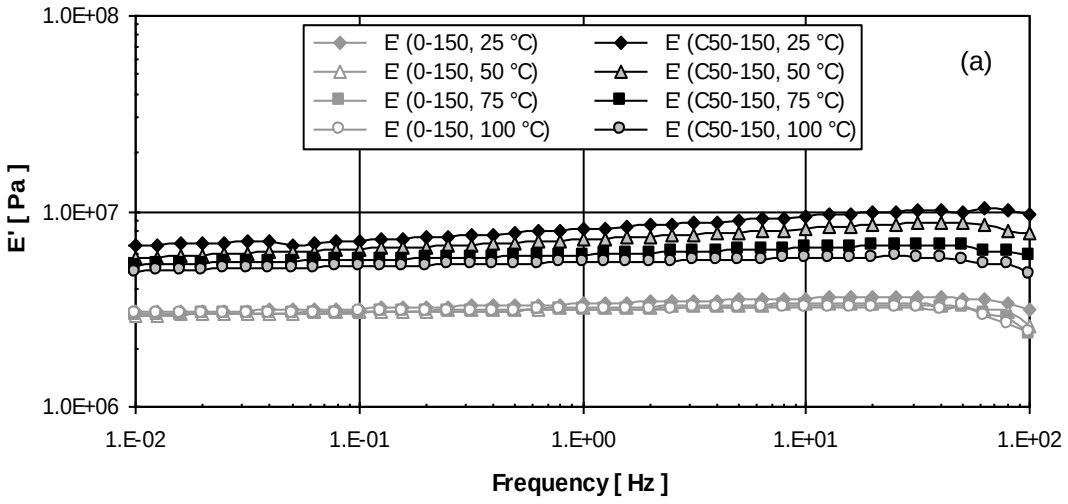

Figure 6.18, cont. on next page

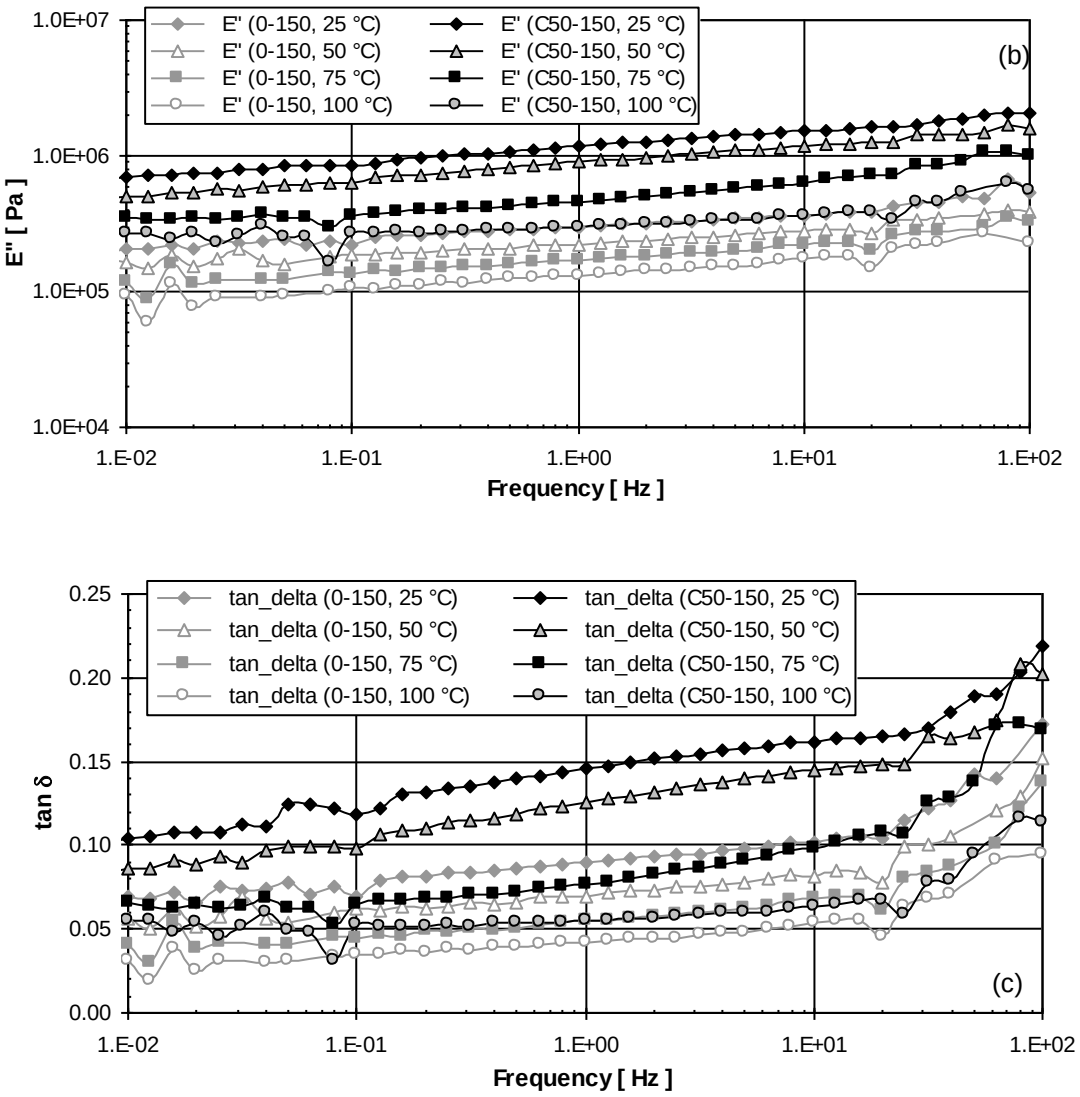

Figure 6.18: Frequency sweeps of the laminate C50-150 and pure silicone rubber 0-150 at 1% strain and temperatures of 25, 50, 75 and 100 °C. (a) Storage modulus (E'); (b) Loss modulus (E"); (c) Loss tangent (tan δ).

6.3.6.3 Strain sweep

In the strain sweep the behaviour of the dynamic properties towards increasing cyclic strain is studied. It is tried to reach the whole (tensile) strain range that a peristaltic tubing material will experience in the pump, i.e. up to 70% (see chapter 4). Unfortunately this is beyond the capabilities of the apparatus, allowing a maximum displacement of only 1 mm. The range of strains measured is therefore limited to about 3 decades, from 0.01% up to 10%. With increasing strain it is expected that at a certain point (the critical strain, γ_c) the non-linear region is reached where the polymer chains start to lose their organisation. Chain segments and eventually, if not crosslinked, whole chains start to slip past one another causing a rapid decrease in

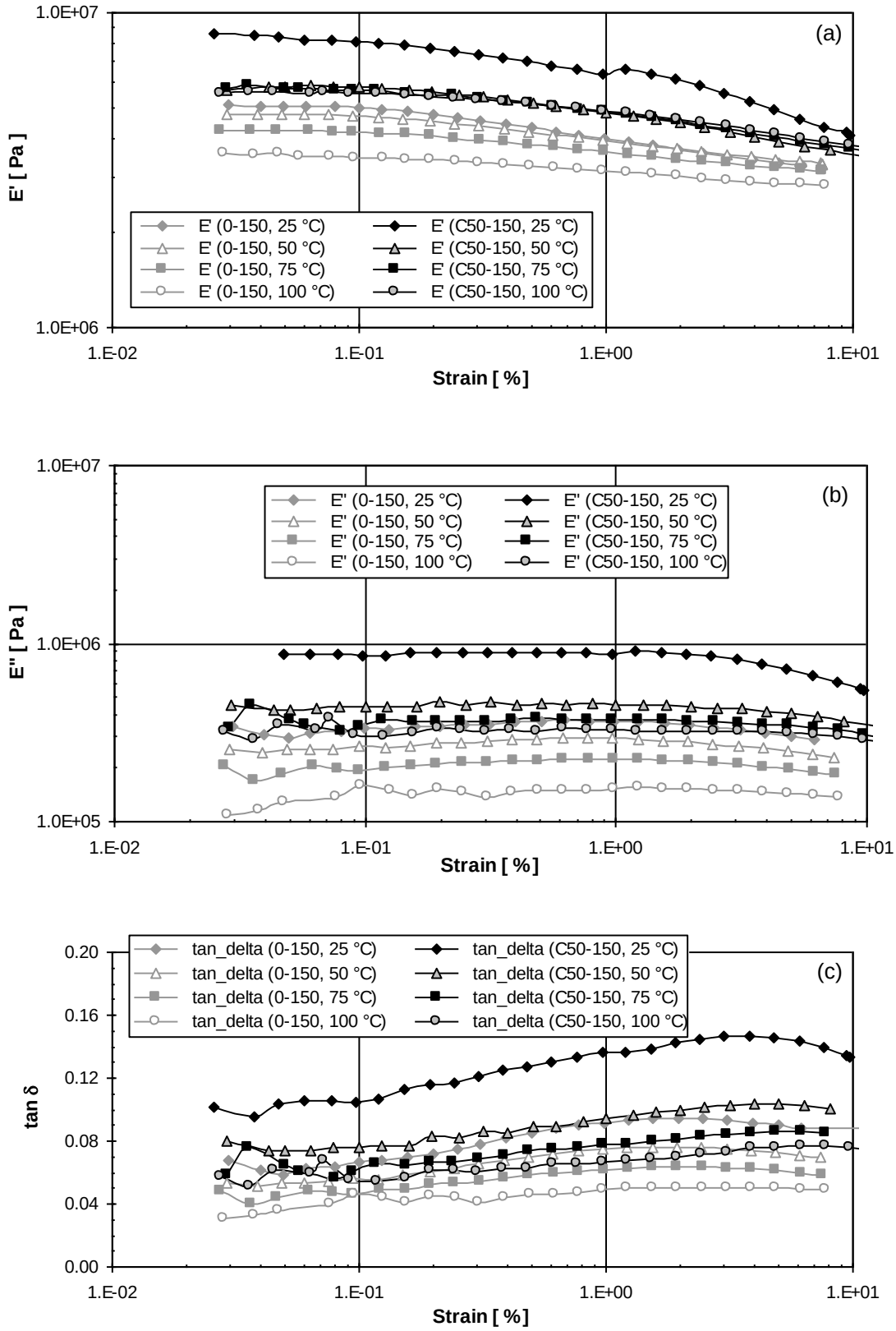

Figure 6.19: Strain sweeps of the laminate C50-150 and pure silicone rubber 0-150 at a frequency of 1Hz and temperatures of 25, 50, 75 and 100 °C. (a) Storage modulus (E'); (b) Loss modulus (E"); (c) Loss tangent (tan δ).

the storage modulus and an increase in the loss modulus. Figure 6.19 shows the results of the strain sweeps for the C50-150 laminate and the silicone rubber 0-150, again at four different temperatures. It can be seen that no major changes in the viscoelastic properties occur and the critical strain has not yet been reached for these materials. The largest effect is a small decrease in storage modulus observed for the laminate at 25 °C, because this measurement is close to the T_g of the nylon6 (see section 6.3.6.1).

6.3.7 Conclusions

Electrospun nanofibre membranes, in this case nylon6, can be used as the fibrous component in a laminate with a silicone elastomer. A clear reinforcing effect of these membranes is observed in the laminates. Furthermore, experimental evidence is found to support the possibility to produce laminates with a reduced through-the-thickness Poisson's ratio using these membranes. More layers of the membrane combined with a better uniformity in the layer thickness will likely pronounce this effect on the Poisson's ratio even more.

7 Tubular laminate structures

To put the laminate material to the test in a peristaltic pump it is necessary to manufacture tubes. This chapter describes this manufacturing, followed by the characterisation of the tubes and actual pump tests. Finally a comparison is made with tubes made with PTFE membrane reinforcement in order to see whether the incorporation of electrospun membranes could be a step towards peristaltic tube improvement or not.

7.1 Manufacturing

A compression mould for producing tubes with a bore of 4.8 mm, a wall thickness of 2.4 mm and a length of 15 cm was made from stainless steel and is shown in Figure 7.1. The preparation of the silicone rubber compound and the laminating process are analogous to what is described in the sections 6.2.1 and 6.2.2, except that the strips of electrospun nylon6 now have a width of 15 cm.

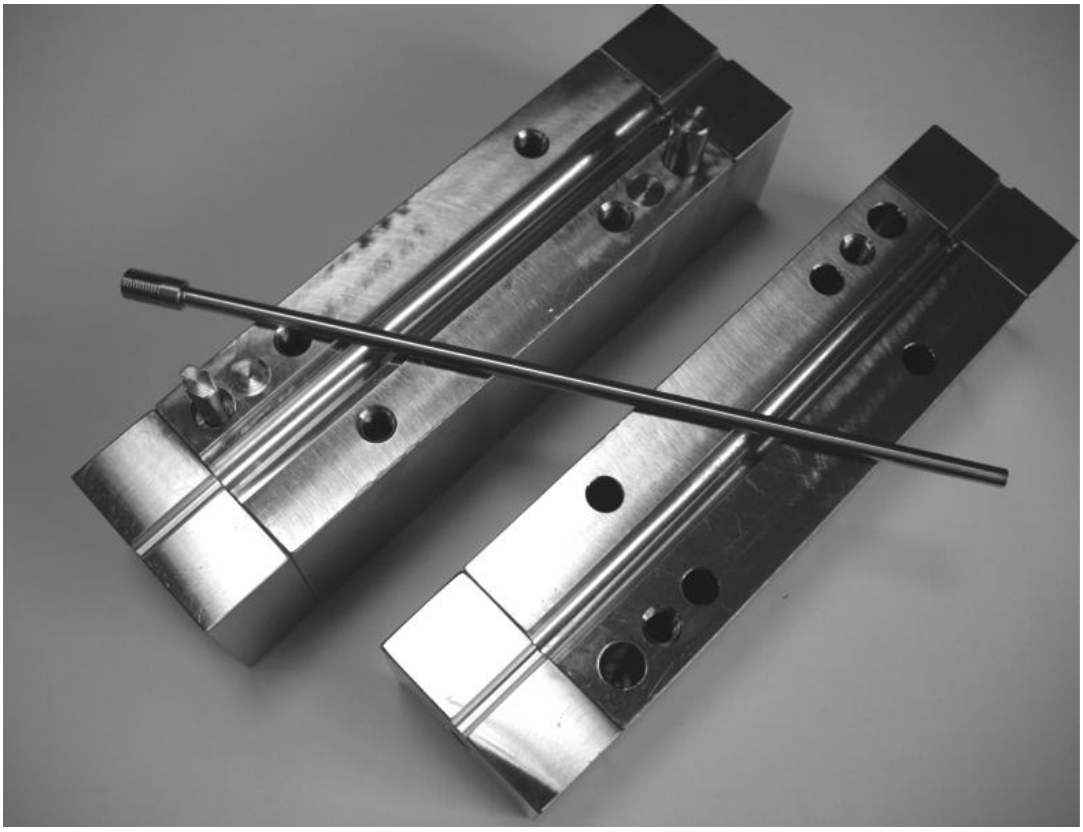

Figure 7.1: The compression mould to manufacture a 4.8 x 2.4 x 1500 mm laminate tube.

The basic manufacturing method for the tubes was as follows: The outer halves of the mould are preheated in an oven at the curing temperature. Release agent

(ELASTOSIL® AUX Mold Release Agent 32, Wacker Silicones, Munich, Germany) is applied on the mandrel with a brush to ensure easy mandrel extraction after curing. The coated electrospun nylon6 is then wrapped around the mandrel like a Swiss roll up to an outer diameter of 10-11 mm. This corresponds with a length of approximately 33 cm from the nylon6 membrane. The last 4-5 cm of the wrapped nylon6 is pulled back and flipped over to give a silicone rubber layer on the outer surface. The bottom half of the mould is then removed from the oven, brushed with the release agent and the mandrel (with the wrapped silicone rubber coated nylon6) is put in place. The top half of the mould is removed from the oven, painted with release agent and the mould is closed. Compression is applied by tightening the bolts as far as possible. The mould is put in the oven for curing for 10 minutes at 165 °C. The curing time is longer than for the flat sheets because of the cold mandrel, cooling of the outer halves when closing the mould and the less efficient heat transfer in an oven compared to a press. After curing the mould is removed and the mandrel extracted from the tube. Finally, the tube is post-cured for 2 hours at 150 °C.

Some deviations on the manufacturing method are made on a small number of tubes. One tube is produced using a length of approximately 50 cm from the nylon6 membrane. The mould could not properly accommodate this much material and was unable to be closed completely (there was still a small gap between the top and bottom half of the mould).
Another variation was to cure some tubes under vacuum in order to get a better impregnation of the nylon6 membrane with silicone rubber. A drawback of the use of vacuum is a higher distortion of the membrane position in the seams where both halves of the mould meet. Therefore this is not used as the standard tube manufacturing method.

For comparison also some pure silicone rubber tubes are manufactured using this mould. For this curing under vacuum was required in order to keep bubble formation in the final tube to a minimum.

7.2 Characterisation of the tubes

The manufactured tubes are characterised using scanning electron microscopy. Some mechanical properties of the tubes are determined by tensile tests. Special attention goes to seams in the tubes that are predominantly present as a

consequence of the mould design. These seams will clearly influence the tube's behaviour and are likely to give a negative impact on tube performance.

7.2.1 Scanning Electron Microscopy

A cross-section of one of the laminated tubes is studied by scanning electron microscopy and the images are shown in Figure 7.2. The left image (a) shows the total wall thickness of the tube. The number of nylon6 layers in the tube wall is 11 to 12. The layers are reasonably well distributed through the wall, but get somewhat closer together towards the tube's bore. At the bottom right of this image the pulled back and flipped over nylon6 membrane is clearly visible. The right images (b) zooms in at one individual layer of nylon6 in the tube wall. In here the membrane is compacted in the thickness direction as well to a similar level as in the flat sheet laminate (see section 6.3.1). A clear difference however, when comparing this image with Figure 6.7a, is the impregnation of the membrane with the silicone rubber. More voids are visible inside the nylon6 layer. This is due to the lower inner mould pressure that can be achieved in the tubular mould.

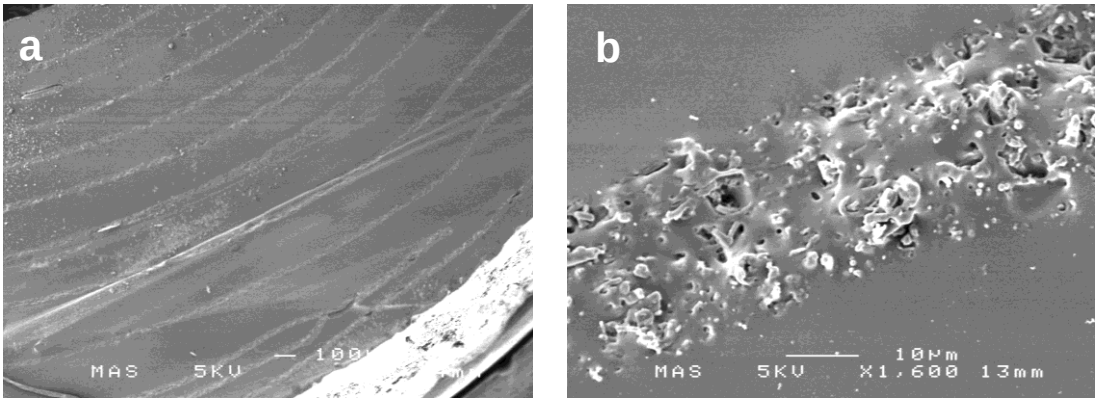

Figure 7.2: SEM images of the cross-section of a laminated nylon6−silicone rubber tube. (a) a low magnification (45x) covering the entire wall thickness of the tube. (b) one layer of nylon6 in the silicone rubber matrix of the tube.

Figure 7.3 shows the large distortion of the nylon6 reinforcement layers around the seam. The flow of the silicone rubber that occurs when the mould is closed, drags the nylon6 membrane along. Applying a vacuum around the mould when curing the tube only increases this effect as already mentioned in section 7.1. The seam clearly looks to be a weak spot in the tube.

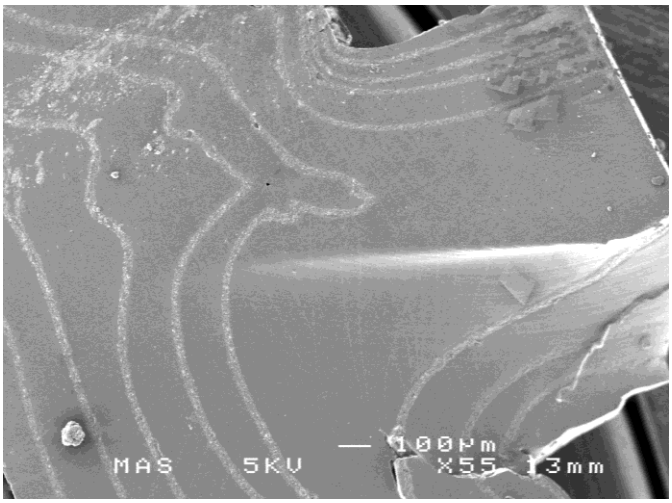

Figure 7.3: SEM image of the seam in the cross-section of a laminated nylon6−silicone rubber tube.

7.2.2 Tensile tests

Similar to what is described in section 4.1, tensile tests are done on sections of some of the manufactured tubes. The specimens are prepared to measure the tensile properties in the circumferential direction, half of them cut through the seam from the mould and the other half cut in between the seams. In the latter case, the

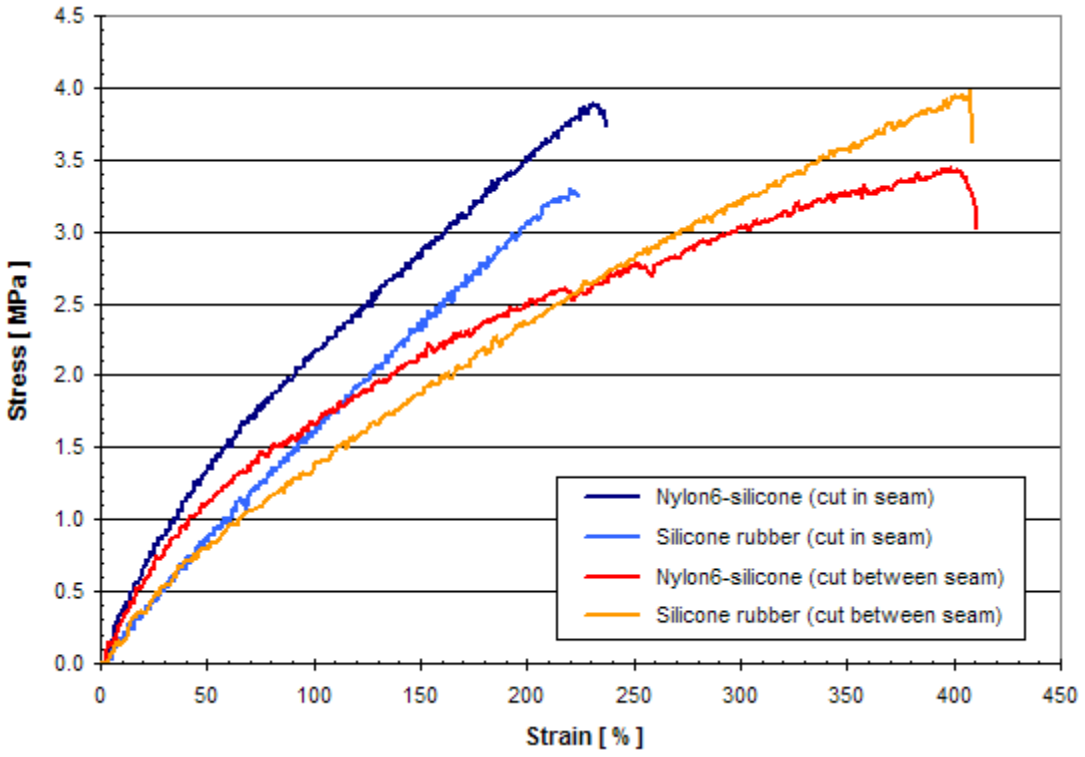

Figure 7.4: Influence of the mould seam on the tensile curves for sections of the produced nylon6−silicone rubber and silicone rubber tubes. The specimens are tested in the circumferential direction.

specimens were placed in such a way that the seams were inside the clamps of the tensile machine. This will give an idea on how much influence this seam has on the mechanical (tensile) properties of the material. The results of these tensile tests (an

average of three specimens) are shown in Figure 7.4. Again, the reinforcing effect of the nylon6 is clearly present. The seam is influencing the stiffness and the strain at break of the specimens. The relatively thick lump of material at the seam inhibits stretching of the material in one direction causing it to break earlier and increase the local stiffness. From these tensile tests can be derived that it is best to locate the seams *not* in the cheeks of the tube when mounted in a peristaltic pump. As described and shown in sections 4.2 and 5.2, the seams will then experience the least amount of tensile deformation.

7.3 Tube tests in the peristaltic pump

Tests on the tubes were done in several peristaltic pumps from the Watson-Marlow 323 series equipped with a 3 roller pump head and set to accommodate a tube with 2.4 mm wall thickness. The fluid being pumped is water and is sucked from an open container by the pump's suction line and then pumped back into the same container. In the beginning a few trials have been made to run the tests with some back pressure in the discharge line using a pressure vessel. This increased pressure however caused the tubes to fail relatively quick through the seam splitting open. Therefore further tests are done at transfer, i.e. a free flow of the water back into the container.

7.3.1 Test results

All the test results are summarised in Table 7.1 showing the test settings, seam orientation and the tube life in hours and number of occlusions. The number of occlusions is calculated by (7.1) with *R* the number of rollers, *n* the pump speed in rpm and *L* the tube life in hours.

$$\#occlusions\ (in\ kcycles) = \frac{R \cdot n \cdot 60 \cdot L}{1000} \qquad (7.1)$$

The results show a large improvement in tube life, from several hours to a few days, when the pressure is taken away and the load on the seams is decreased. Tube lives of more than one million occlusions can be considered good for a first trial. Noticeable is the mode of failure where all the tubes failed through a split in the seams. The orientation of the seam, located in the cheek or at the roller, had no influence on this. This is remarkable since (extruded) peristaltic tubes always fail in the cheek. The seams are definitely the weak areas of these manufactured tubes as was already suspected from the tube characterisations and in order to see the more

of the potential of nylon6−silicone rubber laminate tubes the dominance of the seams has to be decreased.

Tube ID [N6−sil.-]	**Vacuum cured?**	**Pressure** [bar]	**Speed** [rpm]	**Seam orientation**	**Tube life** [hours]	[kcycles]
2	No	2	220	Cheek	2.5	97.7
3	No	0	220	Cheek	27.9	1105.5
4	No	0	220	Cheek	45.0	1782.0
5	No	2 → 1	220	Cheek	5.0	196.7
6	Yes	0	220	Roller	20.0	792.0
7	Yes	0	220	Roller	30.6	1211.1
9	No	0	100	Roller	40.4	727.2
10	No	0	100	Roller	36.0	648.0
11	No	0	100	Roller	36.0	648.0

Table 7.1: Results for the tests of the produced nylon6−silicone rubber tubes in a Watson-Marlow 323 series peristaltic pump.

For comparison several tubes made solely from the silicone rubber have been put to test in the pumps as well. The results of these tests are shown in Table 7.2. The general result is that the tube life of the silicone rubber tubes is about half that of the tubes reinforced with the electrospun nylon6 nanofibre membrane. Also these tubes

Tube ID [sil.-]	**Pressure** [bar]	**Speed** [rpm]	**Seam orientation**	**Tube life** [hours]	[kcycles]
A	0	220	Roller	10.0	396.0
B	0	220	Roller	10.0	396.0
C	0	220	Roller	16.7	661.3
D	0	220	Roller	23.2	918.7

Table 7.2: Results for the tests of the silicone rubber tubes in a Watson-Marlow 323 series peristaltic pump.

failed through a split in the seams. It seems that the nylon6 membrane postpones the fatal failure by providing barrier layers which slow down the split formation. More tests on both type of tubes will be necessary to find out the statistical significance of this.

7.3.2 Characterisation of the failed nylon6−silicone rubber tubes

Inspection of the failed tubes shows that besides the main failure of the seam split also some other damages occur to the tubes as well. Small "pinhole" punctures can be seen in the cusp at the inner surface in the area of the highest compression. The water enters these pinholes into the tube wall and causes delamination between the nylon6 and silicone rubber layers. This continues until the delamination meets the splitting seam. At that point there is a direct route for the water to go through the tube wall and the fatal tube failure is a fact.

Taking a closer look at the tubes with a relative short life a manufacturing issue arises. In this tubes it seems that parts of the inner (first) wrapping of the nylon6 reinforcement is directly at the inner surface. This immediately gives water the opportunity to get into the tube wall through the voids present still present in the laminate (see Figure 7.2b).

In order to have a closer look at the seam split failure, the fracture surface is studied in more detail using scanning electron microscopy and images of this are shown in Figure 7.5. A direct view on a nylon6 layer at the crack face is can be seen in Figure 7.5a. The other two, b and c, are views inside a nylon6 layer. In all three images, the fibres are clearly visible and look to be well coated with silicone rubber. Although lots of fibres are broken, there are still many left bridging over local cracks and voids. Apparently in the end, the nylon6 nanofibre reinforcement layers are not strong enough to withstand the propagating crack from the splitting seam. With a mould design as is used for these tubes, it is necessary to have more layers, better impregnation and stronger fibres (i.e. less degradation of the nylon6, or another higher stiffness material).

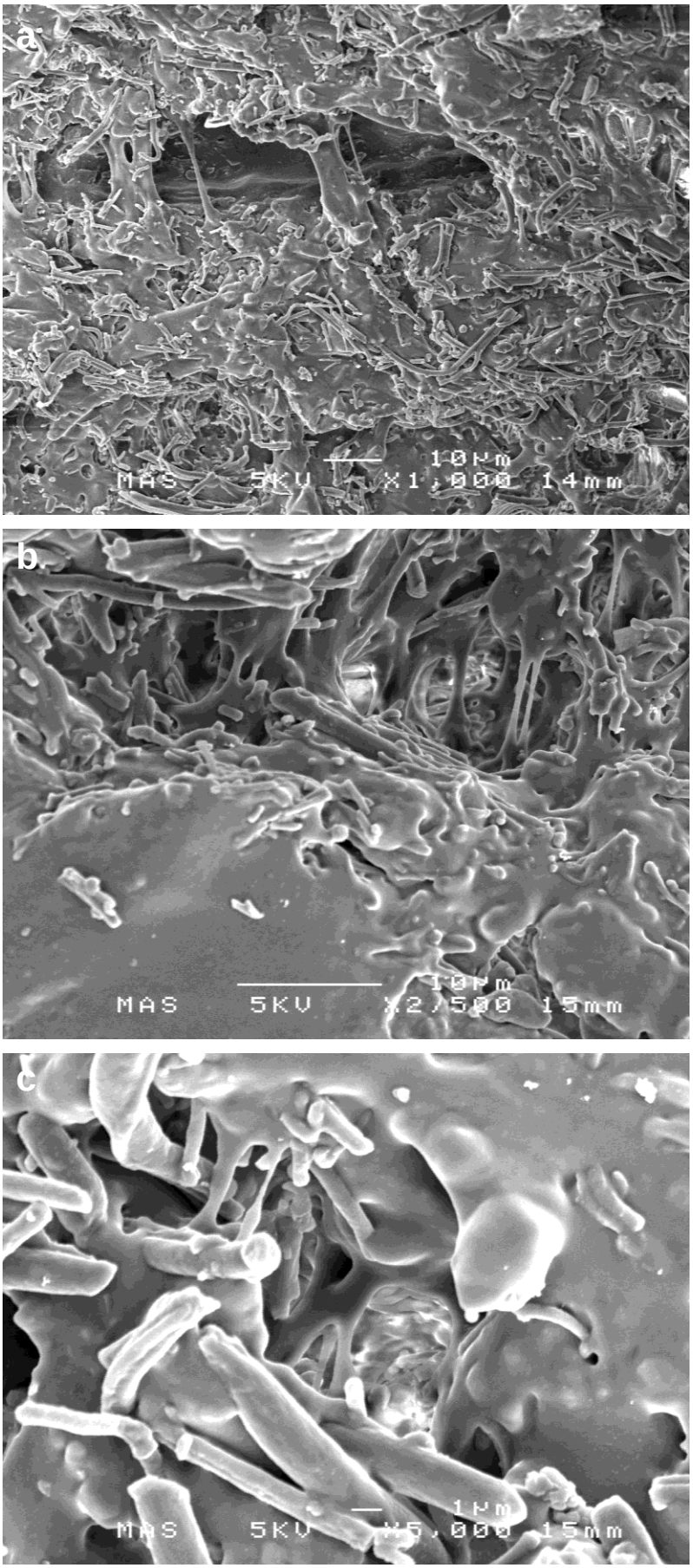

Figure 7.5: SEM images of the seam split crack surface of one of the nylon6−silicone rubber tubes, tube 3.
The images are at various magnifications (1,000x, 2,500x and 5,000x) showing increasing detail of the silicone rubber coated nylon6 nanofibres in the seam split.

7.4 Comparison with other membrane reinforcement

A few more tubes have been manufactured in the mould and using the same method as described in section 7.1, but with different membrane reinforcements.
One tube is produced with the ultrahigh molecular weight polyethylene (UHMWPE) porous film SUNMAP from NITTO DENKO UK Ltd. Two more tubes are produced with PTFE porous membrane from Goodfellow Cambridge Ltd., England. The specifications of these membranes are shown in Table 7.3. The specifications for the electrospun nylon6 are added as well as a reference.

	UHMWPE (SUNMAP)	**PTFE**	**Electrospun nylon6**
Size (length x width)	295 x 210 mm	300 x 150 mm	1016 x 305
Thickness (μm)	100	63	50
Pore size (μm)	17	0.45	0.2 - 2
Porosity (%)	26	84	87

Table 7.3: Specifications of the membranes used for reinforcement in the manufacturing of tubes.

The SUNMAP porous film is an off the shelf material and is used to see if just any randomly selected membrane can be used to produce a laminated tube for a peristaltic pump. Because UHMWPE has a melting point around 110 °C, it was necessary to lower the curing temperature of laminated tube. The curing temperature for this UHMWPE−silicone rubber tube is therefore set at 80 °C. From general curing curves of time vs. temperature it is derived that the time should be 60 minutes to achieve full curing [172]. The post-cure is also done at 80 °C, but extended to 4 hours because of the lower temperature.
In order to get a comparison with the same material as is used as reinforcement in STA-PURE™, microporous PTFE membrane is produced to specifications close to the values of the electrospun nylon6 nanofibre membranes. The settings for curing are kept the same as for the nylon6 reinforcement, 10 minutes at 165 °C followed by 2 hours of post-curing at 150 °C.

The pump test results of these tubes are shown in Table 7.4. The test on the UHMWPE−silicone rubber tube ended already after about 20 minutes with delamination and a split of the seams. The low porosity of the UHMWPE layer does not allow sufficient impregnation by the silicone rubber for a durable bonding or

fixation between both layers. The mechanical load of the pump on the tube causes almost immediately the delamination. Loosing its structural integrity, splitting of the seams follows quickly and the tube fails.

Tube ID	**Pressure** [bar]	**Speed** [rpm]	**Seam orientation**	**Tube life** [hours]	[kcycles]
UHMWPE	0	100	Roller	0.3	5.4
PTFE1	0	100	Roller	62.4	1,123
PTFE2	0	100	Cheek	320.9	5,776

Table 7.4: Results for the tests of the UHMWPE−silicone rubber and PTFE−silicone rubber tubes in a Watson-Marlow 323 series peristaltic pump.

The tubes with the PTFE membrane reinforcement however lasted a lot longer. The porosity of the PTFE membrane is high so there is plenty of opportunity for the silicone rubber to penetrate the pores and impregnate the membrane. Delamination did occur, but at a much later point in time and similarly to the tubes with the electrospun nylon6 reinforcement. Final failure for these tubes was again a split in the seams. Tube PTFE1 had with just over a million occlusions a similar tube life as the upper end of the tubes with the electrospun nylon6. The other PTFE tube however lasted significantly longer.

There are a number of reasons why the tubes with the PTFE reinforcement had a general higher tube life than the tubes with the electrospun nylon6. Most importantly is probably that due to its chemical resistance, PTFE is not suffering from any noticeable degradation during the curing and post-curing steps of the tubes. Another difference between the PTFE and the nylon6 membranes is their morphology. The PTFE membrane has more inherent strength derived from its structure. The nylon6 membrane consists of entangled, but loose fibres whereas the PTFE membrane is a microporous sheet. Especially when degradation occurs the loose fibre membranes are at a disadvantage as they draw their strength from physical interactions. Finally, when pumping water PTFE has an advantage over nylon6. When some of the membrane surface at the inside of the tube becomes exposed, PTFE will repel the water which may delay delamination. The nylon6 however takes up some moisture and will, to some extent, cause the fibres to swell and weaken.

7.5 Conclusions

With the use of a simple mould tubular laminates of thermoplastic membranes and silicone rubber could be manufactured. Mechanical and dynamical performance of these tubes has been assessed by putting them in a peristaltic pump. Unfortunately the tests in the peristaltic pump magnified a weakness in the tube's manufacturing process. As a consequence of the mould design the formation of a seam occurs where the two halves of the mould meet. During the curing step, silicone rubber is squeezed into the gap between the two mould halves causing distortions in the positions of the reinforcing membrane. Nevertheless, for first trials with the used production technique and laminated membranes, the results are looking good and promising: several tubes reached well over 1 million occlusions and the laminates outperformed the pure silicone rubber tubes made in the same mould.

Introduction of the membrane reinforcement has resulted in an increase in tube life providing the membrane has a sufficiently high porosity. In order to obtain an auxetic effect of the electrospun nanofibre membrane it is vital to get sufficient and uniform pressure in the mould during the curing step to fully impregnate the membrane. It is uncertain to what extent this has been achieved in the tubes. There is a similar reduction in the thickness of the membrane in the laminate, but in the tubes still voids could be seen. To obtain a more uniform pressure for better impregnation and to reduce the influence of a seam it is necessary to redesign the mould, or use tape wrapping.

Thermal and chemical degradation of the thermoplastic membrane in the curing step should be avoided as much as possible. The strength of the membrane is then compromised resulting in lower and probably also more scatter in tube lives. Normally the properties and characteristics are leading to choose a membrane as the reinforcement in a laminate. Although a balance is needed, carefully selecting the (post-)curing settings is therefore an important factor in achieving a good performing peristaltic tube.

8 Conclusions

In peristaltic pumps the pump element (i.e. the hose or tube) is the most important part as it can make or break the pump's performance. It is the main wearing part and after failure it needs to be replaced to continue pumping. Hose or tube life is therefore an important factor in selecting a peristaltic pump for a certain application or not. Obviously, a long life is often desired by end users, so increasing this is one of the main objectives of peristaltic pump manufacturers.

During its life the pump element is occluded continuously for many millions of times. And not only just occluded, but also overcompressed. This causes high stresses and strains in the pump element and reducing these could increase its life. A key mechanical property has been identified that has a significant influence on this: the Poisson's ratio. Finite element modelling shows dramatic effects when the Poisson's ratio a of the pump element material is changed, especially on the maximum principal stresses. The overall best effect on the stresses and strain is demonstrated to be around a Poisson's ratio in the range of −0.1 to +0.1 and preferably is 0. Also coming down from the maximum isotropic value for the Poisson's ratio of +0.5, a small decrease already has a significant effect.

Most peristaltic pump elements are made of elastomeric materials. Back-spring of the pump element after occlusion gives the pump its suction capabilities, so the recovery properties of these elastomers are required. Elastomers however have a high Poisson's ratio, in case isotropic case close to the maximum value of +0.5. This contradicts the desired value of this mechanical property to be around 0. To achieve a lower Poisson's ratio in an elastomeric pump element composite materials have to be used. A second material needs to be introduced to the elastomer with a sufficiently low Poisson's ratio in order to bring the total Poisson's ratio down. To reach 0, the Poisson's ratio of this second material has to be negative, a class of materials termed "auxetic".

A composite laminate material is developed consisting of alternating elastomer matrix and thermoplastic reinforcement layers. The thermoplastic layers have a morphology that they will behave auxetically when deformed. The particular materials of choice in here have been electrospun nylon6 in a silicone rubber matrix. Manufactured laminates from these materials are tested and characterised and it is indeed observed that the through-the-thickness Poisson's ratio is lower for the laminate than for the pure silicone rubber. The difference between the two is strain

dependent, but the through-the-thickness Poisson's ratio of the laminate remains lower up to around 50% strain, but will eventually equalise at higher strains. Besides the decrease in the Poisson's ratio, the incorporated electrospun nylon6 also has a clear reinforcing effect. Prototype tube tests are run in a peristaltic pump and some of these tubes managed well over 1 million occlusions. These are certainly promising and encouraging results from first trials. Especially considering a number of issues that have not been optimal. Besides the non-uniform distribution of the reinforcement layers there is also still some thermo-chemical degradation of the nylon6 occurring in the production process. And finally the design of the tube mould results in distorted reinforcement layers and seams at the split of the two mould halves. Addressing these issues and increase the number of reinforcement layers by better laminating techniques will likely increase the tube life more. Whether it will reach the desired objectives and in the future can compete with STA-PURE™ is momentarily unsure and has to be verified with new pump experiments.

The cost objective may not be reached with electrospun nanofibre membranes as a reinforcement. Although not as expensive as expanded PTFE membranes, they are still costly. Therefore it will be useful to keep on top of new developments in possibly cheaper, but not yet feasible manufacturing processes for the reinforcements, like 3D (nano)printing, auxetic fibres and fabrics.

9 Recommendations

As mentioned, the first test results from the tubular laminates in a peristaltic pump look promising. The performance of these tubes however is not yet at the required level. In order to achieve this, a number of issues with the manufacturing need to be addressed and optimised. Besides this, also further material investigation has to be done.

To start with the materials, more investigations in nanofibre membranes are necessary to optimise the reinforcing material in the tubular laminate. In this research nylon6 is used as the membrane material. Many polymer materials are available for electrospinning [179] and may be of interest. Especially when the thermo-chemical degradation during (post-)curing can be minimised, but still being able to use the conventional high temperatures to keep processing time for these steps as short as possible.
Another point of attention is the membrane structure itself. Since the membranes here are used as laminate reinforcement and not for their intended purpose of particle filtering, a reasonable question to ask is whether the structure may be less consistent. As long as the fibre orientation remains random and their lengths remain sufficiently high for entanglements this is probably the case. Then faster electrospinning, even though it will be less accurate and consistent in terms of pore size and fibre thickness, could produce a membrane that is significantly cheaper.

On the manufacturing side a number of improvements have to be considered. The simple compression mould used in this work results in seams that influence the tube's performance too much. A new mould design is necessary to reduce the pronounced presence of a seam.
Also improvements can be made on the laminating procedure. The resulting laminates in this work show a non-uniform distribution of the reinforcement layers. More automated and better controlled application of the liquid silicone rubber coating will improve this. Common laminating techniques that coat a fabric with a highly viscous silicone rubber by means of gravure coating or a doctor's blade have limits in the minimal thickness that can be reached. Below 100 μm is very difficult to achieve in this way [180]. To increase the number of reinforcement layers up to an amount as present in the STA-PURE™ tubes, further investigations have to be made towards more advanced laminating techniques available today.

Finally, developments on other techniques for reinforcement manufacturing, such as 3D (nano)printing, should be kept monitored as this may give a feasible alternative to the nanofibre membranes in the upcoming years.

10 References

[1] WIKIPEDIA, n.d. Peristalsis. *In: Wikipedia: the free encyclopaedia [online]*. Wikimedia Foundation. Available from: http://en.wikipedia.org/wiki/Peristalsis [Accessed 28 June 2010].

[2] ALLEN, E.E., 1881. *Instrument for transfusion of blood*. US Patent 249285. 8 November 1881.

[3] LEE, E., 1890. *Surgical pump*. US Patent 419461. 14 January 1890.

[4] HALES, B.F., 1891. *Surgical pump*. US Patent 459002. 8 September 1891.

[5] NICKERSON, W.E. and BERRENBERG, A. (Beacon Vacuum Pump and Electrical Company), 1891. *Vacuum-pump*. US Patent 453277. 2 June 1891.

[6] FAJEN, G., 1885. *Gas meter*. US Patent 312106. 10 February 1885.

[7] DIECKMANN, D. and SCHMIEDTZINSKY, C., 1883. *Pump*. US Patent 289517. 4 December 1883.

[8] KELLY, D.L., 1885. *Rotary pump*. US Patent 314851. 31 March 1885.

[9] SERDINKO, J., 1885. *Rotary force-pump*. US Patent 315667. 14 April 1885.

[10] FALLER, J., 1885. *Pump*. US Patent 328472. 20 October 1885.

[11] FRASER, J.W. and WILSON, J.D., 1893. *Vacuum-pump*. US Patent 496559. 2 May 1893.

[12] FUNK, C.E., 1894. *Pump*. US Patent 513315. 23 January 1894.

[13] DIECKMANN, D., 1898. *Pump*. US Patent 612834. 25 October 1898.

[14] BRYSON, D.K. (Bryson & Howe), 1906. *Cycle-pump*. US Patent 819690. 1 May 1906.

[15] JONES, T.B., 1918. *Improvements in and relating to Fluid Pumps*. British PatentGB 117110 A. 11 July 1918.

[16] DU NOÜY, P.L., 1920. *Device for moving fluids*. US Patent 1335672. 30 March 1920.

[17] CHAMPENEY, C.C., 1923. *An Improved Appliance for Raising Liquids*. British Patent GB 193574 A. 1 March 1923.

[18] POHL, E., 1926. *Pumpe*. German Patent DE 427746 C. 17 April 1926.

[19] BAUMANN, A. (AG Brown Bovert & Cie), 1930. *Rotary pump*. US Patent 1765360. 24 June 1930.

[20] OWEN, N.T., 1932. *Apparatus for use in blood transfusion, intravenous medication and the like*. US Patent 1848024. 1 March 1932.

[21] SANTIAGO, M.C. and DE BRUYNE, J., 1935. *Pump*. US Patent 1988337. 15 January 1935.

[22] DE BAKEY, M.E. and SCHMIDT, C.E., 1935. Surgical pump. US Patent 2018998. 19 October 1935.

[23] DE BAKEY, M.E. and SCHMIDT, C.E., 1935. Surgical pump. US Patent 2018999. 29 October 1935.

[24] BENNETT, C.G.M., 1937. *Improvements in and relating to pumps*. British Patent GB 467288 A. 15 June 1937.

[25] FERRARA, S.J. and DEEN, W.E., 1937. *Blood transfusion machine*. US Patent 2102523. 14 December 1937.

[26] MOULINIER, E.J., 1940. *Pompe à usages divers et notament médicaux chirurgicaux et scientifiques*. French Patent FR 854088 A. 4 April 1940.

[27] HUBER, C.J. (Downington Manufacturing Company), 1941. *Pump*. US Patent 2231579. 11 February 1941.

[28] BUTLER, R.S. (Nordberg Manufacturing Co.), 1933. *Pump*. US Patent 1922196. 15 August 1933.

[29] WIKIPEDIA, n.d. Cardiopulmonary bypass. *In: Wikipedia: the free encyclopaedia [online]*. Wikimedia Foundation. Available from: http://en.wikipedia.org/wiki/Heart-lung_machine [Accessed 28 June 2010].

[30] WIKIPEDIA, n.d. Michael E. DeBakey. *In: Wikipedia: the free encyclopaedia [online]*. Wikimedia Foundation. Available from: http://en.wikipedia.org/wiki/Michael_E._DeBakey [Accessed 28 June 2010].

[31] HORNICEK, H. and PAZMANN, A., 1957. *Schlauchpumpe*. German Patent DE 1009030 B. 23 May 1957.

[32] GUSTAFSSON, S. (Watson-Marlow Ltd), 1981. *Peristaltic fluid-machines*. British Patent GB 2051253 A. 14 January 1981.

[33] EVANS, C.W., 1979. *Hose Technology*. 2nd ed. Barking, Essex: Applied Science Publishers.

[34] GERRITSEN, J.W., 1974. *Slang voor een slangenpomp*. Dutch Patent NL 7301380. 2 August 1974.

[35] GERRITSEN, J.W., 1976. *Slangpomp*. Dutch Patent NL 7601867. 26 August 1976.

[36] POSTMA, T., 2005. High-pressure peristaltic pumps tackle petrochemicals. *World Pumps*, 2005(468*),* September 2005*,* pp.24-26.

[37] POSTMA, T., SCHIPPERS, D. and KRUISINGA, H.J.J., 2007. *Peristaltic pump, method for manufacturing a hose therefore, and hose for such a pump*. European Patent EP 1847711 (A1). 24 October 2007.

[38] ZUMBRUM, M.A. and MULLER, J.W. (Gore Enterprise Holdings, Inc.), 2002. *Flexure Endurant Composite Elastomer Compositions*. US Patent 6451396. 17 Sept. 2002.

[39] ZUMBRUM, M.A. and MULLER, J.W. (Gore Enterprise Holdings, Inc.), 2004. *Flexure Endurant Composite Elastomer Compositions*. US Patent 6673455. 6 January 2004.

[40] McCLINTOCK, F.A. and ARGON, A.S., ed., 1966. *Mechanical behavior of materials*. pp.79-80. Reading, Massachusetts: Addison-Wesley Publishing Company Inc.

[41] TODHUNTER, I. and PEARSON, K., 1960. *A history of the theory of elasticity and of the strength of materials from Galilei to Lord Kelvin*. New York: Dover Publications.

[42] LOVE, A.E.H., 1944. *A treatise on the mathematical theory of elasticity*. 4th ed. p.163. New York: Dover Publications.

[43] FORTES, M.A. and NOGUEIRA, M.T., 1989. The Poisson effect in cork. *Materials Science & Engineering A*, 122(2), pp.227-232.

[44] LAKES, R., 1987. Foam Structures with a Negative Poisson's Ratio. *Science*, 235(4792), pp.1038-1040.

[45] GIBSON, L.J., ASHBY, M.F., SCHAJER, G.S. and ROBERTSON, C.I., 1982. The Mechanics of Two-Dimensional Cellular Materials. *Proceedings of the Royal Society of London. Series A, Mathematical and Physical Sciences*, 382(1782), pp.25-42.

[46] HERAKOVICH, C.T., 1984. Composite Laminates with Negative Through-the-Thickness Poisson's Ratios. *Journal of Composite Materials*, 18(5), pp.447-455.

[47] KOLPAKOV, A.G., 1985. Determination of the average characteristics of elastic frameworks. *Journal of Applied Mathematics and Mechanics*, 49(6), pp.739-745.

[48] GLEICK, J., 1987. A perverse creation of science: anti-rubber. *New York Times*, 14 April 1987.

[49] MILTON, G.W., 1992. Composite materials with Poisson’s ratios close to –1. *Journal of the Mechanics and Physics of Solids*, 40(5), pp.1105-1137.

[50] EVANS, K.E., NKANSAH, M.A., HUTHINSON, I.J. and ROGERS, S.C., 1991. Molecular network design. *Nature*, 353(6340), p.124.

[51] OBERG, E., JONES, F.D., HORTON, H.L. and RYFFEL, H.H., 2008. *Machinery's handbook*. 28th ed. pp.201, 394. New York: Industrial Press.

[52] BLACK, J. and HASTINGS, G., 1998. Handbook of Biomaterial Properties. pp. 288-289. Springer - Verlag.
Available from: http://knovel.com/web/portal/browse/display?_EXT_KNOVEL_DISPLAY_bookid=1229&VerticalID=0 [Accessed 22 January 2009].

[53] HOLOWNIA, B.P., 1975. Effect of carbon black on Poisson’s ratio of elastomers. *Rubber Chemistry and Technology*, 48(2), pp.246-253.

[54] RAMACHANDRAN, V.S., 1995. *Concrete Admixtures Handbook - Properties, Science, and Technology*. 2nd ed. p. 601. William Andrew Publishing/Noyes.
Available from: http://knovel.com/web/portal/browse/display?_EXT_KNOVEL_DISPLAY_bookid=365&VerticalID=0 [Accessed 22 January 2009].

[55] BANSAL, N.P. and DOREMUS, R.H., 1986. *Handbook of Glass Properties*. pp.34, 38. Elsevier.

Available from: http://knovel.com/web/portal/browse/display?_EXT_KNOVEL_DISPLAY_bookid=2266&VerticalID=0 [Accessed 22 January 2009].

[56] EVANS, K.E., 1991. The Design of Doubly Curved Sandwich Panels with Honeycomb Cores. *Composite Structures*, 17(2), pp.95-111.

[57] LAKES, R.S. and ELMS, K., 1993. Indentability of Conventional and Negative Poisson's Ratio Foams. *Journal of Composite Materials*, 27(12), pp.1193-1202.

[58] CHOI, J.B. and LAKES, R.S., 1992. Non-linear properties of polymer cellular materials with a negative Poisson's ratio. *Journal of Materials Science*, 27(19), pp.5375-5381.

[59] CHOI, J.B. and LAKES, R.S., 1996. Fracture toughness of re-entrant foam materials with a negative Poisson's ratio: experiment and analysis. *International Journal of Fracture*, 80(1), pp.73-83.

[60] CHOI, J.B. and LAKES, R.S., 1992. Non-linear properties of metallic cellular materials with a negative Poisson's ratio. *Journal of Materials Science*, 27(17), pp.4678-4684.

[61] DONOGHUE, J.P., ALDERSON, K.L. and EVANS, K.E., 2009. The fracture toughness of composite laminates with a negative Poisson's ratio. *Physica Status Solidi (b)*, 246(9), pp.2011-2017.

[62] BAUGHMAN, R.H., SHACKLETTE, J.M., ZAKHIDOV, A.A. and STAFSTROM, S., 1998. Negative Poisson's ratios as a common feature of cubic metals. *Nature*, 392(6674), pp.362-365.

[63] YEGANEH-HAERI, A., WEIDNER, D.J. and PARISE, J.B., 1992. Elasticity of α-Cristobalite: A Silicon Dioxide with a Negative Poisson's Ratio. *Science*, 257(5070), pp.650-652.

[64] GRIMA, J.N., GATT, R., ZAMMIT, V., WILLIAMS, J.J., EVANS, K.E., ALDERSON, A. and WALTON, R.I., 2007. Natrolite: A zeolite with negative Poisson's ratios. *Journal of Applied Physics*, 101(8), pp.086102.

[65] VERONDA, D.R. and WESTMANN, R.A., 1970. Mechanical characterization of skin – finite deformations. *Journal of Biomechanics*, 3(1), pp.111-124.

[66] LEES, C., VINCENT, J.F.V. and HILLERTON, J.E., 1991. Poisson’s ratio in skin. *Bio-Medical Materials and Engineering: an international journal*, 1(1), pp.19-23.

[67] WILLIAMS, J.L. and LEWIS, J.L., 1982. Properties and an Anisotropic Model of Cancellous Bone From the Proximal Tibial Epiphysis. *Journal of Biomechanical Engineering*, 104(1), pp.50-56.

[68] PEURA, M., GROTKOPP, I., LEMKE, H., VIKKULA, A., LAINE, J., MÜLLER, M. and SERIMAA, R., 2006. Negative Poisson Ratio of Crystalline Cellulose in Kraft Cooked Norway Spruce. *Biomacromolecules*, 7(5), pp. 1521-1528.

[69] FRIIS, E.A., LAKES, R.S. and PARK, J.B., 1988. Negative Poisson's Ratio Polymeric and Metallic Foams. *Journal of Materials Science*, 23(12), pp.4406-4414.

[70] CHAN, N. and EVANS, K.E., 1999. The Mechanical Properties of Conventional and Auxetic Foams. Part I: Compression and Tension. *Journal of Cellular Plastics*, 35(2),

pp.130-165.

[71] MOORE, J.S., 1993. Odd solid predictions. *Nature*, 365(6448), p.690.

[72] BAUGHMAN, R.H. and GALVÃO, D.S., 1993. Crystalline networks with unusual predicted mechanical and thermal properties. *Nature*, 365(6448), pp.735-737.

[73] GARDNER, G.B., VENKATARAMAN, D., MOORE, J.S. and LEE, S., 1995. *Nature*, 374(6525) pp.792-795.

[74] SIGMUND, O., 1995. Tailoring materials with prescribed elastic properties, *Mechanics of Materials*, 20(4), pp.351-368.

[75] BAUGHMAN, R.H., GALVÃO, D.S., CUI, C. and DANTAS, S.O., 1997. Hinged and chiral polydiacetylene carbon crystals. *Chemical Physics Letters*, 269(3), pp.356-364.

[76] MOORE, J.S. and ZHANG, J., 1992. Efficient Synthesis of Nanoscale Macrocyclic Hydrocarbons. *Angewandte Chemie International Edition in English*, 31(7), pp.922-924.

[77] GUO, Y. and GODDARD III, W.A., 1995. Is carbon nitride harder than diamond? No, but its girth increases when stretched (negative Poisson's ratio). *Chemical Physics Letters*, 237(1), pp.72-76.

[78] CHAN, N. and EVANS, K.E., 1997. Fabrication methods for auxetic foams. Journal of Materials Science, 32(22), pp5945-5953.

[79] BRANDEL, B. and LAKES, R.S., 2001. Negative Poisson's ratio polyethylene foams. *Journal of Materials Science*, 36(24), pp.5885-5893.

[80] CHAN, N. and EVANS, K.E., 1997. Microscopic examination of the microstructure and deformation of conventional and auxetic foams. *Journal of Materials Science*, 32(21), pp.5725-5725.

[81] CHAN, N. and EVANS, K.E., 1999. The Mechanical Properties of Conventional and Auxetic Foams. Part II: Shear. *Journal of Cellular Plastics*, 35(2), pp.166-183.

[82] WAN, H., OHTAKI, H., KOTOSAKA, S. and HU, G., 2004. A study of negative Poisson's ratios in auxetic honeycombs based on a large deflection model. European Journal of Mechanics A/Solids, 23(1), pp.95-106.

[83] SCARPA, F., CIFFO, L.G. and Yates, J.R., 2004. Dynamic properties of high structural integrity auxetic open cell foam. *Smart Materials and Structures*, 13(1), pp. 49-56.

[84] CHEKKAL, I., BIANCHI, M., REMILLAT, C., BÉCOT, F.-X., FAOUEN, L. and SCARPA, F., 2010. Vibro-Acoustic Properties of Auxetic Open Cell Foam: Model and Experimental Results. *Acta Acustica united with Acustica*, 96(2), pp.266-274.

[85] BIANCHI, M., SCARPA, F., BANSE, M. and SMITH, C.W., 2011. Novel generation of auxetic open cell foams for curved and arbitrary shapes. *Acta Materialia*, 59(2), pp.686-691.

[86] LIM, T-C., 2002. Functionally graded beam for attaining Poisson-curving. *Journal of Materials Science Letters*, 21(24), pp.1899-1901.

[87] EVANS, K.E., 1989. Tensile network microstructures exhibiting negative Poisson's ratios. *Journal of Physics D: Applied Physics*, 22(12), pp.1870-1876.

[88] CADDOCK, B.D. and EVANS, K.E., 1989. Microporous materials with negative Poisson's ratios: I. Microstructure and mechanical properties. *Journal of Physics D: Applied Physics*, 22(12), pp.1877-1882.

[89] EVANS, K.E. and CADDOCK, B.D., 1989. Microporous materials with negative Poisson's ratios: II. Mechanisms and interpretation. *Journal of Physics D: Applied Physics*, 22(12), pp.1883-1887.

[90] ALDERSON, A. and Evans, K.E., 1995. Microstructural modelling of auxetic microporous polymers. *Journal of Materials Science*, 30(13), pp.3319-3332.

[91] ALDERSON, K.L. and EVANS, K.E., 1992. The fabrication of microporous polyethylene having a negative Poisson's ratio. *Polymer*, 33(20), pp.4435-4438.

[92] EVANS, K.E. and AINSWORTH, K.L. (National Research Development Corporation), 1991. *Polymeric materials*. International Publication Number WO 91/01210 A1. 7 February 1991.

[93] PICKLES, A.P., WEBBER, R.S., ALDERSON, K.L., NEALE, P.J. and EVANS, K.E., 1995. The effect of the processing parameters on the fabrication of auxetic polyethylene. Part I. The effect of compaction conditions. *Journal of Materials Science*, 30(16), pp.4059-4068.

[94] ALDERSON, K.L., KETTLE, A.P., NEALE, P.J., PICKLES, A.P. and EVANS, K.E., 1995. The effect of the processing parameters on the fabrication of auxetic polyethylene. Part II. The effect of sintering temperature and time. *Journal of Materials Science*, 30(16), pp.4069-4075.

[95] NEALE, P.J., PICKLES, A.P., ALDERSON, K.L. and EVANS, K.E., 1995. The effect of the processing parameters on the fabrication of auxetic polyethylene. Part III. The effect of extrusion conditions. *Journal of Materials Science*, 30(16), pp.4087-4094.

[96] PICKLES, A.P., ALDERSON, K.L. and EVANS, K.E., 1996. The Effects of Powder Morphology on the Processing of Auxetic Polypropylene (PP of Negative Poisson's Ratio). *Polymer Engineering and Science*, 36(5), pp.636-642.

[97] ALDERSON, K.L., ALDERSON, A. and EVANS, K.E., 1997. The interpretation of the strain-dependent Poisson's ratio in auxetic polyethylene. *The Journal of Strain Analysis for Engineering Design*, 32(3), pp.201-212.

[98] ALDERSON, K.L., ALDERSON, A., WEBBER, R.S. and EVANS, K.E., 1998. Evidence for uniaxial drawing in the fibrillated microstructure of auxetic polymers. *Journal of Materials Science Letters*, 17(16), pp.1415-1419.

[99] WEBBER, R.S., ALDERSON, K.L. and EVANS, K.E., 2000. Novel Variations in the Microstructure of the Auxetic Microporous UHMWPE. Part 1: Processing and Microstructure. *Polymer Engineering and Science*, 40(8), pp.1894-1905.

[100] ALDERSON, K.L., WEBBER, R.S. and EVANS, K.E., 2000. Novel Variations in the Microstructure of the Auxetic Microporous UHMWPE. Part 2: Mechanical Properties. *Polymer Engineering and Science*, 40(8), pp.1906-1914.

[101] ALDERSON, K.L., WEBBER, R.S. and EVANS, K.E., 2007. Microstructural evolution in the processing of auxetic microporous polymers. *Physica Status Solidi (b)*, 244(3), pp.828-841.

[102] ALDERSON, K.L., WEBBER, R.S., KETTLE, A.P. and EVANS, K.E., 2005. Novel Fabrication Route for Auxetic Polyethylene. Part 1. Processing and Microstructure. *Polymer Engineering and Science*, 45(4), pp. 568-578.

[103] WEBBER, R.S., ALDERSON, K.L. and EVANS, K.E., 2008. A Novel Fabrication Route for Auxetic Polyethylene, Part 2: Mechanical Properties. *Polymer Engineering and Science*, 48(7), pp.1351-1358.

[104] ALDERSON, K.L. and SIMKINS, V.R. (Bolton Institute of Higher Education), 2000. *Auxetic materials*. International Publication Number WO 00/53830 A1. 14 September 2000.

[105] ALDERSON, K.L., ALDERSON, A., SMART, G., SIMKINS, V.R. and DAVIES, P.J., 2002. Auxetic polypropylene fibres: Part 1 - Manufacture and characterisation. *Plastics, Rubber and Composites*, 31(8), pp.344-349.

[106] RAVIRALA, N., ALDERSON, A., ALDERSON, K.L. and DAVIES, P.J., 2005. Expanding the range of auxetic polymeric products using a novel melt spinning route. *Physica Status Solidi (b)*, 242(3), pp.653-664.

[107] RAVIRALA, N., ALDERSON, K.L., DAVIES, P.J., SIMKINS, V.R. and ALDERSON, A., 2006. Negative Poisson's Ratio Polyester Fibers. *Textile Research Journal*, 76(7), pp.540-546.

[108] ALDERSON, K.L., ALDERSON, A., DAVIES, P.J., SMART, G., RAVIRALA, N. and SIMKINS, G., 2007. The effect of processing parameters on the mechanical properties of auxetic polymeric fibers. *Journal of Materials Science*, 42(19), pp.7991-8000.

[109] SIMKINS, V.R., ALDERSON, A., DAVIES, P.J. and ALDERSON, K.L., 2005. Single fibre pullout tests on auxetic polymeric fibres. *Journal of Materials Science*, 40(16), pp.4355-4364.

[110] HOOK, P. (Auxetix Ltd), 2006. *Uses of auxetic fibres*. International Publication Number WO 2006/021763 A1. 2 March 2006.

[111] MILLER, W., HOOK, P.B., SMITH, C.W., WANG, X. and EVANS, K.E., 2009. The manufacture and characterisation of a novel, low modulus, negative Poisson's ratio composite. *Composites Science and Technology*, 69(5), pp.651-655.

[112] RAVIRALA, N., ALDERSON, A., ALDERSON, K.L. and DAVIES, P.J., 2005. Auxetic polypropylene films. *Polymer Engineering and Science*, 45(4), pp.517-528.

[113] CHIRIMA, G., RAVIRALA, N., RAWAL, A., SIMKINS, V.R., ALDERSON, A. and ALDERSON, K.L., 2008. The effect of processing parameters on the fabrication of auxetic extruded polypropylene films. *Physica Status Solidi (b)*, 245(11), pp.2383-2390.

[114] ALDERSON, K.L., FITZGERALD, A., EVANS, K.E., 2000. The strain dependent indentation resilience of auxetic microporous polyethylene. *Journal of Materials Science*, 35(16), pp.4039-4047.

[115] HE, C., LIU, P. and GRIFFIN, A.C., 1998. Toward Negative Poisson Ratio Polymers through Molecular Design. *Macromolecules*, 31(9), pp.3145-3147.

[116] HE, C., LIU, P., McMULLAN, P.J. and GRIFFIN, A.C., 2005. Toward molecular auxetics: Main chain liquid crystalline polymers consisting of laterally attached para-quaterphenyls. *Physica Status Solidi (b)*, 242(3), pp.576-584.

[117] HE, C., LIU, P., GRIFFIN, A.C., SMITH, C.W. and EVANS, K.E., 2005. Morphology and Deformation Behaviour of a Liquid Crystalline Polymer Containing Laterally Attached Pentaphenyl Rods. *Macromolecular Chemistry and Physics*, 206(2), pp.233-239.

[118] LIU, Y., ZHANG, L., SHI, J. and CAO, S., 2005. Synthesis and characterization of liquid crystalline copolyesters containing horizontal and lateral rods in main chain (II). *Reactive & Functional Polymers*, 64(1), pp.35-46.

[119] ALDRED, P. and MORATTI, S.C., 2005. Dynamic simulations of potentially auxetic liquid-crystalline polymers incorporating swivelling mesogens. *Molecular Simulation*, 31(13), pp.883-887.

[120] REN, W., McMULLAN, P.J. and GRIFFIN, A.C., 2008. Poisson's Ratio of Monodomain Liquid Crystalline Elastomers. *Macromolecular Chemistry and Physics*, 209(18), pp.1896-1899.

[121] HULL, D. and CLYNE, T.W., 1996. *An introduction to composite materials*. Cambridge: Cambridge University Press.

[122] PEEL, L.D., 2007. Exploration of high and negative Poisson's ratio elastomer-matrix laminates. *Physica Status Solidi (b)*, 244(3), pp.988-1003.

[123] MIKI, M. and MUROTSU, Y., 1989. The Peculiar Behavior of the Poisson's Ratio of Laminated Fibrous Composites. *The Japan Society of Mechanical Engineers International Journal. Series 1 - Solid mechanics, strength of materials*, 32(1), pp.67-72.

[124] ZHANG, R., YEH, H-L. and YEH, H-Y., 1999. A Discussion of Negative Poisson's Ratio Design for Composites. *Journal of Reinforced Plastics and Composites*, 18(17), pp.1546-1556.

[125] ZHANG, R., YEH, H-L. and YEH, H-Y., 1999. A Study of Negative Poisson's Ratio in Randomly Oriented Quasi-Isotropic Composite Laminates. *Journal of Composite Materials*, 33(19), pp.1843-1857.

[126] EVANS, K.E., DONOGHUE, J.P. and ALDERSON, K.L., 2004. The Design, Matching and Manufacture of Auxetic Carbon Fibre Laminates. *Journal of Composite Materials*, 38(2), pp.95-106.

[127] CLARKE, J.F., DUCKETT, R.A., HINE, P.J., HUTCHINSON, I.J. and WARD, I.M., 1994. Negative Poisson's ratios in angle-ply laminates: theory and experiment. *Composites*, 25(9), pp.863-868.

[128] HINE, P.J., DUCKETT, R.A. and WARD, I.M., 1997. Negative Poisson's ratios in angle-ply laminates. *Journal of Materials Science Letters*, 16(7), pp.541-544.

[129] HARKATI, E.H., BEZAZI, A., SCARPA, F., ALDERSON, K. and ALDERSON A.,

2007. Modelling the influence of the orientation and fibre reinforcement on the Negative Poisson's ratio in composite laminates. *Physica Status Solidi (b)*, 244(3), pp.883-892.

[130] YEH, H-L. and YEH, H-Y., 2000. Dilatation and Through-the-Thickness Poisson's Ratio of Composite Laminates. *Journal of Reinforced Plastics and Composites*, 19(12), pp.966-991.

[131] YEH, H-L. and YEH, H-Y., 2001. Transverse Moduli Effect on Dilatation and Through-Thickness Poisson's Ratio of Composite Laminates. *Journal of Reinforced Plastics and Composites*, 20(12), pp.1066-1085.

[132] YEH, H-L. and YEH, H-Y., 2002. The Effect of Transverse Moduli on Dilatation and Through-Thickness Poisson's Ratio in Angle-Ply Laminates. *Journal of Reinforced Plastics and Composites*, 21(18), pp.1653-1670.

[133] YEH, H-L. and YEH, H-Y., 2003. Effect of lamina material properties on dilatation and through-thickness Poisson's ratio of angle-ply laminates. *Journal of Reinforced Plastics and Composites*, 22(16), pp.1477-1496.

[134] TATLIER, M. and BERHAN, L., 2009. Modelling the negative Poisson's ratio of compressed fused fibre networks. *Physica Status Solidi (b)*, 246(9), pp. 2018-2024.

[135] JAYANTY, S., CROWE, J. and BERHAN, L., 2011. Auxetic fibre networks and their composites. *Physica Status Solidi (b)*, 248(1), pp.73-81.

[136] VINSON, J.R., 1999. *The behavior of sandwich structures of isotropic and composite materials*. Chap. 1. Lancaster (PA): Technomic Publishing Company.

[137] WHITTY, J.P.M., ALDERSON, A., MYLER, P and KANDOLA, B., 2003. Towards the design of sandwich panel composites with enhanced mechanical and thermal properties by variation of the in-plane Poisson's ratios. *Composites. Part A, applied science and manufacturing*, 34(6), pp.525-534.

[138] SCARPA, F. and TOMLINSON, G., 2000. Theoretical characteristics of the vibration of sandwich plates with in-plane negative Poisson's ratio values. *Journal of Sound and Vibration*, 230(1), pp.45-67.

[139] RUZZENE, M. and SCARPA, F., 2003. Control of Wave Propagation in Sandwich Beams with Auxetic Core. *Journal of Intelligent Material Systems and Structures*, 14(7), pp.443-453.

[140] WEI, G and EDWARDS, S.F., 1998. Auxeticity windows for composites. *Physica A*, 258(1), pp.5-10.

[141] WEI, G and EDWARDS, S.F., 1999. Effective elastic properties of composites of ellipsoids (I). Nearly spherical inclusions. *Physica A*, 264(3), pp.388-403.

[142] WEI, G and EDWARDS, S.F., 1999. Effective elastic properties of composites of ellipsoids (II). Nearly disk- and needle-like inclusions. *Physica A*, 264(3), pp.404-423.

[143] WEI, G and EDWARDS, S.F., 1998. Poisson ratio in composites of auxetics. *Physical Review E*, 58(5), pp.6173-6181.

[144] PRALL, D. and LAKES, R.S., 1997. Properties of a Chiral Honeycomb with a Poisson’s Ratio of –1. *International Journal of Mechanical Sciences*, 39(3), pp.305-

314.

[145] SPADONI, A., RUZZENE, M. and SCARPA, F., 2005. Global and local linear buckling behavior of a chiral cellular structure. *Physica Status Solidi (b)*, 242(3), pp.695-709.

[146] GASPAR, N., REN, X.J., SMITH, C.W., GRIMA, J.N. and EVANS, K.E., 2005. Novel honeycombs with auxetic behaviour. *Acta Materialia*, 53(8), pp.2439-2445.

[147] GRIMA, J.N. and EVANS, K.E., 2000. Auxetic behavior from rotating squares. *Journal of Materials Science Letters*, 19(17), pp.1563-1565.

[148] GRIMA, J.N., ALDERSON, A. and EVANS, K.E., 2005. Auxetic behaviour from rotating rigid units. *Physica Status Solidi (b)*, 242(3), pp.561-575.

[149] GRIMA, J.N. and EVANS, K.E., 2006. Auxetic behavior from rotating triangles. *Journal of Materials Science*, 41(10), pp.3193-3196.

[150] GRIMA, J.N., FARRUGIA, P-S., GATT, R. and ZAMMIT, V., 2007. Connected Triangles Exhibiting Negative Poisson's Ratios and Negative Thermal Expansion. *Journal of the Physical Society of Japan*, 76(2), pp.025001.

[151] GRIMA, J.N., GATT, R., ALDERSON, A. and EVANS, K.E., 2005. On the Auxetic Properties of 'Rotating Rectangles' with Different Connectivity. *Journal of the Physical Society of Japan*, 74(10), pp.2866-2867.

[152] GRIMA, J.N., FARRUGIA, P-S., GATT, R. and ATTARD, D., 2008. On the auxetic properties of rotating rhombi and parallelograms: A preliminary investigation. *Physica Status Solidi (b)*, 245(3), pp.521-529.

[153] ISHIBASHI, Y. and IWATA, M, 2000. A Microscopic Model of a Negative Poisson's Ratio in Some Crystals. *Journal of the Physical Society of Japan*, 69(8), pp.2702-2703.

[154] GRIMA, J.N., ALDERSON, A. and EVANS, K.E., 2005. An Alternative Explanation for the Negative Poisson's Ratio in Auxetic Foams. *Journal of the Physical Society of Japan*, 74(4), pp.1341-1342.

[155] ATTARD, D., MANICARO, E., GATT, R and GRIMA, J.N., 2009. On the properties of auxetic rotating stretching squares. *Physica Status Solidi (b)*, 246(9), pp.2045-2054.

[156] GRIMA, J.N., MANICARO, E. and ATTARD, D., 2011. Auxetic behaviour from connected different-sized squares and rectangles. *Proceedings of the Royal Society A*, 467(2126), pp.439-458.

[157] XU, B., ARIAS, F., BRITTAIN, S.T., ZHAO, X-M., GRZYBOWSKI, B., TORQUATO, S. and WHITESIDES, G.M., 1999. Making Negative Poisson's Ratio Microstructures by Soft Lithography. *Advanced Materials*, 11(14), pp.1186-1189.

[158] ALDERSON, A., RASBURN, J., AMEER-BEG, S., MULLARKEY, P.G., PERRIE, W. and EVANS, K.E., 2000. An Auxetic Filter: A Tuneable Filter Displaying Enhanced Size Selectivity or Defouling Properties. *Industrial & Engineering Chemistry Research*, 39(3), pp.654-665.

[159] ALDERSON, A., RASBURN, J., EVANS, K.E. and GRIMA, J.N., 2001. Auxetic polymeric filters display enhanced de-fouling and pressure-compensation properties.

Membrane Technology, 137(2001), pp.6-8.

[160] RASBURN, J., MULLARKEY, P.G., EVANS, K.E., ALDERSON, A., AMEER-BEG, S. and PERRIE, W., 2001. Auxetic Structures for Variable Permeability Systems. *AIChE Journal*, 47(11), pp.2623-2626.

[161] ALDERSON, A, ALDERSON, K.L., HUDSON, G.D. and SKERTCHLY, D.E. (Auxetic Technologies Ltd), 2007. *A Composite Material*. International Publication Number WO 2007/135447 A1. 27 May 2007.

[162] Celgard® Electrolytic Membranes | Lithium-Ion Battery Separators. Available from: http://www.celgard.com/products/ [Accessed 16 September 2009].

[163] XIA, Y. and WHITESIDES, G.M., 1998. Soft lithography. *Annual Review of Materials Science*, 28, pp.153-184

[164] XIA, Y. and WHITESIDES, G.M., 1998. Soft Lithography. *Angewandte Chemie: International Edition*, 37(5), pp.550-575.

[165] XU, B., ARIAS, F. and WHITESIDES, G.M., 1999. Making Honeycomb Microcomposites by Soft Lithography. *Advanced Materials*, 11(6), pp.492-495.

[166] ARIAS, F., KENIS, P.J.A., XU, B., DENG, T., SCHUELLER, O.J.A., WHITESIDES, G.M., SUGIMURA, Y. AND EVANS, A.G., 2001. Fabrication and characterization of microscale sandwich beams. *Journal of Materials Research*, 16(2), pp.597-605.

[167] The International Nickel Company, Inc. 1983. *The Corrosion Resistance of Nickel-Containing Alloys in Sulfuric Acid and Related Compounds*. Available from: http://www.nickelinstitute.org/~/Media/Files/TechnicalLiterature/TheCorrosionResistanceofNickel_ContainingAlloysinSulphuricAcidandRelatedCompounds_1318_.pdf [Accessed 9 June 2010].

[168] Objet Connex500™ - The World's First Multi-Material 3D Printing System. Available from: http://www.objet.com/3D-Printer/Objet_connex500 [Accessed 23 May 2011]

[169] BLEVINS, R.D., 1979. *Formulas for natural frequency and mode shape*. Reprint edition 1987. Chapters 5 and 8. Malabar (FL): Robert E. Krieger Publishing Co.

[170] WACKER SILICONES. Technical Data Sheet for: *Elastosil® LR 3043 A, B, Liquid Silicone Rubber*. Version 6.10, 01-04-08. Munich, Germany.

[171] BS ISO 37:2005. *Rubber, vulcanized or thermoplastic – Determination of tensile stress-strain properties*. BSI.

[172] LYNCH, W., 1978. *Handbook of silicone rubber fabrication*. 2nd ed. New York: Van Reinhold Company.

[173] HOFMANN, W., 1989. *Rubber Technology Handbook*. Reprint edition 1996. Chapter 6. Munich: Carl Hanser Verlag.

[174] BS ISO 7619-1:2010. *Rubber, vulcanized or thermoplastic – Determination of the indentation hardness. Part 1: Durometer method (Shore hardness)*. BSI.

[175] BS 903-A3:1995 / ISO 34-1:1994. *Physical testing of rubber – Part A3: Method for determination of tear strength (trouser, angle and crescent test pieces*). BSI.

[176] BLOM, C., JONGSCHAAP, R.J.J. and MELLEMA, J. 1991. *Inleiding in de Reologie*. 3rd ed. Deventer: Kluwer Technische Boeken B.V.

[177] FERRY, J.D., 1970. *Viscoelastic Properties of Polymers*. 2nd ed. New York: John Wiley & Sons, Inc.

[178] MARK, J.E. (ed), 2009. *Polymer Data Handbook*. 2nd ed. Oxford: Oxford University Press.

[179] HUANG, Z.-M., ZHANG, Y.-Z., KOTAKI, M. and RAMAKRISHNA, S., 2003. A review on polymer nanofibres by electrospinning and their applications in nanocomposites. *Composites Science and Technology*, 63(15), pp.2223-2253.

[180] INOUE, Y and MOMII, K. (Shin-Etsu Chemical Co., Ltd.), 1995. *Air bag coating composition and airbag*. US Patent 5399402. 21 March 1995.

[181] YAO, Y.T., ALDERSON, A. and ALDERSON, K.L., 2008. Can nanotubes display auxetic behaviour? *Physica Status Solidi (b)*, 245(11), pp. 2373-2382.

Appendix

Complete overview of the baseline test results and the modelling results of the Poisson's ratio effect on a tube under occlusion are shown in the Figures A1 – A25 on the next pages.

- Tensile tests (Figures A1 – A6)
- Occlusion tests (Figures A7 – A13)
- Finite Element Modelling results (Figures A14 – A25)

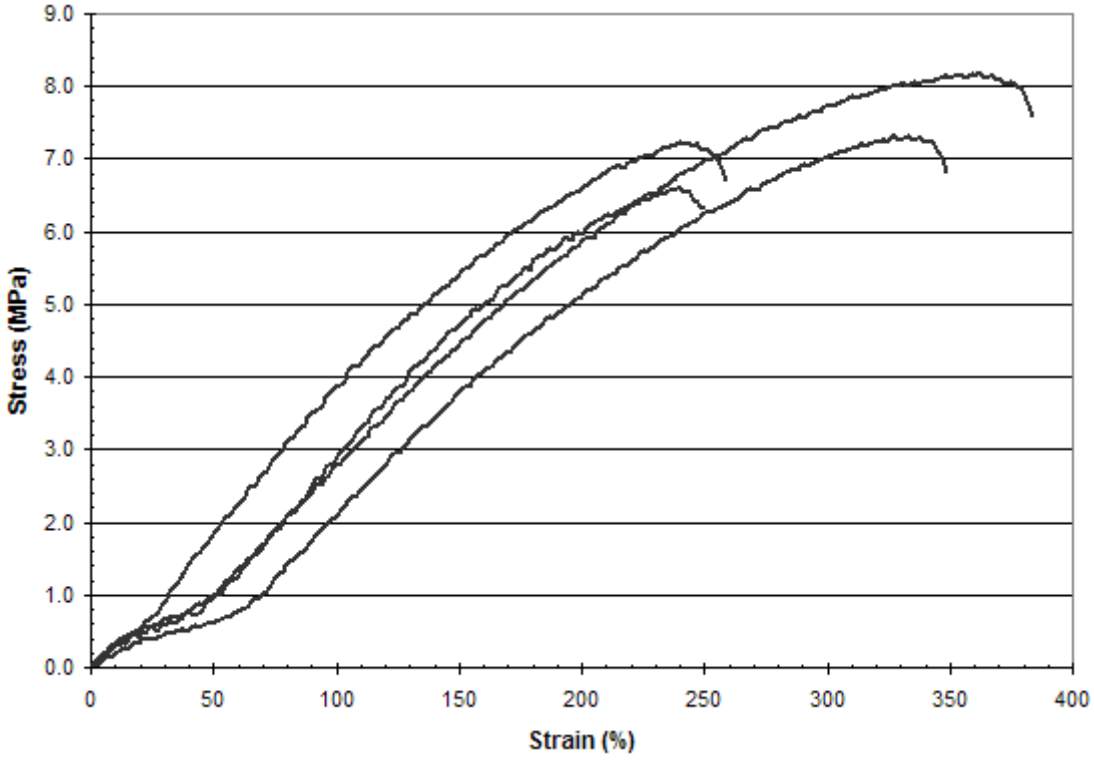

Figure A1: Stress-strain curves for STA-PURE™ from a 4.8 x 2.4 mm tube tested in the circumferential (θ-x) direction.

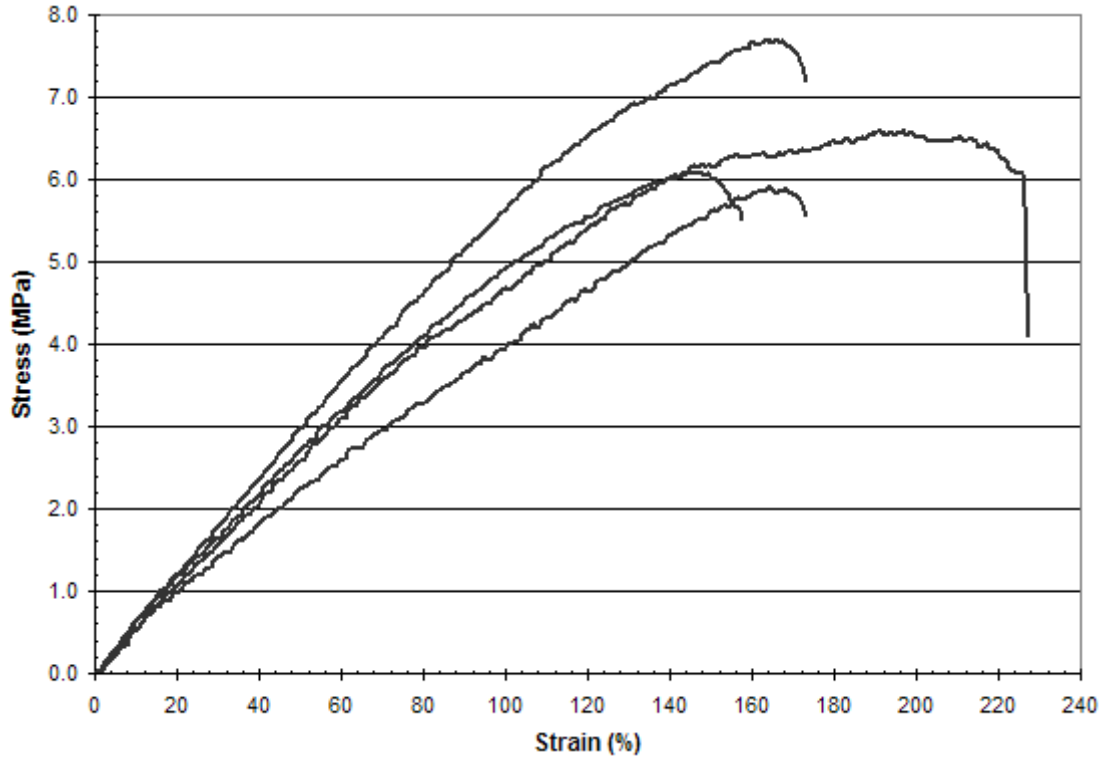

Figure A2: Stress-strain curves for STA-PURE™ from a 9.6 x 2.4 mm tube tested in the circumferential (θ-x) direction.

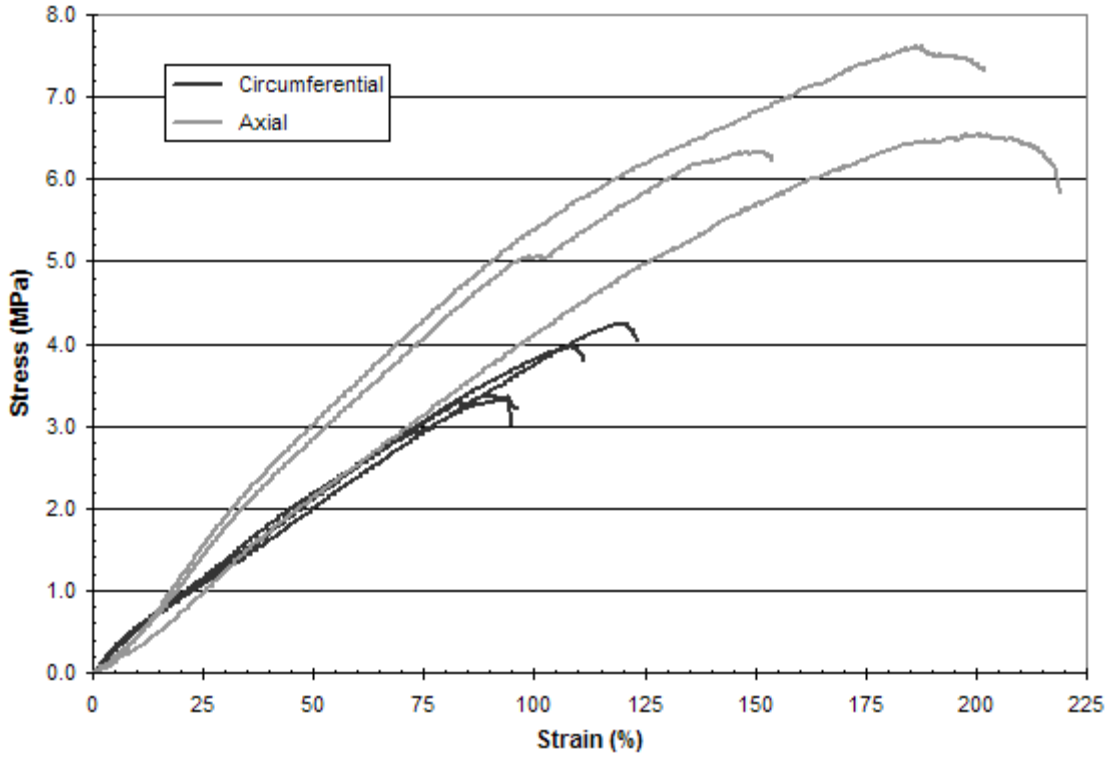

Figure A3: Stress-strain curves for STA-PURE™ from a 12.7 x 4.8 mm tube tested in the axial (x-θ) and the circumferential (θ-x) direction.

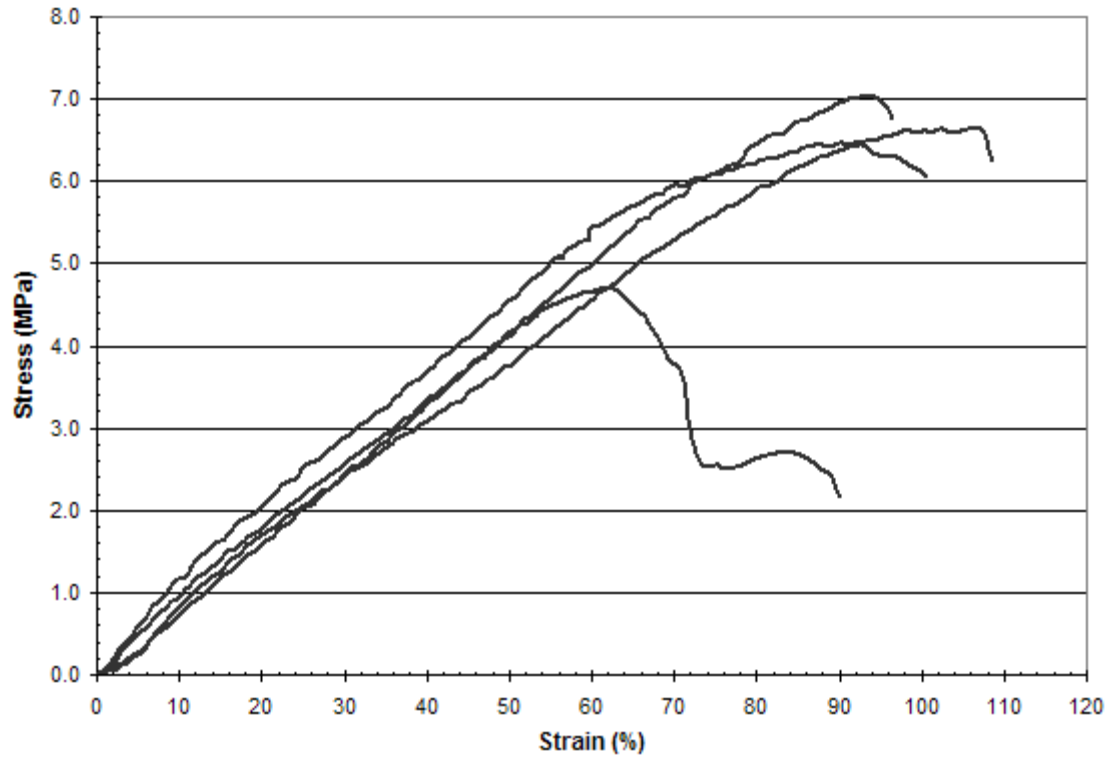

Figure A4: Stress-strain curves for STA-PURE™ "high pressure" from a 6.4 x 2.54 mm tube tested in the circumferential (θ-x) direction.

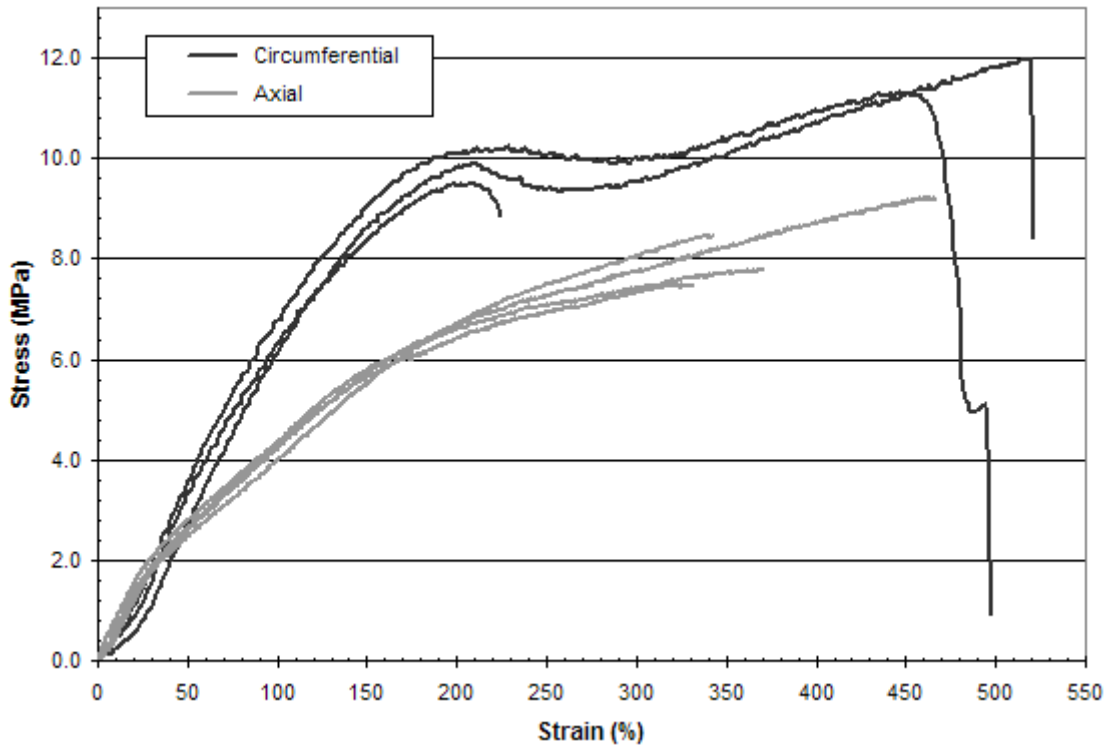

Figure A5: Stress-strain curves for ePTFE/FKM from a 4.8 x 2.4 mm tube tested in the circumferential (θ-x) direction.

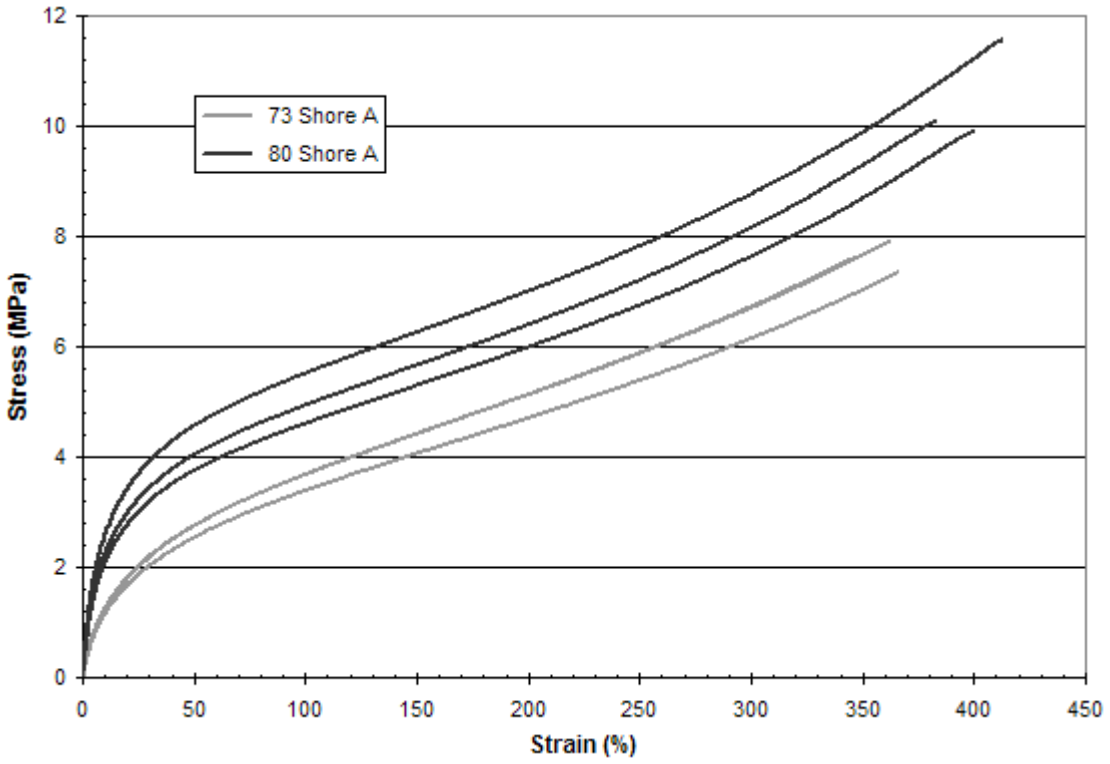

Figure A6: Stress-strain curves for two hardness grades of Bioprene® from a 40 x 12.75 mm tube tested in the axial (x-r) direction.

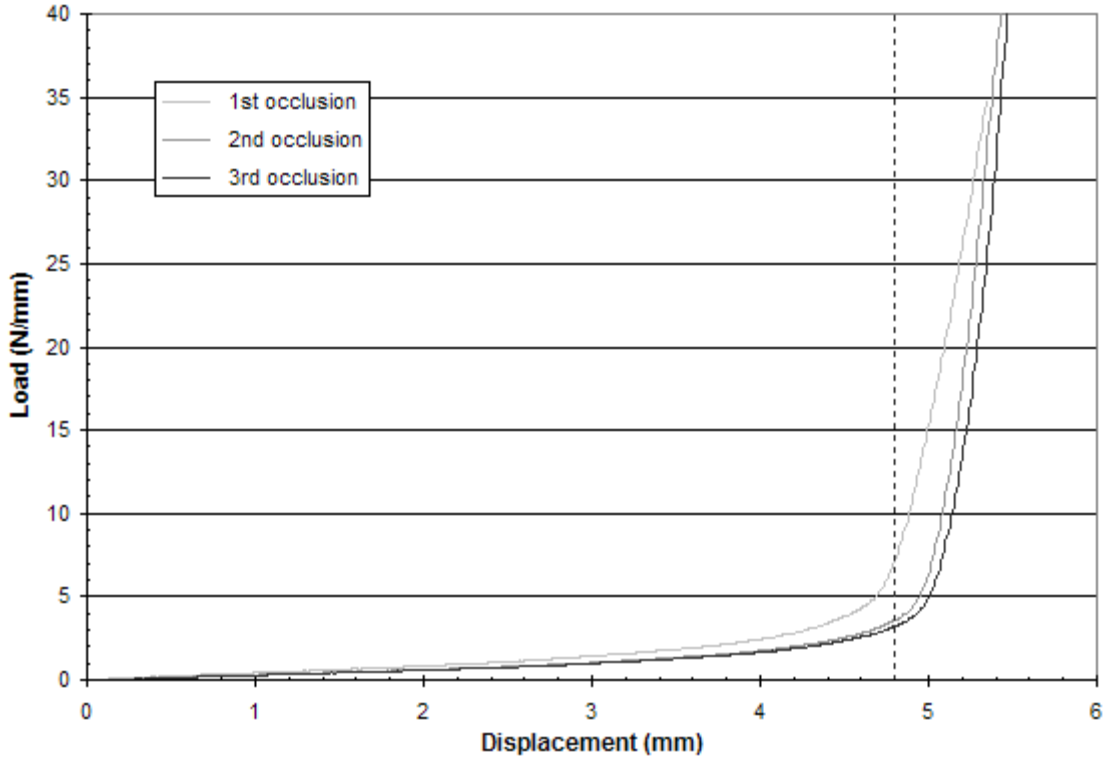

Figure A7: The first three occlusion curves for a 4.8 x 2.4 mm tube section of STA-PURE™. The dashed line denotes the inner diameter of the tube.

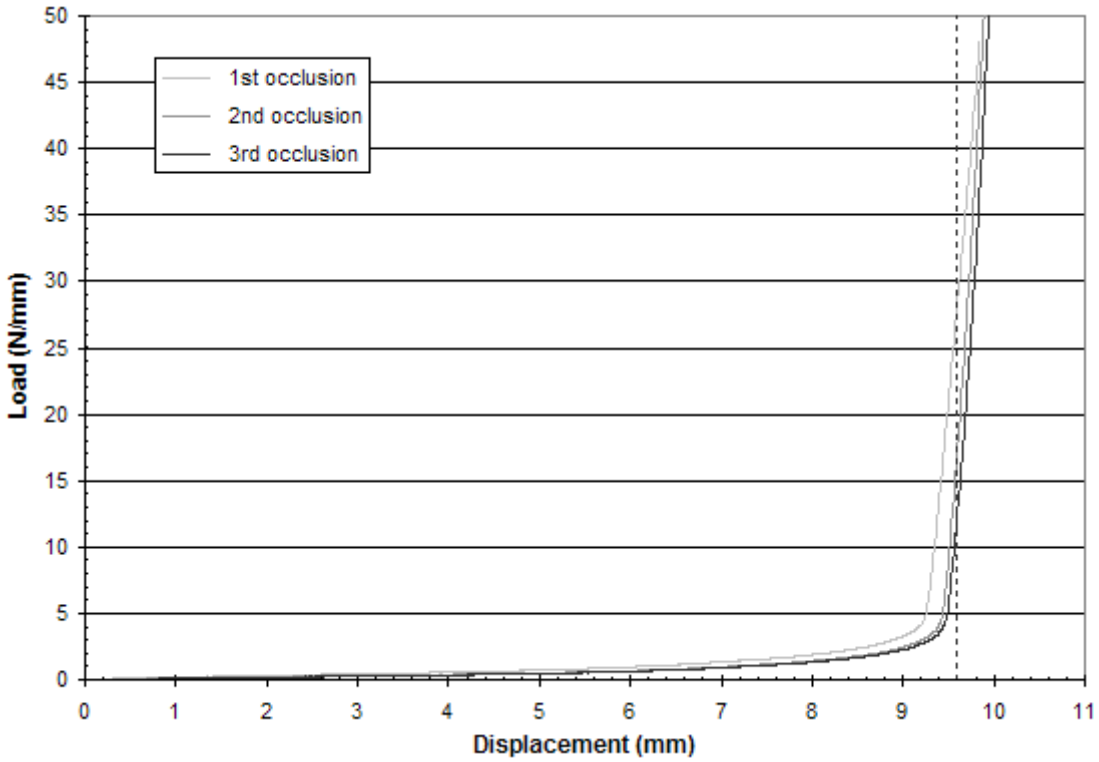

Figure A8: The first three occlusion curves for a 9.6 x 2.4 mm tube section of STA-PURE™. The dashed line denotes the inner diameter of the tube.

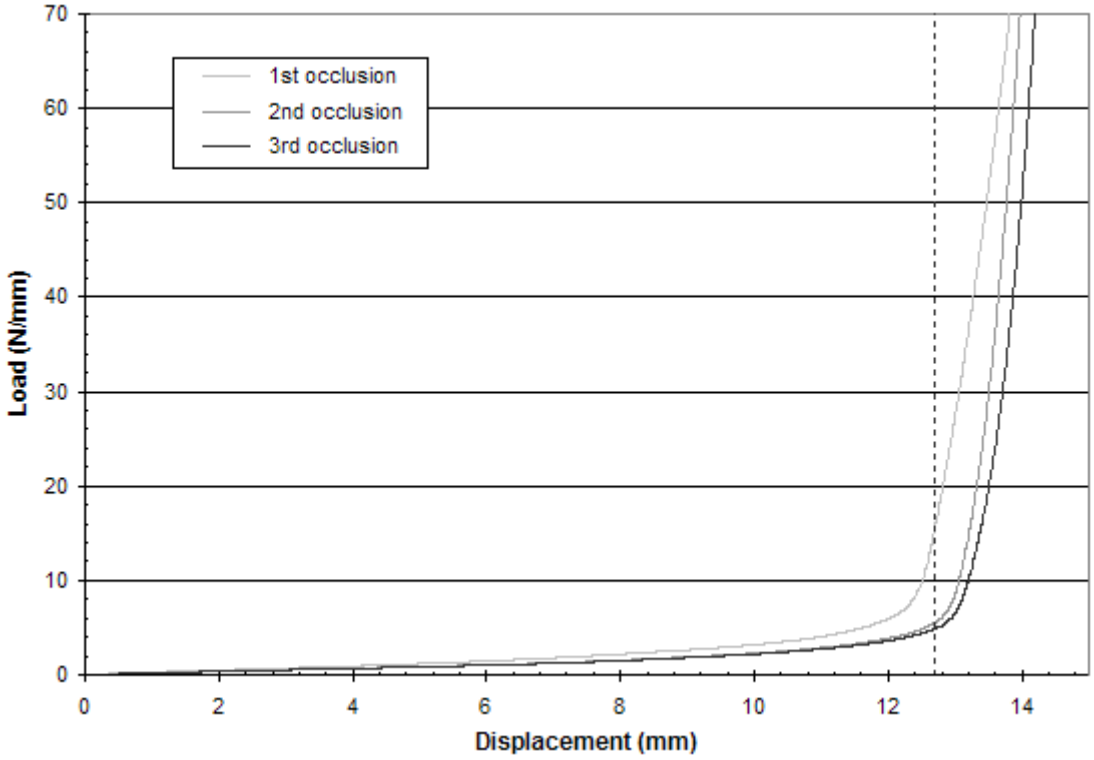

Figure A9: The first three average occlusion curves for 12.7 x 4.8 mm tube sections of STA-PURE™. Each curve is an average of 3 samples. The dashed line denotes the inner diameter of the tube.

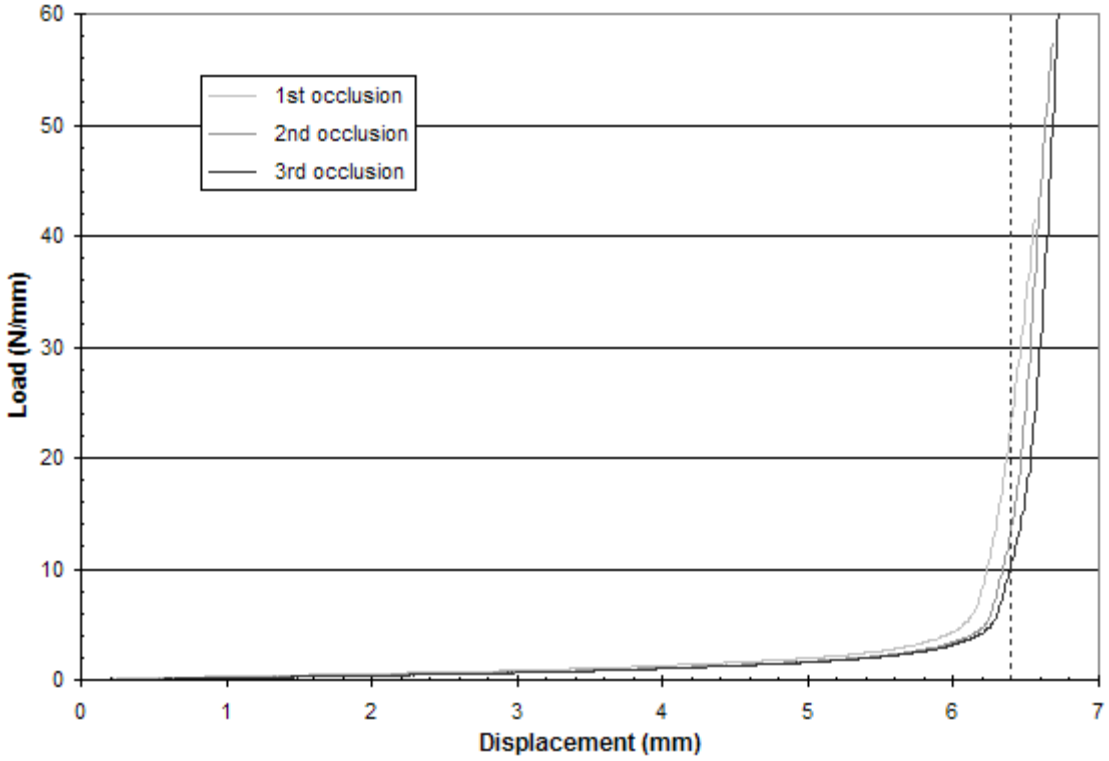

Figure A10: The first three occlusion curves for a 6.4 x 2.54 mm tube section of STA-PURE™ "high pressure". The dashed line denotes the inner diameter of the tube.

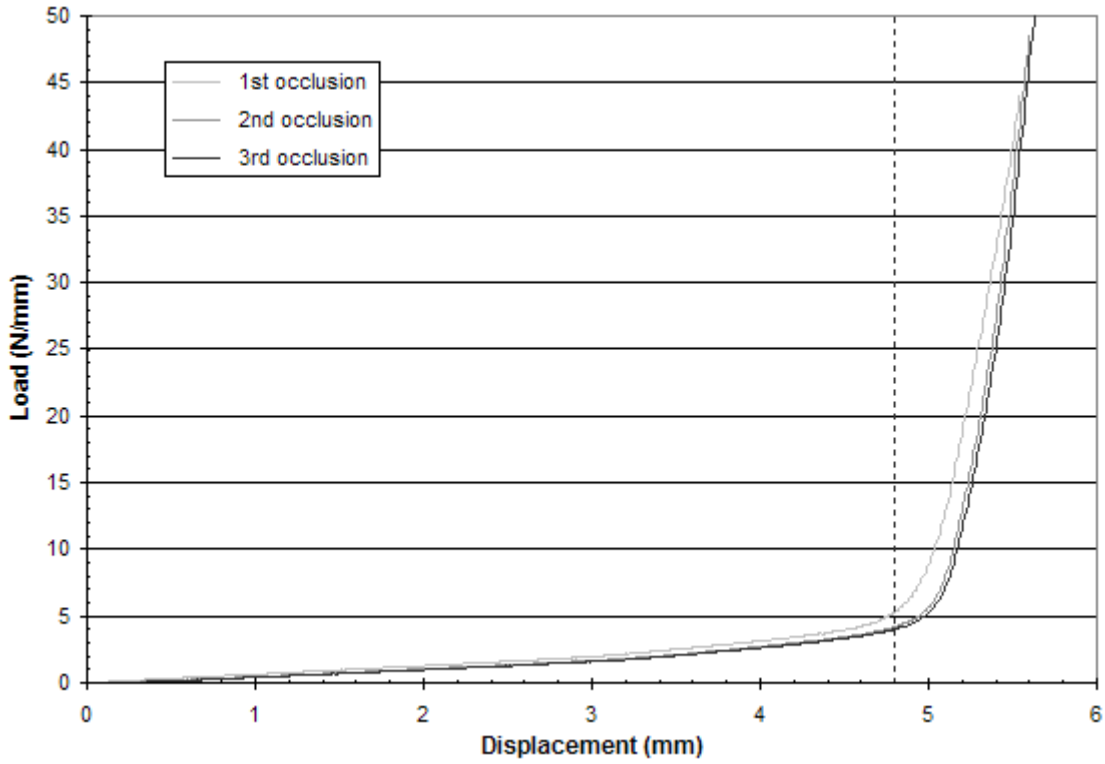

Figure A11: The first three occlusion curves for a 4.8 x 2.4 mm tube section of ePTFE/FKM. The dashed line denotes the inner diameter of the tube.

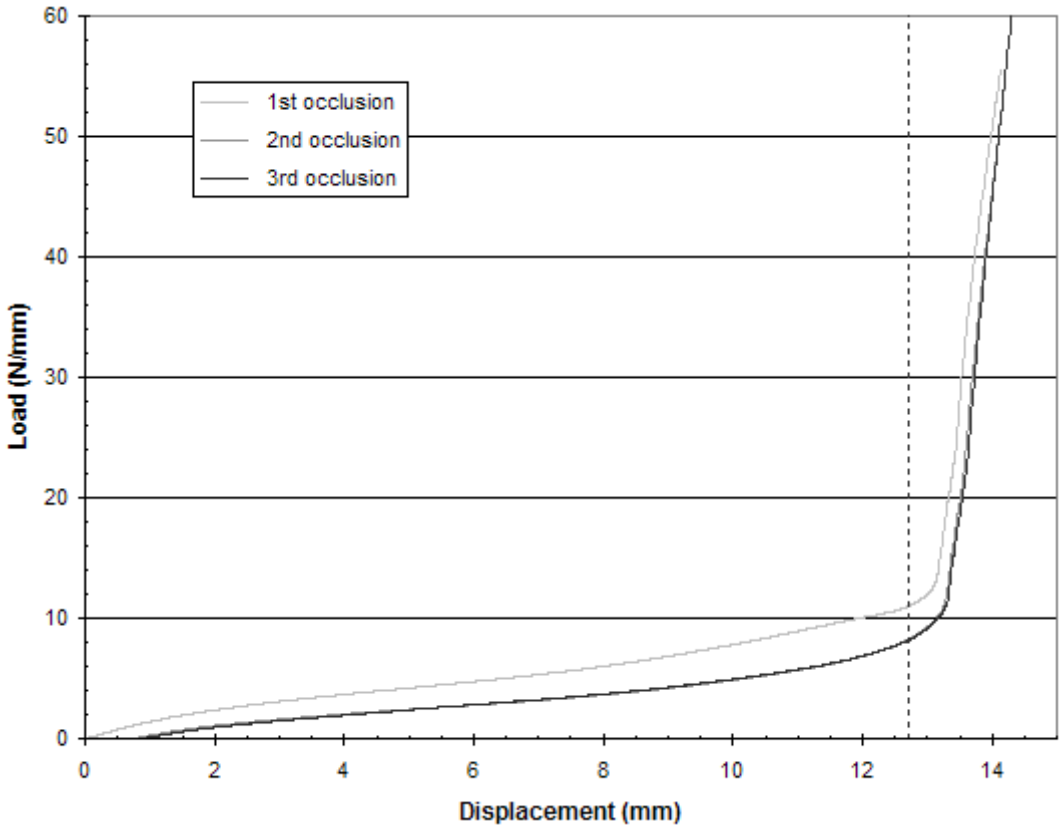

Figure A12: The first three average occlusion curves for 12.7 x 4.8 mm tube sections of 73 Shore A Bioprene®. Each curve is an average of 2 samples. The dashed line denotes the inner diameter of the tube.

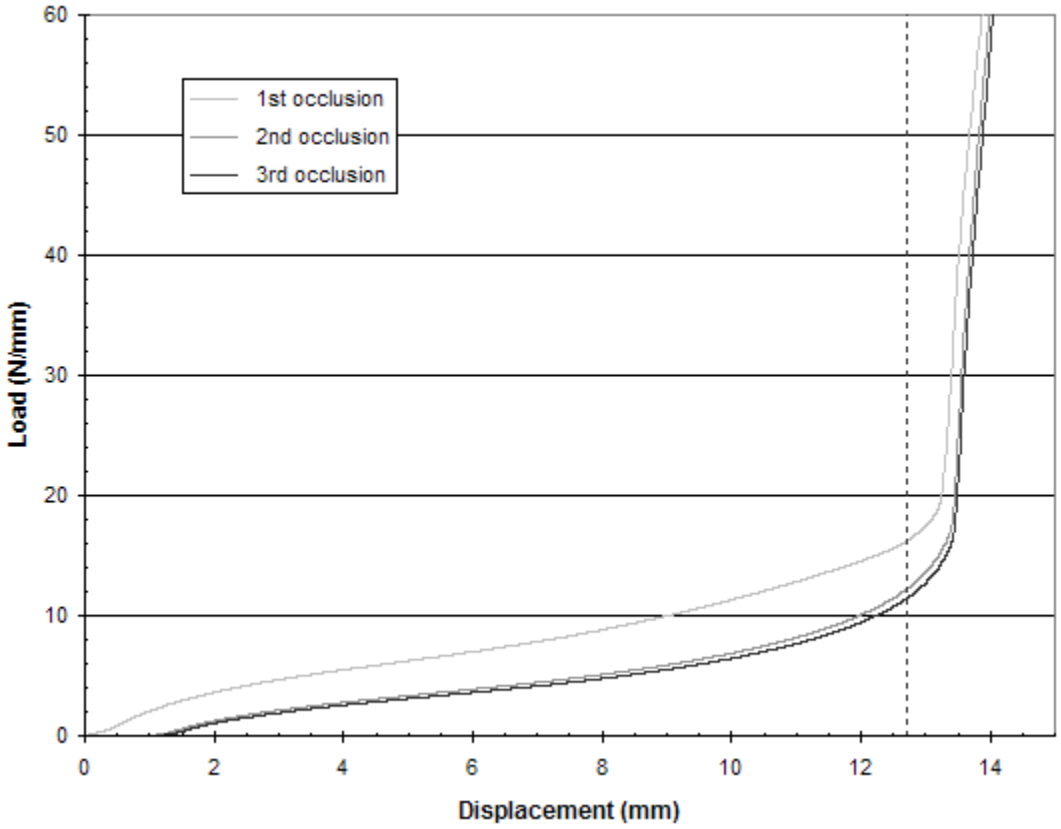

Figure A13: The first three average occlusion curves for 12.7 x 4.8 mm tube sections of 80 Shore A Bioprene®. Each curve is an average of 2 samples. The dashed line denotes the inner diameter of the tube.

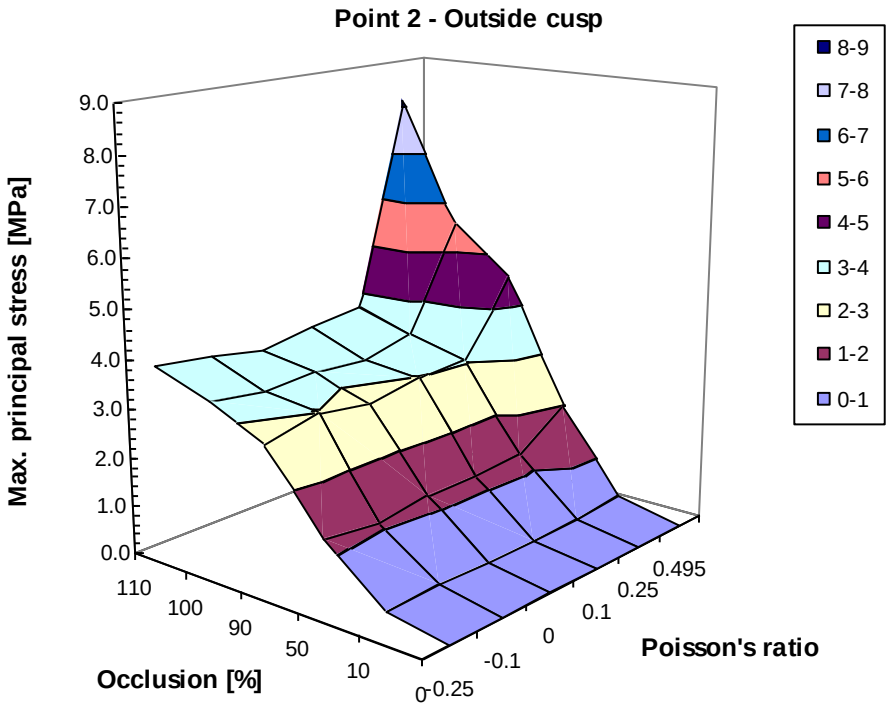

Figure A14: Maximum principal stresses in the outside cusp (point 2) related to the level of occlusion and the Poisson's ratio.

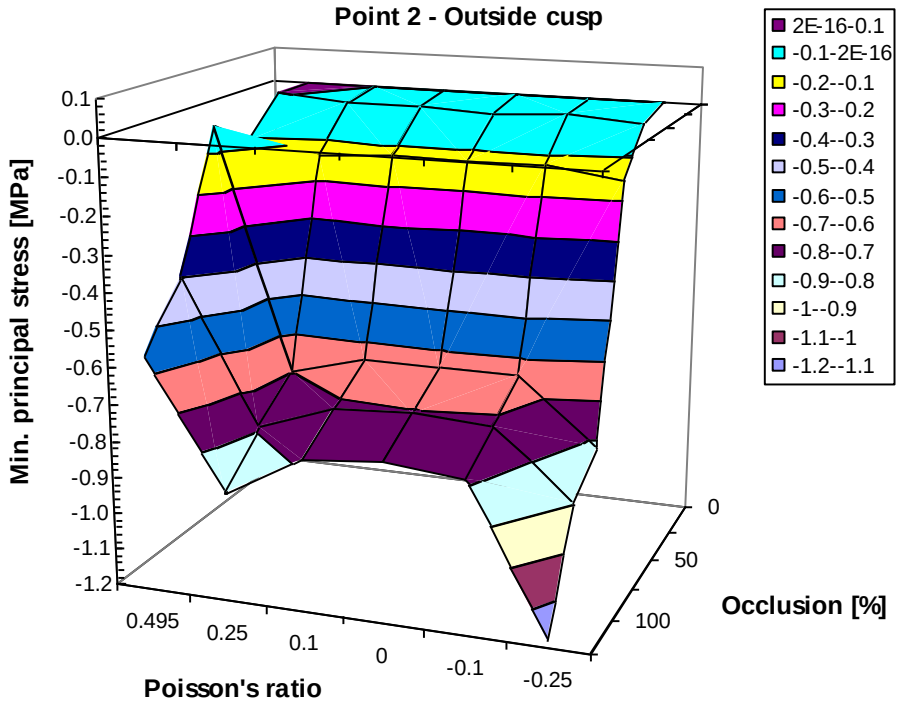

Figure A15: Minimum principal stresses in the outside cusp (point 2) related to the level of occlusion and the Poisson's ratio.

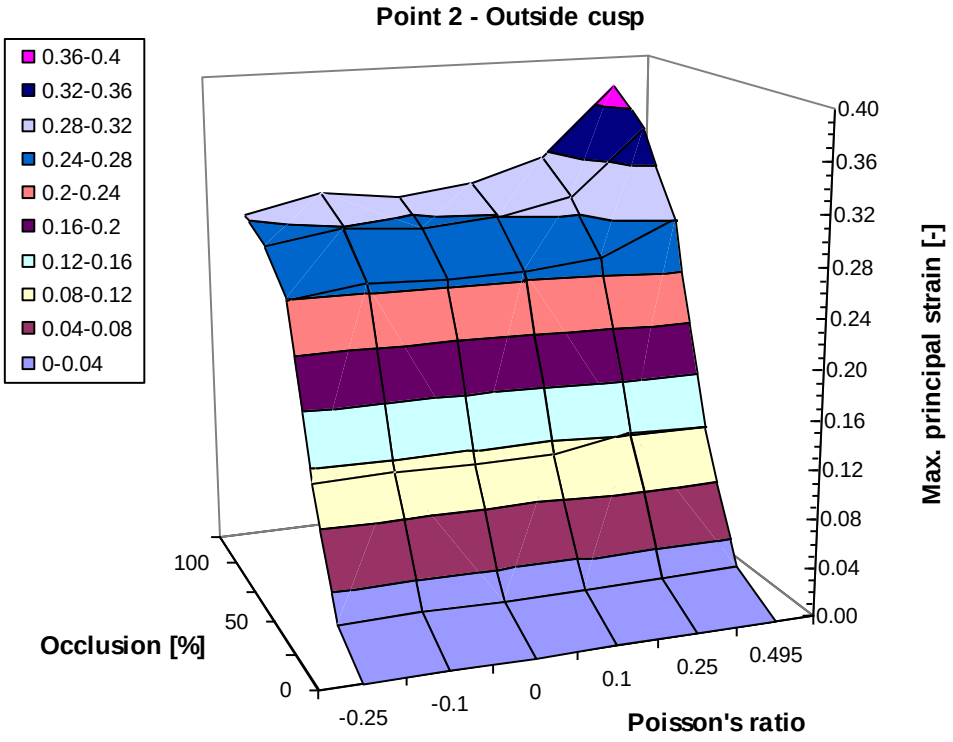

Figure A16: Maximum principal strains in the outside cusp (point 2) related to the level of occlusion and the Poisson's ratio.

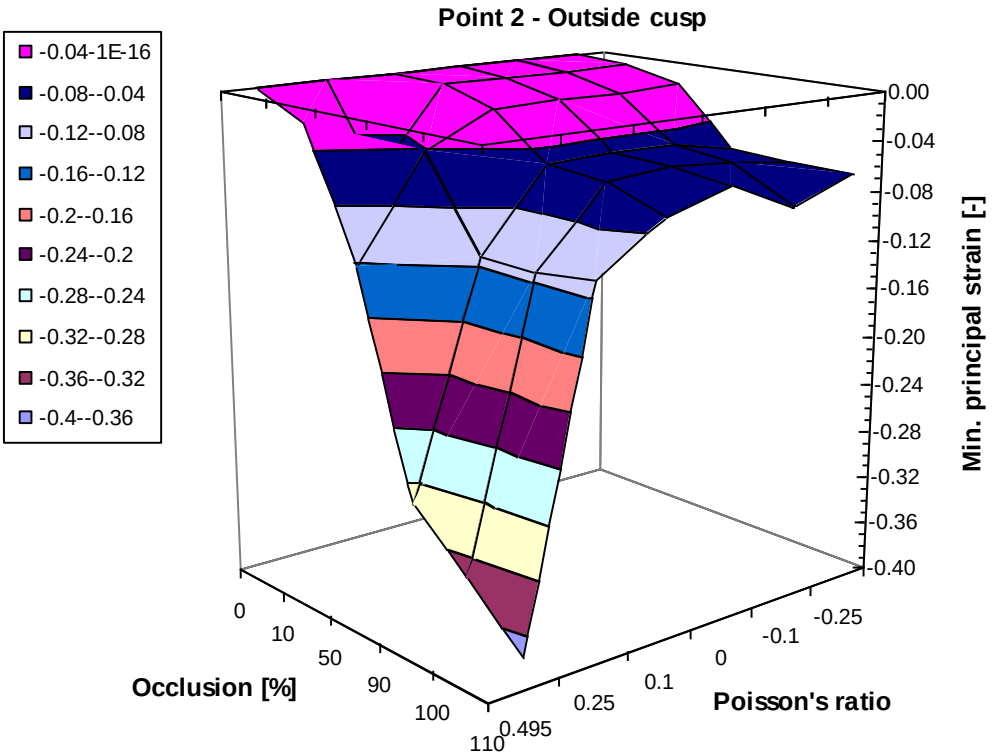

Figure A17: Minimum principal strains in the outside cusp (point 2) related to the level of occlusion and the Poisson's ratio.

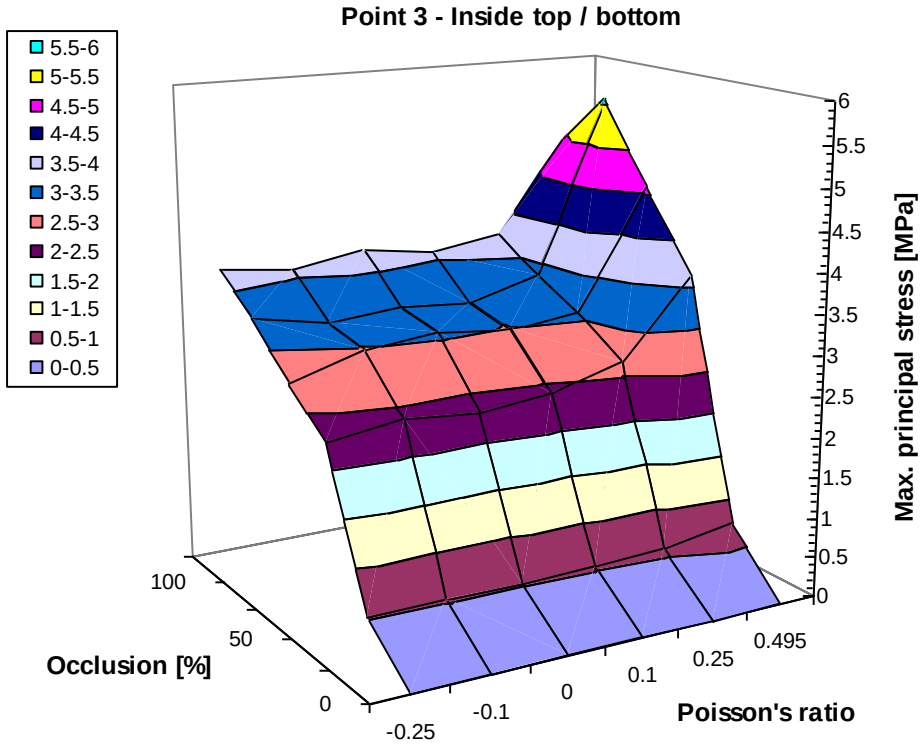

Figure A18: Maximum principal stresses in inside top / bottom (point 3) related to the level of occlusion and the Poisson's ratio.

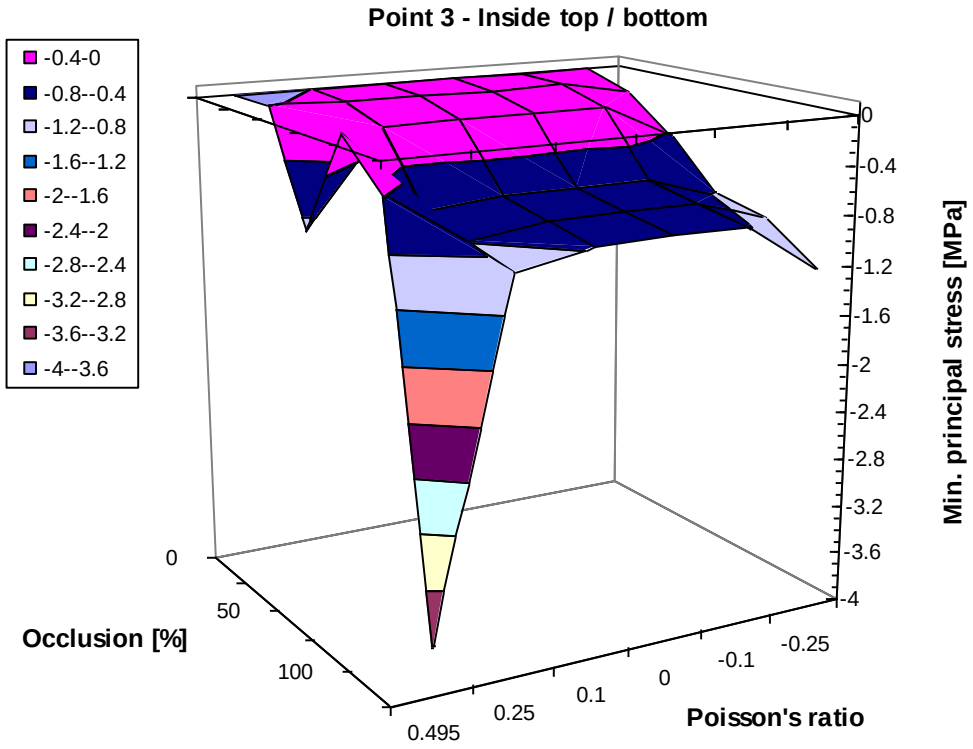

Figure A19: Minimum principal stresses in inside top / bottom (point 3) related to the level of occlusion and the Poisson's ratio.

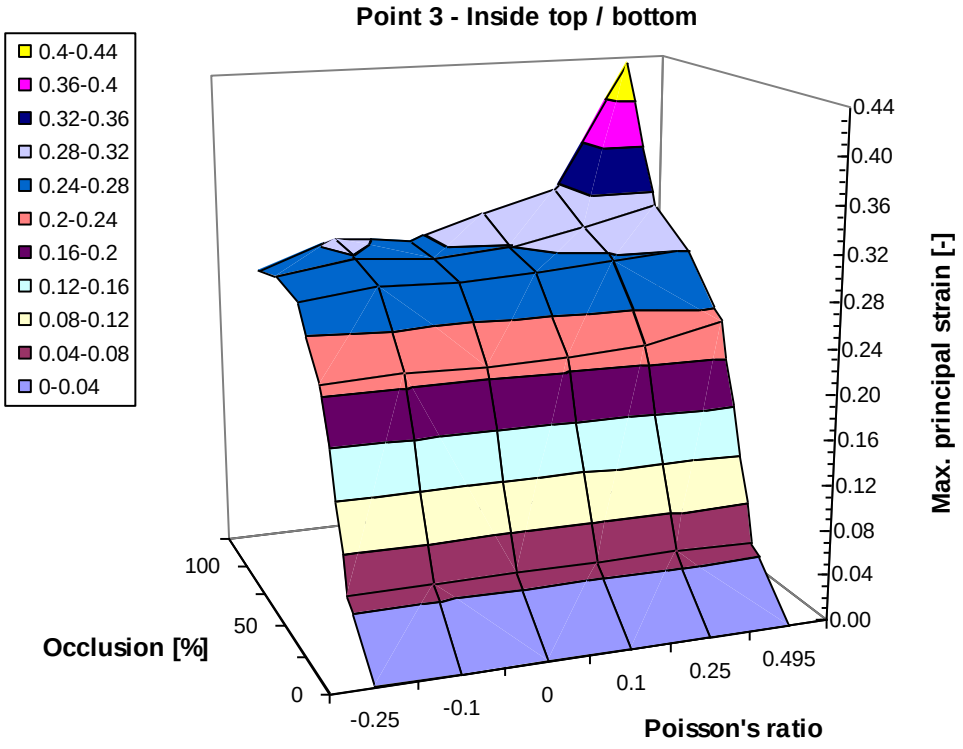

Figure A20: Maximum principal strains in inside top / bottom (point 3) related to the level of occlusion and the Poisson's ratio.

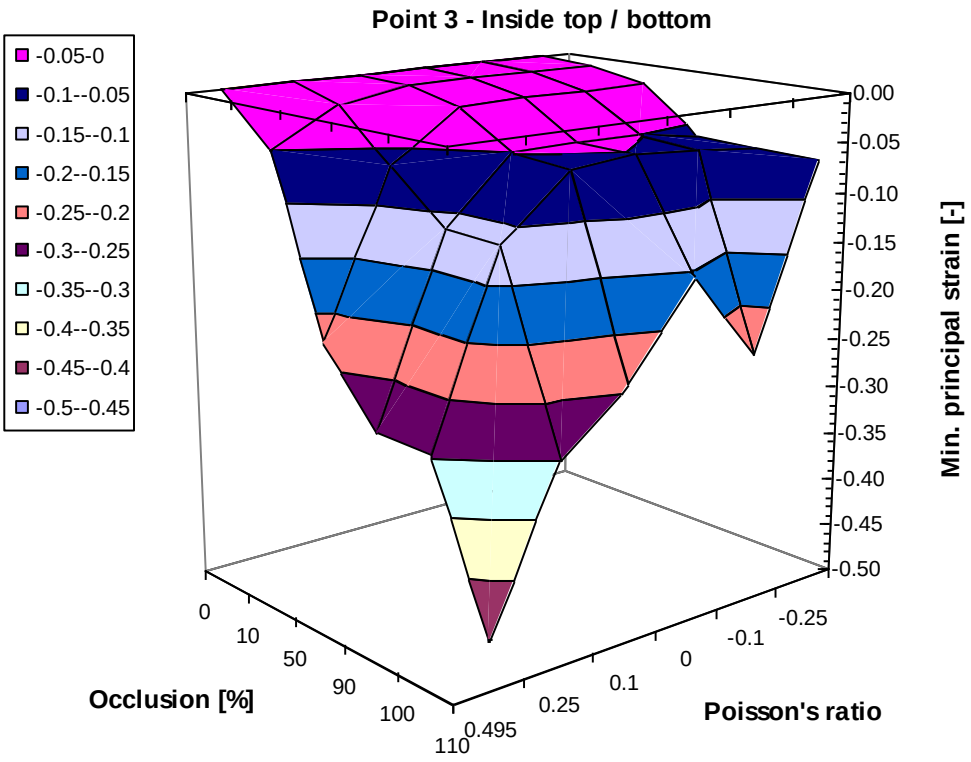

Figure A21: Minimum principal strains in inside top / bottom (point 3) related to the level of occlusion and the Poisson's ratio.

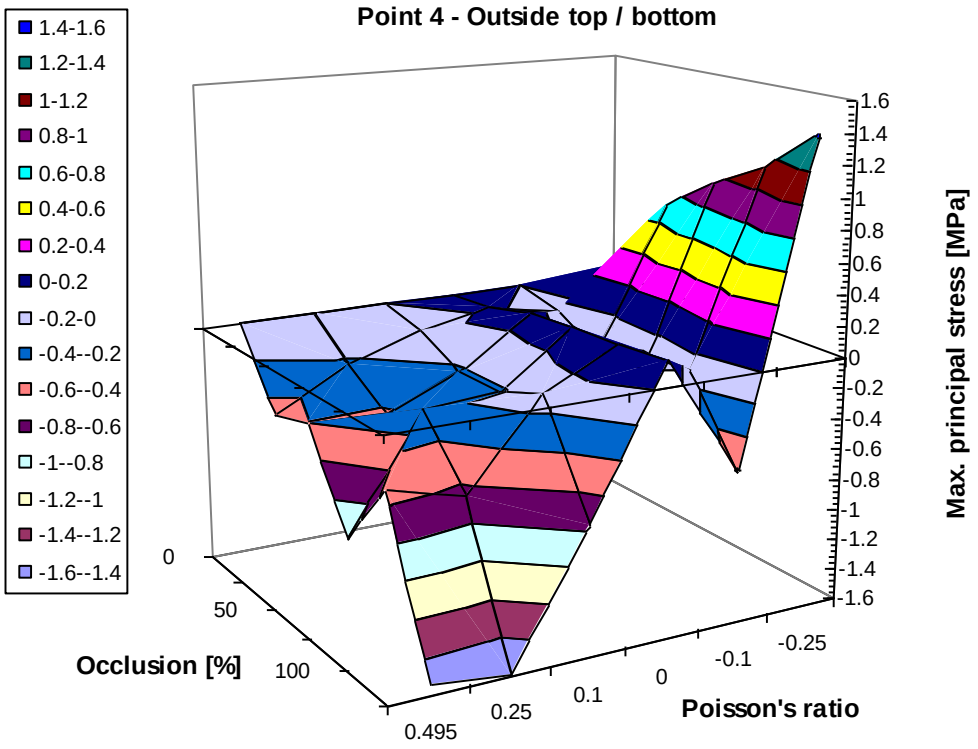

Figure A22: Maximum principal stresses in outside top / bottom (point 4) related to the level of occlusion and the Poisson's ratio.

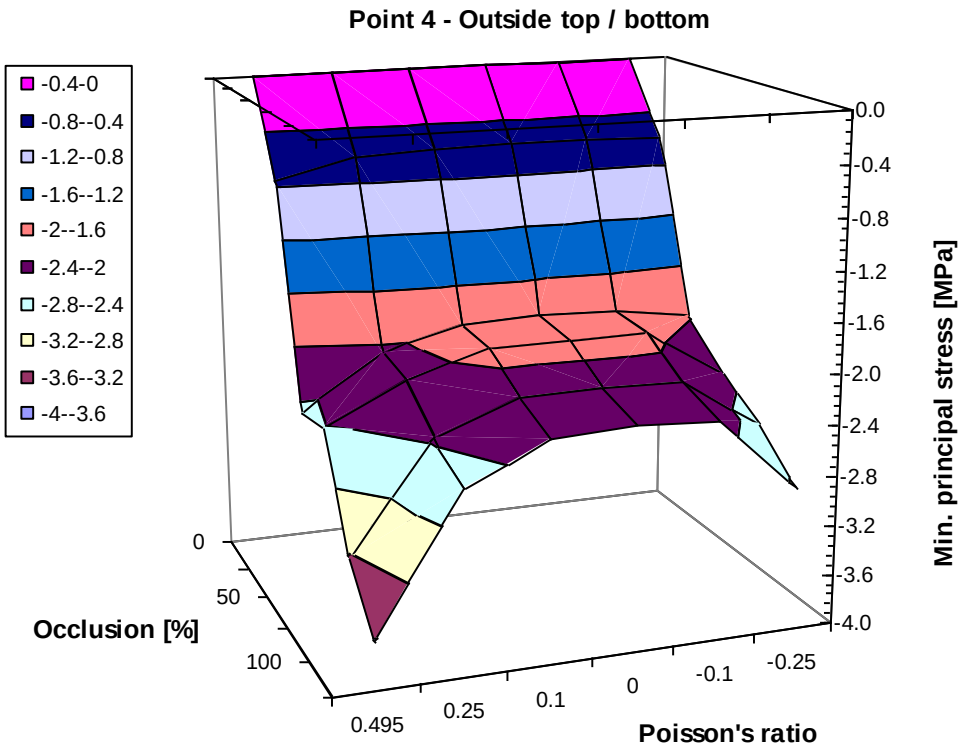

Figure A23: Minimum principal stresses in outside top / bottom (point 4) related to the level of occlusion and the Poisson's ratio.

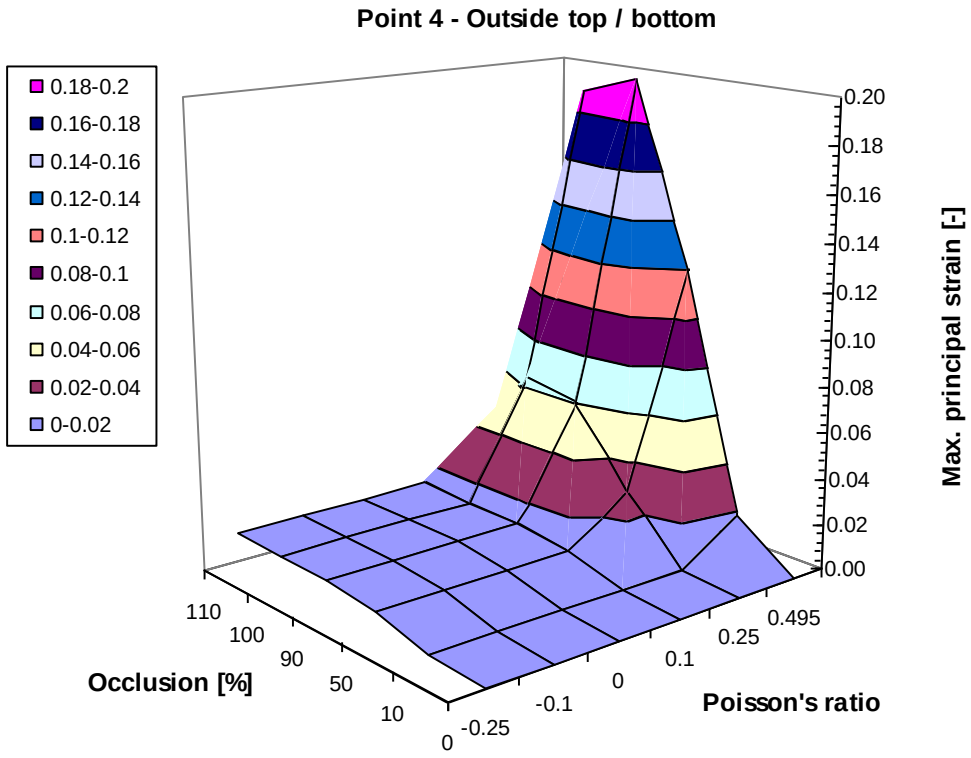

Figure A24: Maximum principal strains in outside top / bottom (point 4) related to the level of occlusion and the Poisson's ratio.

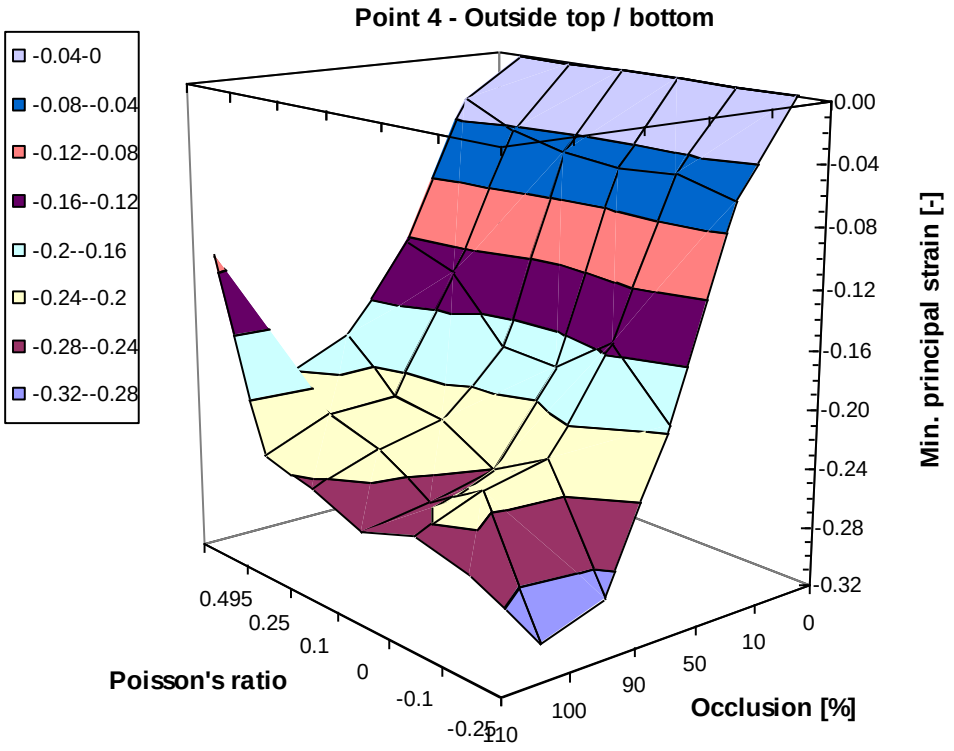

Figure A25: Minimum principal strains in outside top / bottom (point 4) related to the level of occlusion and the Poisson's ratio.